CAL-2150

National Aeronautics and Space Administration

HEA Gamma Ray Astronomy Research and Analysis Program

Annual Status Report for NAGW-2013

Submitted to:

Dr. Louis J. Kaluzienski
Astrophysics Division
Code SZC (GRA)
National Aeronautics and Space Administration
Washington, DC 20546

Submitted by:

The Trustees of Columbia University
in the City of New York
Box 20, Low Memorial Library
New York, New York 10027

Prepared by:

Columbia Astrophysics Laboratory
Departments of Astronomy and Physics
Columbia University
538 West 120^{th} Street
New York, New York 10027

Title of Research:

"A High Resolution Liquid Xenon Imaging Telescope for 0.3–10 MeV Gamma-Ray Astrophysics: Construction and Initial Balloon Flights"

Principal Investigator:

Prof. Elena Aprile
Columbia University

Report Period:

1 January 1993 – 31 December 1993

ANNUAL STATUS REPORT FOR NASA GRANT NAGW-2013

1. Introduction

The project entitled "A High Resolution Liquid Xenon Imaging Telescope for 0.3-10 MeV Gamma-Ray Astrophysics: Construction and Initial Balloon Flights" was initiated with the submission in August 1992 of the proposal CAL-2015 in response to NASA Announcement of Opportunity NRA 92-OSSA-8.

For the first year of the project, covering the period 1 January 1993 through 31 December 1993 funds in the amount of $250,000 were allocated, under NASA Grant NAGW-2013.

The results achieved with a 3.5 liter LXe-TPC prototype during the first year can be summarized as follows:

- The efficiency of detecting the primary scintillation light for event triggering has been measured to be higher than 85% (See Section 2.1).
- The charge response has been measured to be stable to within 0.1% for a period of time of about 30 hours.
- The electron lifetime has been measured to be in excess of 1.3 ms, corresponding to attenuation an length of the order of meters.
- The energy resolution has been measured to be consistent with previous results obtained with small volume chambers. At a drift field of 4 kV/cm the FWHM of 662 keV gamma-rays is 7% after corrections for electronic noise, shielding inefficiency and rise time effects (See Section 2.2).
- $X - Y$ gamma-ray imaging has been demonstrated with a non-destructive orthogonal wires readout (See Section 2.3).
- Monte Carlo Simulation Results: detection efficiency, expected background count rate at balloon altitude; background reduction algorithms; telescope's response to pointlike and diffuse sources; polarization sensitivity calculations (See Section 2.4).
- Design of a 10 liter LXe-TPC laboratory prototype and associated 100 channels of readout electronics was completed (See Section 2.5).
- Construction of a gas purification/recovery system for 10 liter or larger LXe-TPC prototype was completed and tested.

The results obtained in these areas are discussed in details in the following sections. They represent a significant progress towards the goal of construction and

test of the 10 liter laboratory prototype, with about half the sensitive area and depth of the proposed space flight instrument. The work has also addressed and answered the questions of technical concern raised by the proposal review panel as specified in the proposal CAL-2015 evaluation sheet.

Three articles published or accepted for publication in refereed journals are attached as Appendix 1–3. Three more articles, on which much work was devoted in 1993, are in the final stage of preparation: the first deals with studies of the different background components expected in the LXe-TPC/Coded Mask Telescope in the near space environment and their reduction based on imaging (to be submitted to *Nucl. Instrum. & Methods* in January 1994); the second deals with the scientific use of a LXe-TPC/ Coded mask gamma-ray telescope, with special emphasis on the determination of the ^{26}Al celestial source distribution (to be submitted to *Ap.J.* in February 1994); the third paper summarizes the results obtained with the 3.5 liter LXe chamber triggered by the scintillation light (to be submitted to *Nucl. Instrum. & Methods* in March 1994).

2.1. Triggering on Primary Scintillation Light in LXe

While the induction signals detected by orthogonal X and Y wire planes give two dimensional image of an interaction point inside the detector, triggering with the primary scintillation light gives the third coordinate of the interaction point, using the known drift velocity.

The scintillation light trigger efficiency has been studied in great detail with our 3.5 LXe liter detector, shown in Fig. 1. It is a gridded ionization chamber with a drift gap of 5 cm; the electrode sensitive area is 8×8 cm^2. On the side of the chamber body there are two quartz windows with about 70% transmission at the wavelength of 175 nm. Two UV sensitive photomultipliers can be fixed on the outer cryogenic vessel with vacuum insulation. The distance between the photocathode surface of the PMTs and the center of the detector sensitive volume is about 16 cm. Two different PMTs have been tested for comparison: an Hamamatsu R2059, and an EMI 9813QB. A collimated ^{137}Cs (10 mCi) γ-ray source is used to irradiate the detector

Each γ-ray interaction inside the detector produces both ionization and scintillation signals. The scintillation light is detected by the PMTs and used as a trigger, while the ionization charge is drifted under the applied electric field and is collected by the anode. Fig. 2 shows two typical triggered events, the first one is

single photoabsorption event, and the second one is a photoabsorption followed by a Compton interaction.

The waveforms of the light and charge signals are amplified and digitized by a CAMAC based LeCroy 2262 FADC, using the light signal as trigger for the FADC. Offline data analysis finds the trigger position and the height of the steps of charge collection. The steps are fitted with the function,

$$f(a,b,c,d,e) = \begin{cases} d+et & t<b \\ \frac{a(t-b)}{c}e^{-\frac{t-b}{tf}}+d+et, & b\le t<b+c \\ ae^{-\frac{t-b}{tf}}+d+et, & t\ge b+c \end{cases} \quad (1)$$

a – pulse height

b – step starting time position

c – rise time of the step

tf – fall time of electronics.

The delay between the trigger and the time of start of a charge step corresponds to the drift time between cathode and grid.

Fig. 3 shows one typical fitted event. The correlation between step height and drift distance is shown in Fig. 4. The dense part in the scatter plot corresponds to the full energy peak in the pulse height spectrum. The fact that the peak position stays invariant with increasing drift distance, means that there is no charge loss during the charge "blob" drift, indicating very good purity of the liquid xenon. With the information of the pulse height dependence on drifting distance, one can directly infer the attenuation length of electrons in LXe.

The pulse height distribution gives the spectrum as shown in Fig. 5a. The peak is fitted with a Gaussian and a FWHM resolution of 9.8% is obtained at a field of 2 kV/cm, which is similar to or better than the resolution of the spectrum directly obtained by a MCA, (see Fig. 5b). This shows that the fitting algorithm can precisely find the step height, with good noise filtering. It also shows the power of the digitized information which permits to reject "bad events" such as those interacting in the grid-anode region.

The geometry of this detector is not optimized for light detection yet. The solid angle subtended by the PMTs to the center of the sensitive volume is only about 0.5%. The spectrum of scintillation light at zero field and 1.5 kV/cm field with ^{137}Cs light 662 keV γ-ray source is shown in Fig. 6. It shows clearly the effect

of light quenching by the external field which reduces the recombination rate. For the field higher than 500 V/cm, the light spectra are almost the same. This means that the quenching effect has reached a saturated value. It can be seen that many events produce a single or double photoelectron. However a triggering efficiency better than 85% was already achieved for energy depositions larger than 511 keV (see Table 1). In Fig. 7, the lower spectrum is from events triggered by a coincidence of two PMTs, while the upper is the spectrum from direct charge signal. From the ratio of the total events under the peak, one gets the trigger efficiency of 73.3% for two PMT coincidence triggering. Random coincidences, which are less than 0.1% of the total counts, were subtracted when estimating the triggering efficiency.

Table 1. Triggering efficiency for different energy lines with single PMT

	511 keV	662 keV	1.274 keV
Trig. Eff. (%)	86.9	87.2	100

The triggering efficiency is expected to be improved for the 10 liter LXe-TPC prototype due to the better geometry for light detection.

2.2. Charge and Energy Resolution Response

The same 3.5 liter chamber shown in Fig. 1, with a drift distance of 5 cm, was used for studies of charge collection and energy resolution dependence on: gamma-ray energy, shielding effects, pulse rise time variation, and source collimation. Excellent LXe purity was achieved for the 3.5 liter sample, as demonstrated by the ionization pulses of cosmic ray muons traversing the 5 cm gap and recorded at a filed of 5 V/cm and 2 V/cm (Fig. 8). The drifting electron lifetime is in excess of 1.3 ms, which is the longest pulse rise time recorded at the lowest field.

Charge collection stability and energy resolution was measured with a collimated ^{137}Cs source, as well as with ^{22}Na and ^{207}Bi sources. The relevant results obtained with 662 keV gamma-rays are shown in Fig. 9(a-d). Fig. 9a shows the charge yield as a function of applied electric field; Fig 9b shows the dependence of the noise subtracted energy resolution on the drift field. At 5 kV/cm the FWHM resolution at 662 keV is 8%, in good agreement with previous results obtained at the same field with small volume LXe chambers. The degradation of resolution

due to shielding inefficiency and pulse rise time variation is not negligible in the present data. The contribution was estimated by Monte Carlo. When subtracted in quadrature, along with the electronic noise contribution, the intrinsic resolution becomes on the order or 7% FWHM at 662 keV. Fig. 9c shows the measured resolution dependence on gamma-ray energy. A good fit with a $1/\sqrt{E}$ function is obtained. The data were obtained at a drift field of 2.5 kV/cm. Typical ^{137}Cs and ^{22}Na spectra obtained at low fields are shown in Fig. 10. Fig 9d shows the variation of the collected charge as a function of time. Over a period of about 30 hours the detector's response was stable to within 0.1%. This demonstrates that there should be no concerns about the lifetime of LXe against buildup of impurities due to outgassing. As for radiation damage in the space environment, it is known that one of the advantages of liquid rare gases is their radiation hardness.

2.3. X-Y Gamma-Ray Imaging

In the few MeV region, Compton interaction dominates and produces events of multiple interaction sites in the LXe γ-ray detector. These multiple-site events are characterized by the spatially separated point-like charge blobs. These might give the ambiguity of event localization and degrade the resolution of imaging. Therefore it is necessary to accurately localize these charge blobs and precisely measure the energy deposited in each site, in order to reconstruct the event based on the Compton kinematics.

We adopted in our proposal a simple non-destructive readout, schematically shown in Fig. 11a, for imaging the point-like charge blobs produced by γ-ray interactions in LXe. It consists of two orthogonal induction wire planes, separated from the drift region by a screening mesh. The sense wires have a spacing that is a multiple of the mesh pitch and are aligned with the mesh so that they don't intercept the drifting electrons. The induced signals on the wires provide $X-Y$ information. The measured drift time, referred to the scintillation trigger, and the known drift velocity, provide the $Z-$information. Thus 3-D imaging is achieved for each ionizing event. The charge of each blob can be obtained from the multiple-steps pulse shape recorded by an anode plate placed below the induction wires.

Such a readout geometry turns out to be very suitable for accurate localization of the point-like charge blobs. The amplitude of the induction signal produced by a point-like charge depends strongly on its initial lateral position with respect to the sense wire cell. This position dependence of the induction signals can be

an advantage to localize a point-like charge blob by weighting the signals from adjacent wires. This is schematically shown in Fig. 11b. Without the weighting, the spatial resolution is limited by the wire spacing. By pulse height sharing between adjacent wires and subsequent centroid finding, the position of a charge blob is determined with an effective resolution $< 58\mu\text{m}(2\text{mm}/\sqrt{12})$ for 2 mm wire spacing. The ultimate resolution is therefore determined by the accu- racy of the amplitude measurements, i.e. the signal-to-noise ratio.

We have successfully tested this design concept with the 3.5 liter LXe chamber. The shielding mesh is made of nickel, spot-welded on a stainless steel frame, and has a spacing of 0.8 mm and a wire width of 50 μm. The ratio of electric fields on the two sides of the mesh was chosen to be 2.0 or more to ensure full transparency for the drifting electrons. The sense wires are made of BeCu with a diameter of 50 mm and have a spacing of 4 mm, which is a multiple of the mesh pitch. The tested readout has 10 sense wires for the X-direction and 10 for the Y-direction. The sense wires are stretched on a ceramic (MACOR) holder, electrically isolated from each other and biased with their natural potentials in order not to distort the field distribution. The distances between the plates, determined by the ceramic spacers, are $G_x = 3.25$ mm, $G_y = 3.75$ mm and $G_o = 4.0$ mm (see Fig. 1). The induction signal on each wire is detected, via a decoupling capacitor, with a low noise charge sensitive preamplifier with a decay time of 50 ms. The output of each preamplifier is connected to a FADC through an additional amplification stage. This additional amplification stage has a band-pass filter which greatly enhances the signal-to-noise ratio of the induction signals without changing the triangle shape of the signal.

Fig. 11b shows a typical $X - Y$ image of a γ-ray event from ^{207}Bi, recorded by the FADC readout at a drift field of 0.5 kV/cm. Due to the point-like charge blob produced by the γ-ray, only two adjacent X-wires and two adjacent Y-wires show a signal. The different pulse heights on these adjacent wires give better localization accuracy than that of wire spacing, by weighting the signal amplitudes. This is further demonstrated in Fig. 12 by the pulse height distribution of the induction signals which are induced on a particular X-wire by blobs of fixed amount of charge. The blob with fixed amount of charge was selected by setting a narrow window on the energy spectrum and picking up events with single step pulse shape. These charge blobs are produced by the γ-rays of fixed energy (662 keV) and uniformly interacting within the drift region (uncollimated source). The two bumps correspond to two bunches of possible drifting paths for the charge from the drifting region, which are focused by the shielding mesh, as shown in Fig. 12.

The whole distribution corresponds to the lateral distance away from the monitored wire within the 4 mm pitch for X-wires. The maximum and minimum pulse heights correspond to the interaction point which is laterally closest or farthest from the wire, within a wire cell. The RMS spread of these bumps directly gives the spatial resolution for this horizontal axis, which is obviously better than the wire spacing, on an event-by-event basis and is approaching the intrinsic limit set by the physical extension and diffusion of the charge blobs. The step height of the anode signal gives the total deposited energy.

In this preliminary design and test, we have demonstrated that both γ-ray imaging with submillimeter $X - Y$ localization accuracy and calorimetry can be obtained simultaneously, using such a readout. Fig. 13 shows a distribution of the events when imaging collimated γ-rays from ^{137}Cs with a beam width of about 4 mm.

2.4. Monte Carlo Results

MonteCarlo calculations continued throughout 1993, with the goal of finding the optimum detector and shield configuration for best sensitivity in the energy region of 0.3-10 MeV. The capability of the LXe gamma-ray detector to measure both the deposited energy and the three spatial coordinates of any interaction point inside the sensitive volume, enables one to use the kinematics of the dominant Compton scattering process to identify the direction of a multiple-sited γ-ray event and therefore translates directily into a powerful background rejection capability. The event reconstruction algorithm, based on Compton kinematics and originally discussed in the published NIM paper (Appendix 1), was futher tested and optimized for different modes of telescope operation. Algorithm 1 was developed for operation with a fine resolution mask with the γ-ray source located within a narrow FOV. In this case the initial γ-ray direction is assumed perpendicular to the detector's plane. Algorithm 2 was developed for a wide FOV telescope, optimized for diffuse sources observations. Both algorithms are most efficicient in the energy range 0.5-3 MeV, where Compton cross section is dominant. All events with a single point of interaction are rejected as background and no pair production analysis is done to recover high energy events. The photopeak effiency of the LXe-TPC/Coded Mask Telescope was calculated for the energy range 0.3-10 MeV for 5 cm (laboratory prototype) and 10 cm (flight prototype) active depth of LXe. Fig. 14 shows the efficiency for 5 cm, before and after the Compton event reconstruction. To recover

the efficiency at low energy, more sophisticated analysis based on energy and location can be applied. Similarly high energy events characterized by pair production can be recovered by appropriate analysis. The effect of the event reconstruction on Compton continuum suppression is shown in Fig. 15. To estimate the background rate expected in LXe-TPC/Coded Mask Telescope at balloon altitude (3 g/cm^2 over Palestine), we considered the contribution from atmospheric and cosmic γ-rays, as well as background originating from the detector itself and the materials around the detector. Results from the calculations are shown in Figs. 16-20. The calculations were done with either 5 cm or 10 cm thick active CsI shield around the sides and bottom of the LXe-TPC. The figures show the total background count rate as well as the components considered: aperture flux, shield leakage, mask, spallation and elastic neutron scattering. The reduction of the background count rate by the event reconstruction algorithms is also shown. For spallation induced background the reduction efficiency was assumed to be the same as that for atmospheric background. In reality the reduction factor should be even larger because most of the spallation events will be beta-decays. The background rates for different configurations are summarized in Table 2. The large contribution at low energies (0.1–0.3 MeV) will be strongly reduced by the scintillation trigger threshold as well as by the plastic scintillation counters to be used for charged particles veto in front of the aperture. Results indicate that a shielded LXe instrument will not be dead-time limited, even with a maximum event rate of about 600/s for the entire 0.1–10 MeV region. Calculations with an unshielded detector show that the event rejection technique applied to an unshielded detector can provide the same reduction factor as a detector with thick shield. Details of the background components studies including neutron activation and the reduction techniques based on event imaging are summarized in a paper in preparation for NIM. Here we discuss in particular the secondary radiation from the tungsten coded mask which was considered of particular concern by the proposal review panel.

Table 2. Total Background Rate of LXe Telescope at 3 g/cm^2 Over Palestine, Tx

	Before rejection		After rejection 5 cm shield	
	10 cm shield	5 cm shield	Algorithm 1	Algorithm 2
0.1–10 MeV	580 s^{-1}	630 s^{-1}	70 s^{-1}	50 s^{-1}
0.3–10 MeV	180 s^{-1}	230 s^{-1}	70 s^{-1}	50 s^{-1}

Gamma-ray background may be produced in the mask from (1) ambient γ-rays, (2) charged particles (photons and electrons), and (3) neutrons. The first source, ambient photons, can Compton scatter or produce pairs in the mask material. The scattered photons and bremsstrahlung photons (from electromagnetic cascade,s for example) can then interact in the detector. Using the empirical formula of Owens et al. (1985) and the count rate spectrum measured in a balloon flight by the UNH group (Dunphy et al. 1989), we find that most of the mask background is due to reprocessing of high energy ambient (i.e., atmospheric) photons.

The second source, γ-rays produced by electrons and protons ($>$ 20 MmeV) incident on the mask, can be estimated from measurements and calculations of electron and proton fluxes at balloon altitudes (Verma 1967; Daniel and Stephens 1974; Aitbaev et al. 1981). This can be compared with the atmospheric γ-ray flux (Thompson 1974; Schönfelder et al. 1980). This shows that the flux of γ-rays produced in the mask by charged particles is at least a factor of 5 smaller than that produced by the atmospheric photons, and thus can be neglected. The third source, background photons from the interaction of thermal and fast neutrons in the atmosphere with a tungsten mask, has been evaluated by Butler et al. (1984) using a Monte Carlo code. Using their calculated yields, we find that the photon background from this source is about 4 orders of magnitude smaller than the atmospheric γ-ray background from the region of sky covered by the mask; so this is also negligible.

To calculate the contribution of the mask background to the LXe detector counting rate, we compare it to the background from the atmosphere and the cosmic diffuse gamma-ray flux. Comparing the count rate spectrum from the mask in Dunphy et al. (1989) at 1 MeV with the count rate expected from the atmosphere plus the cosmic diffuse source (Schönfelder et al. 1980; Costa et al. 1984), we conclude that the mask adds a relatively small component (50% or less) to the photon background that comes through the aperture of a coded aperture detector. The estimated background counting rate spectrum in the LXe detector from the mask is shown in the previous Figs. 16-20.

Using the calculated efficiency and background rate after event reconstruction, we have simulated the response of the telescope to various source distributions. To illustrate the point source response we show in Fig. 21 the image of the Crab Nebula in the range 1-2 MeV (10 hr observation). The source is present at a significance level of 10 s. The localization accuracy for this observation is 3 arcminutes, assuming a characteristic pixel size of 30 arcminutes. The performance of the proposed telescope as a Compton Polarimeter is discussed in the Appendix 2. Fig. 22 shows the results

of the calculation for the minimum detectable degree of polarization versus incident photon energy for a 3 s detection of a 100% polarized source with the spectrum of the Crab (10 hr observation).

References for Section 2.4.

Aitbaev, F.B. et al, Proc. 17th ICRC **5**, 426 (1981).
Butler, R.C., et al., Nucl. Instr. and Meth. **221**, 41 (1984).
Costa, E., et al., Astrophys. Space Sci. **100**, 165 (1984).
Daniel, R.R., and Stephens, S.A., Rev. Geophys. Space Phys. **12**, 233 (1974).
Dunphy, P.P. et al., Nucl. Instr. and Meth. **A274**, 362 (1989).
Owens, A. et al., Proc. 19th ICRC **3**, 314 (1985).
Schönfelder, V. et al, Astrophys. J. **240**, 350 (1980).
Thompson, D., JGR **76**, 1309 (1974).
Verma, S.D., JGR **72**, 915 (1967).

2.5 Design of 10 Liter LXe-TPC/Electronics/Gas System

The only convincing evidence of the suitability of the LXe-TPC technology for gamma-ray observations in space is to demonstrate the technology with a laboratory prototype of similar size as that of the proposed flight instrument. With substantial contribution from the Waseda collaborators, the design of a 10 liters LXe-TPC prototype was initiated during 1993. In its final version, the LXe detector and its cryostat is shown in Fig. 23. The internal electrode structure of the TPC is shown schematically in Fig. 24. For cost reasons, the sensitive area and depth of liquid is half the scale of the future balloon version. Fig. 25 shows the gas purification and recovery system associated with the 10 liter detector. Its construction and test were completed in 1993. Xe gas equivalent to five liquid liters were already procured with 1993 funds and purified with such system. The Xe is stored in two SS cylinders (each of 4 gallons capacity). The design of the analog and digital readout electronics for the 10 liter prototype was also done during 1993. A schematic of the readout chain is shown in Fig. 26. The induction signals (50 from X-wires and 50 from Y-wires) and the collection signal from the anode are directly coupled to low noise charge sensitive preamplifiers. Additional signal amplification needed to drive the FADCs is obtained with a second stage amplification system which also include a band pass filter for noise reduction. The analog signals are then digitized with a VME based FADC system. Both the amplitute and the timing of each event is

recorded. For more details on the characteristics of the electronics components we refer to the Proposal Renewal for 1994, submitted separately to NASA.

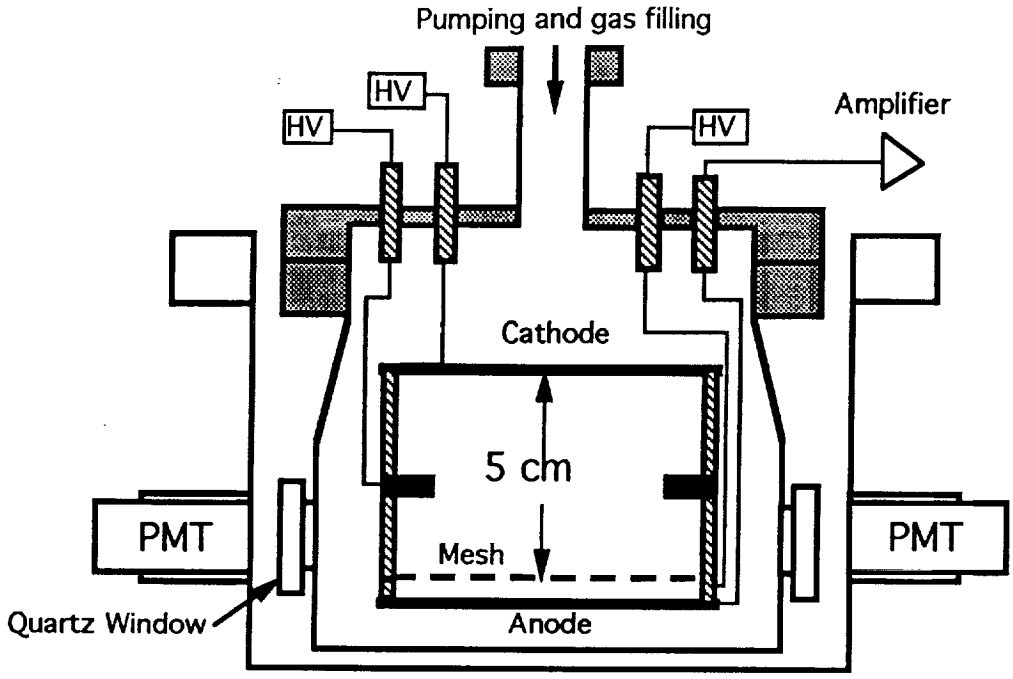
Pumping and gas filling
HV
HV
HV
Amplifier
Cathode
5 cm
Mesh
PMT
PMT
Quartz Window
Anode

Fig. 1

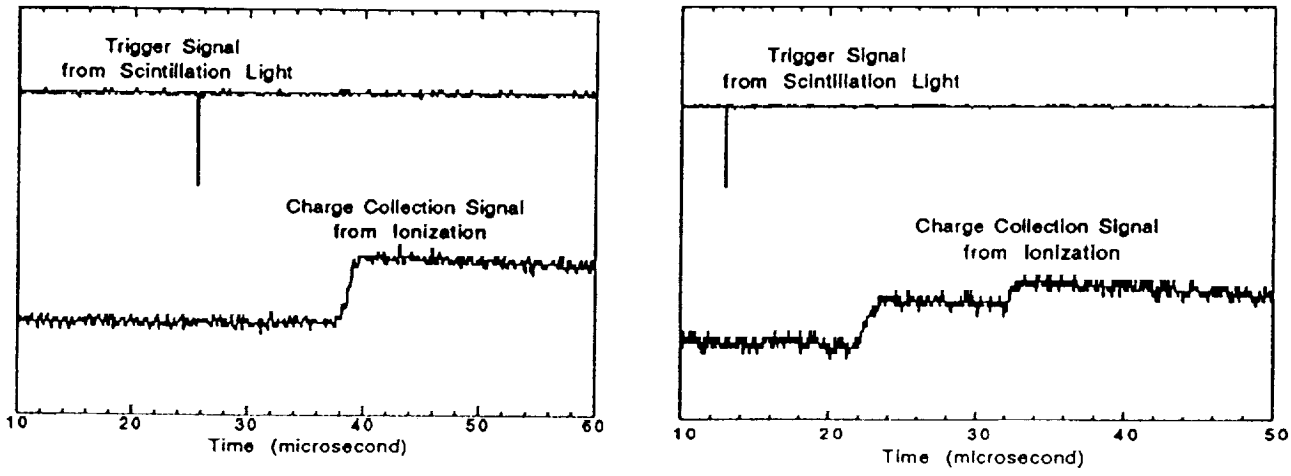
Trigger Signal
from Scintillation Light
Charge Collection Signal
from Ionization
10
20
30
40
50
60
Time (microsecond)
Trigger Signal
from Scintillation Light
Charge Collection Signal
from Ionization
10
20
30
40
50
Time (microsecond)

Fig. 2

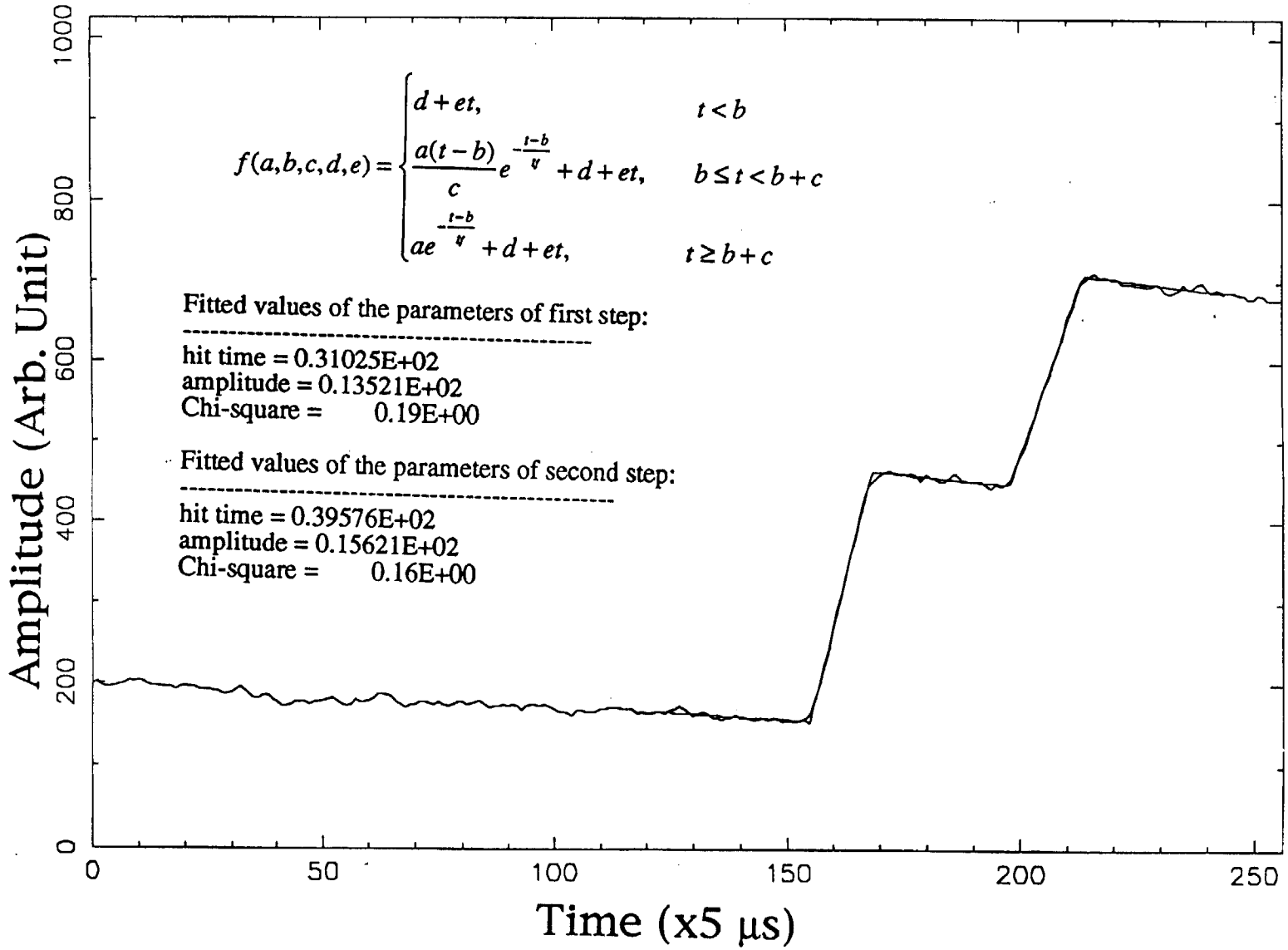
$f(a,b,c,d,e) = \begin{cases} d+et, & t<b \\ \frac{a(t-b)}{c} e^{-\frac{t-b}{\tau}} + d + et, & b \le t < b+c \\ ae^{-\frac{t-b}{\tau}} + d + et, & t \ge b+c \end{cases}$
Fitted values of the parameters of first step:
hit time = 0.31025E+02
amplitude = 0.13521E+02
Chi-square = 0.19E+00
Fitted values of the parameters of second step:
hit time = 0.39576E+02
amplitude = 0.15621E+02
Chi-square = 0.16E+00
Amplitude (Arb. Unit)
Time (x5 μs)
0
200
400
600
800
1000
0
50
100
150
200
250

Fig. 3

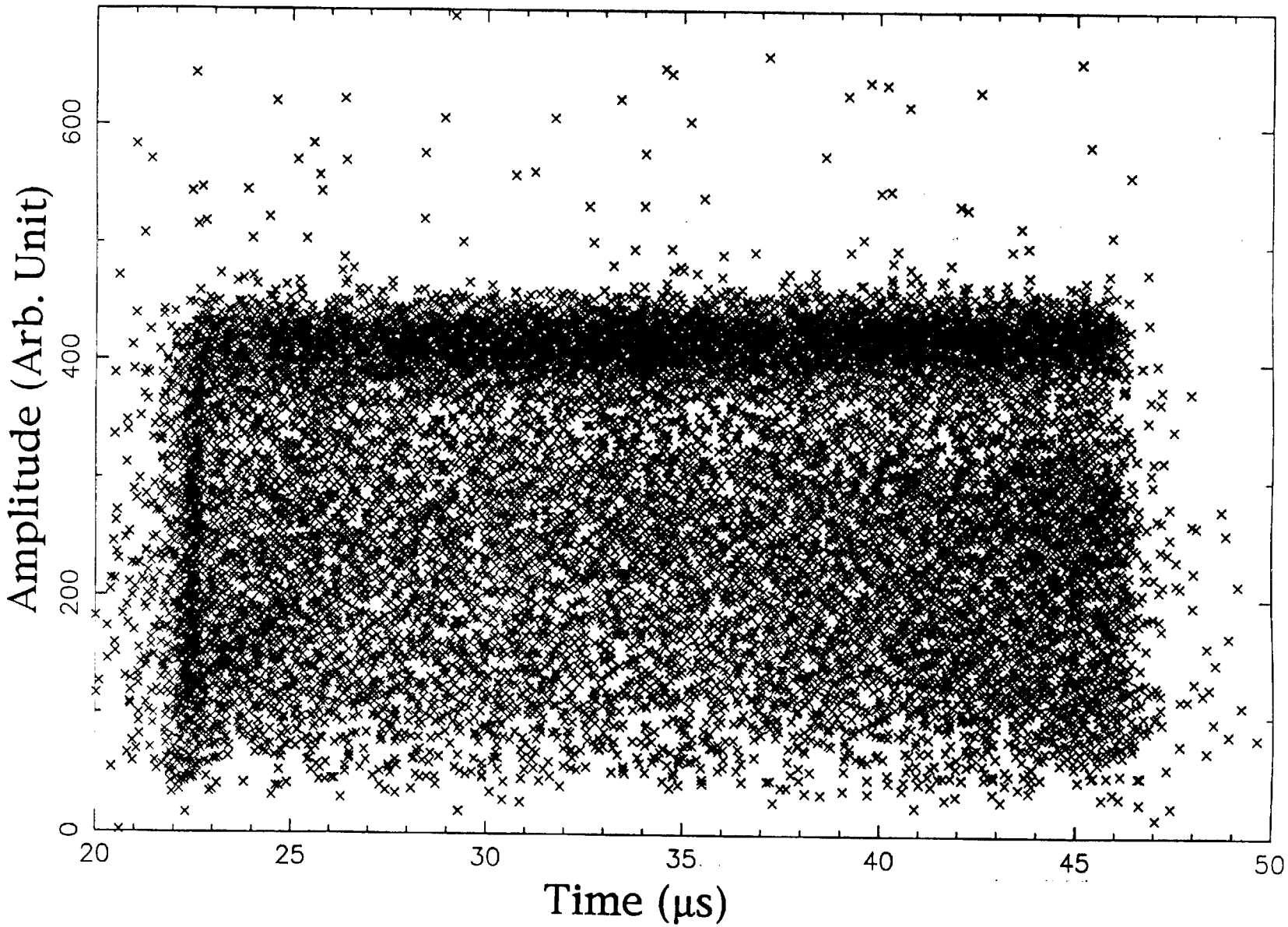

Fig. 4

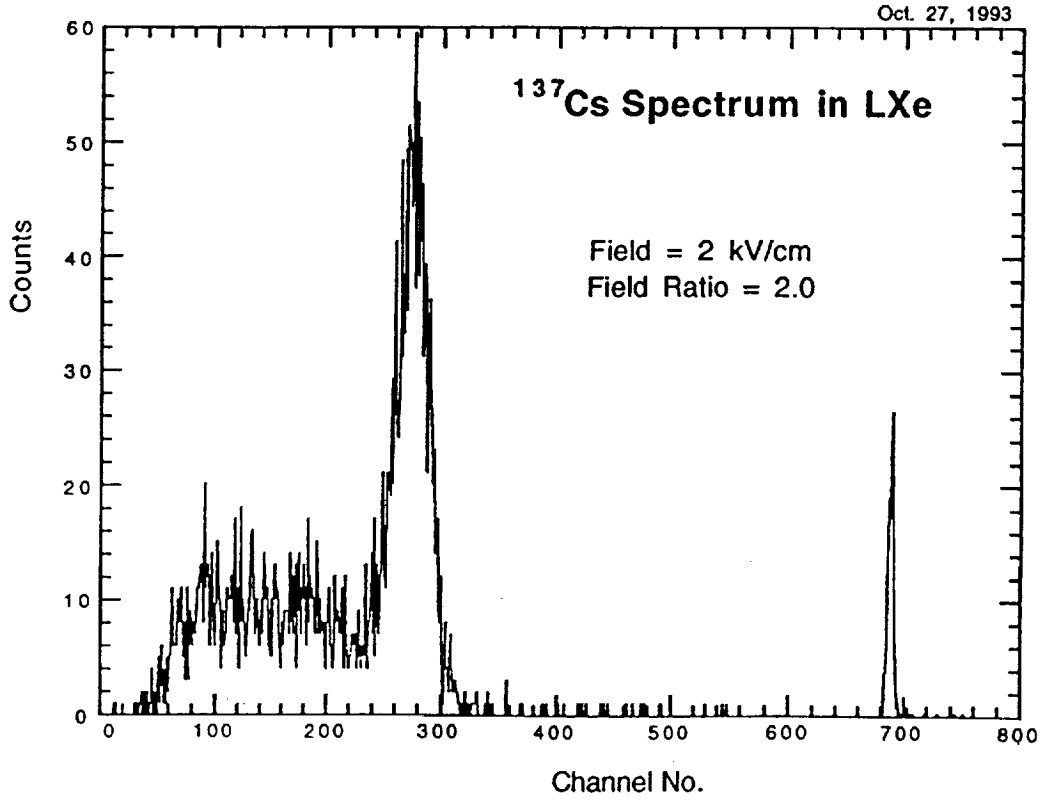
Oct. 27, 1993
^{137}Cs Spectrum in LXe
Field = 2 kV/cm
Field Ratio = 2.0
Counts
Channel No.
0
10
20
30
40
50
60
0
100
200
300
400
500
600
700
800

Fig. 5a

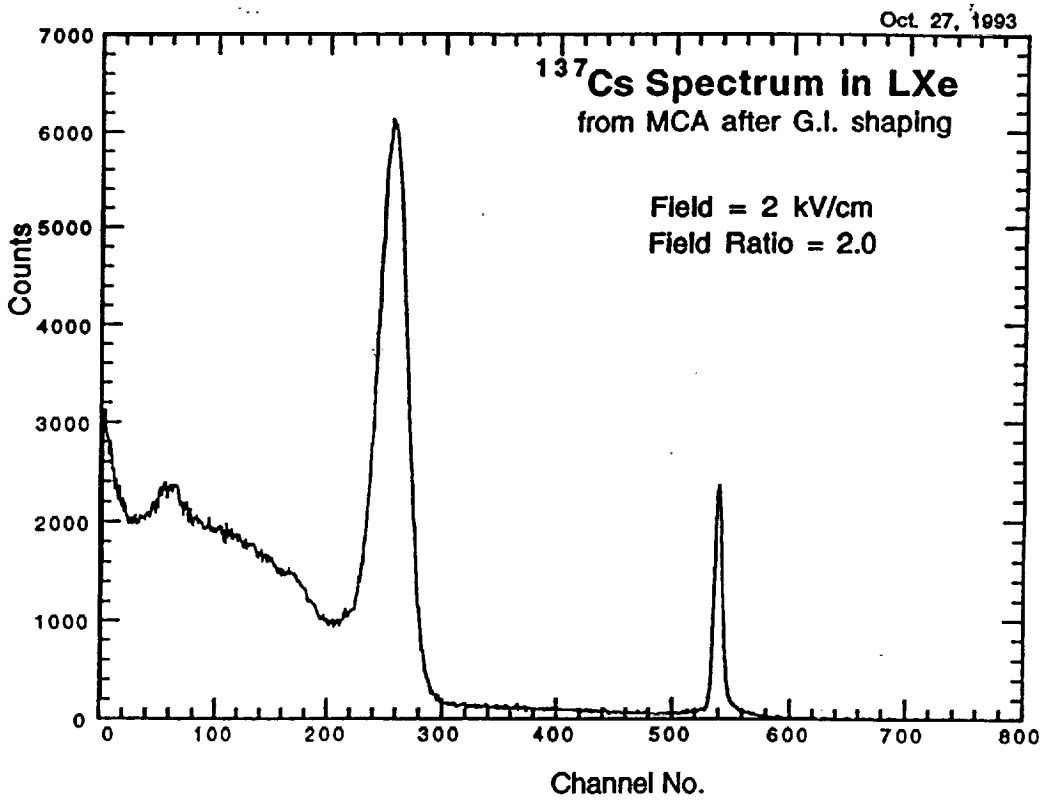
Oct. 27, 1993
^{137}Cs Spectrum in LXe
from MCA after G.I. shaping
Field = 2 kV/cm
Field Ratio = 2.0
Counts
Channel No.
0
1000
2000
3000
4000
5000
6000
7000
0
100
200
300
400
500
600
700
800

Fig. 5b

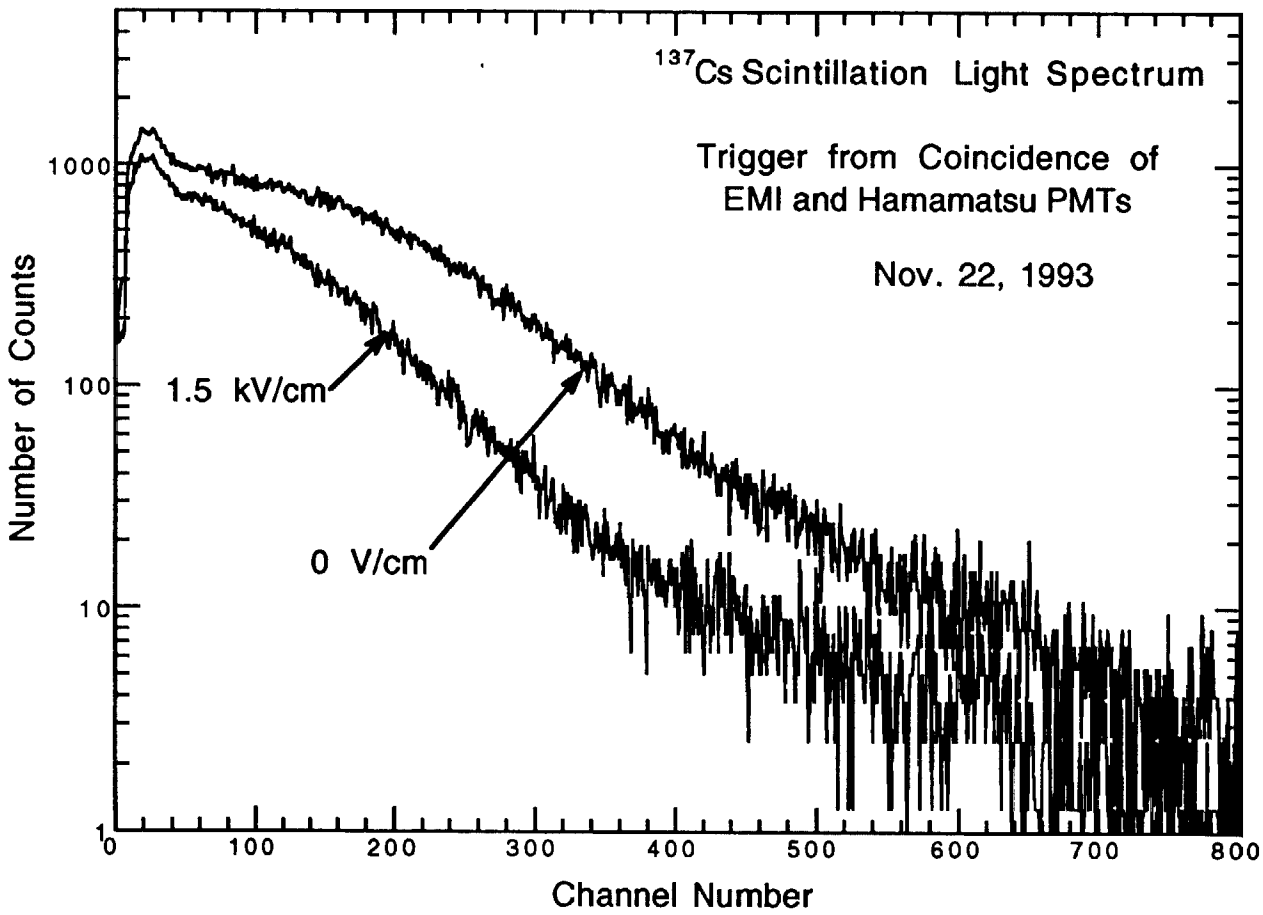
^{137}Cs Scintillation Light Spectrum
Trigger from Coincidence of
EMI and Hamamatsu PMTs
Nov. 22, 1993
1.5 kV/cm
0 V/cm
Number of Counts
Channel Number
1000
100
10
1
0
100
200
300
400
500
600
700
800

Fig. 6

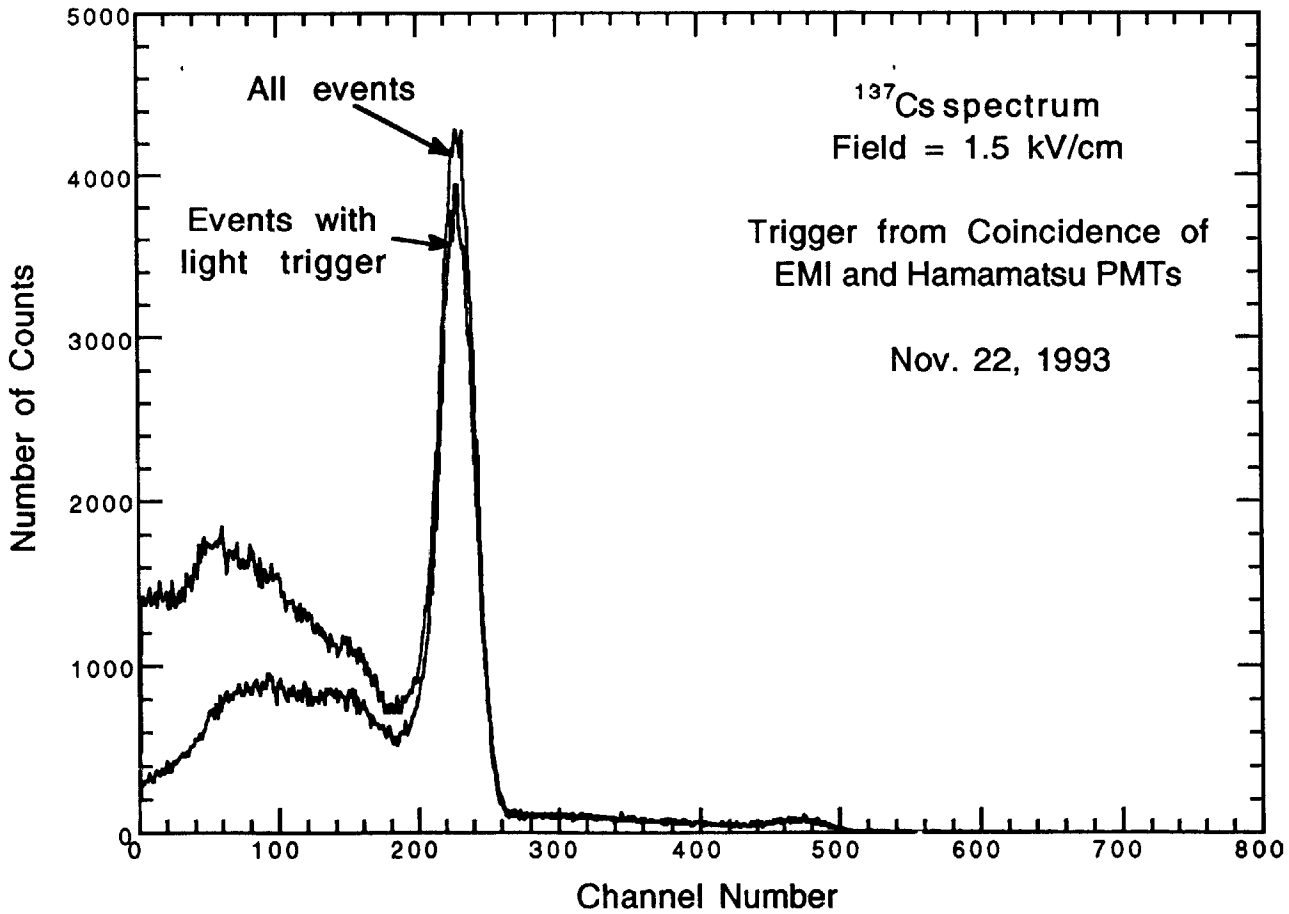
All events
Events with
light trigger
^{137}Cs spectrum
Field = 1.5 kV/cm
Trigger from Coincidence of
EMI and Hamamatsu PMTs
Nov. 22, 1993
Number of Counts
Channel Number
0
1000
2000
3000
4000
5000
0
100
200
300
400
500
600
700
800

Fig. 7

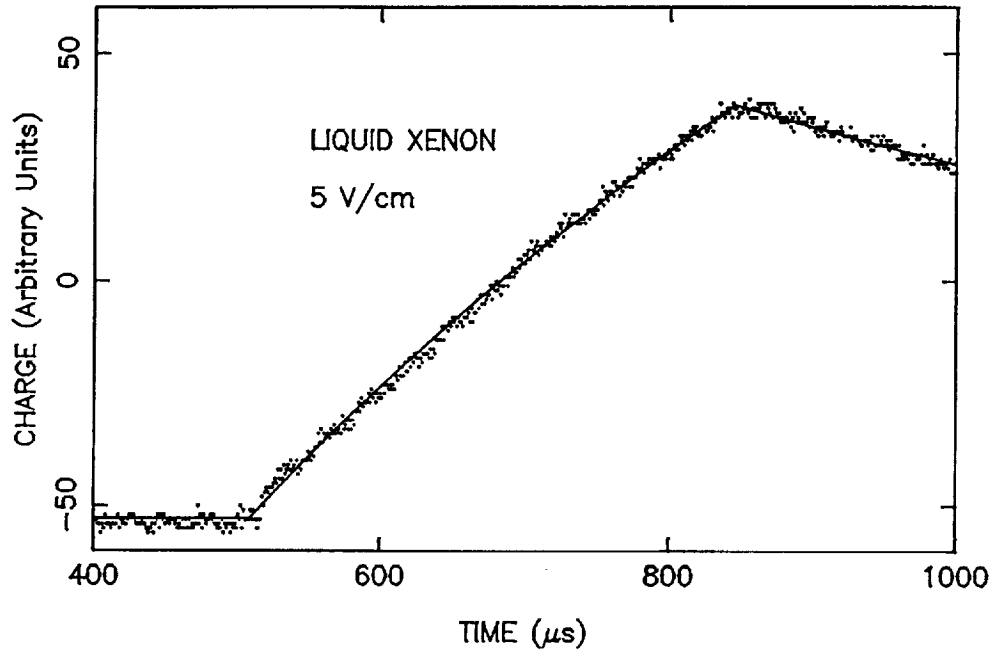
LIQUID XENON
5 V/cm
CHARGE (Arbitrary Units)
50
0
−50
400
600
800
1000
TIME (μs)

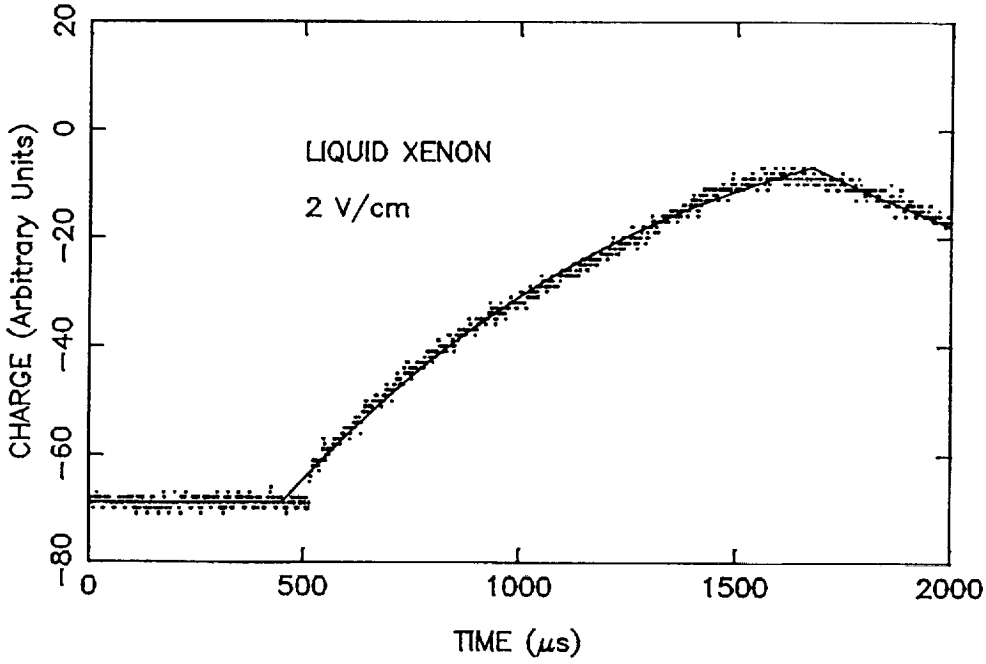
LIQUID XENON
2 V/cm
CHARGE (Arbitrary Units)
20
0
−20
−40
−60
−80
0
500
1000
1500
2000
TIME (μs)

Fig. 8

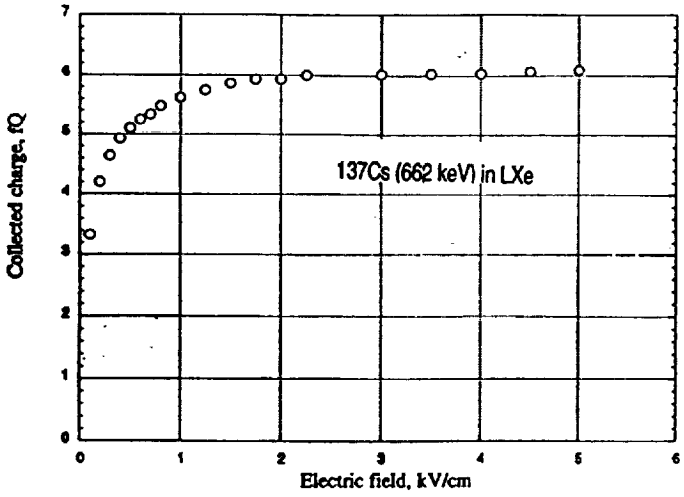

Fig. 9a

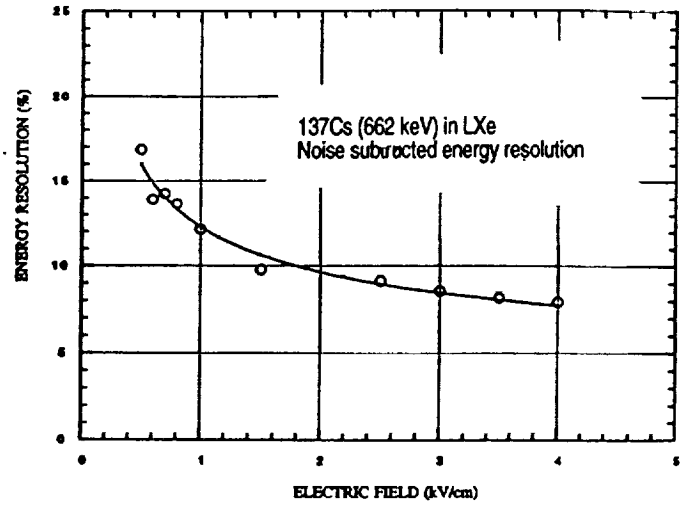

Fig. 9b

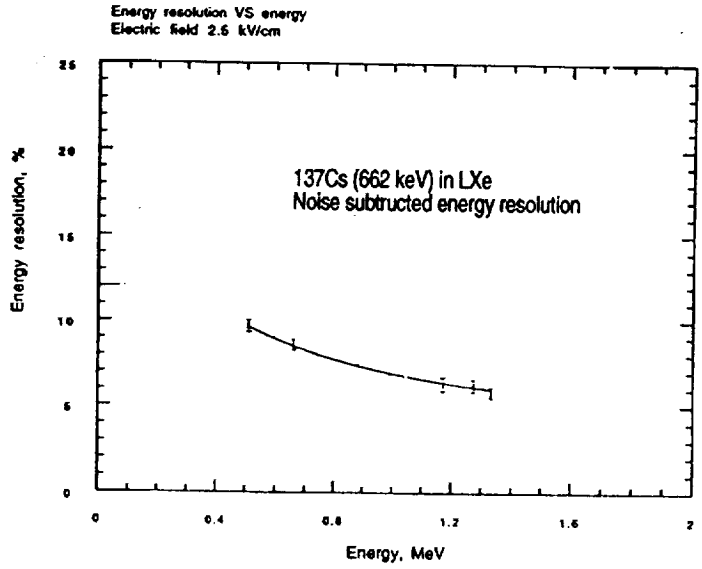

Fig. 9c

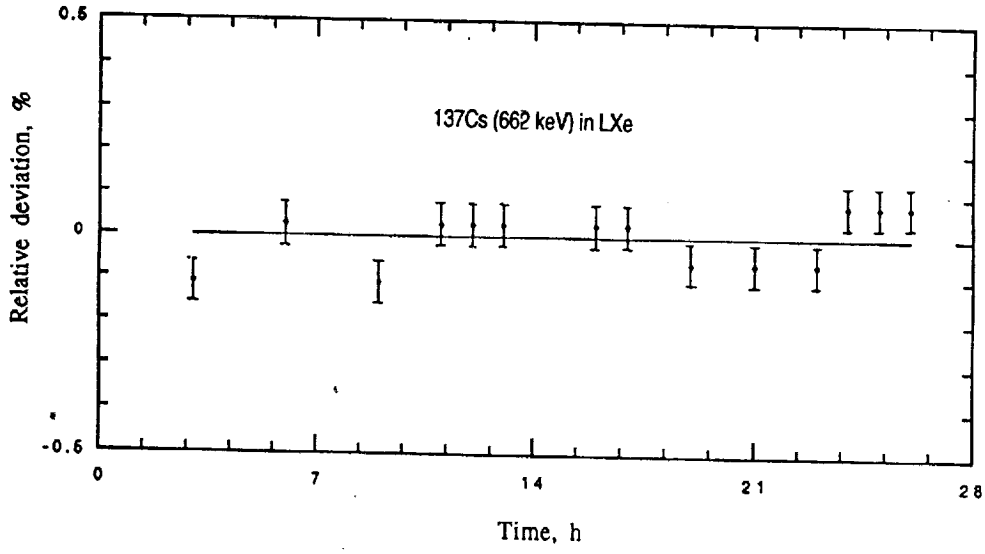

Fig. 9d

Spectroscopy of a 3.5 liter LXe Chamber

with 5 cm Drift Gap

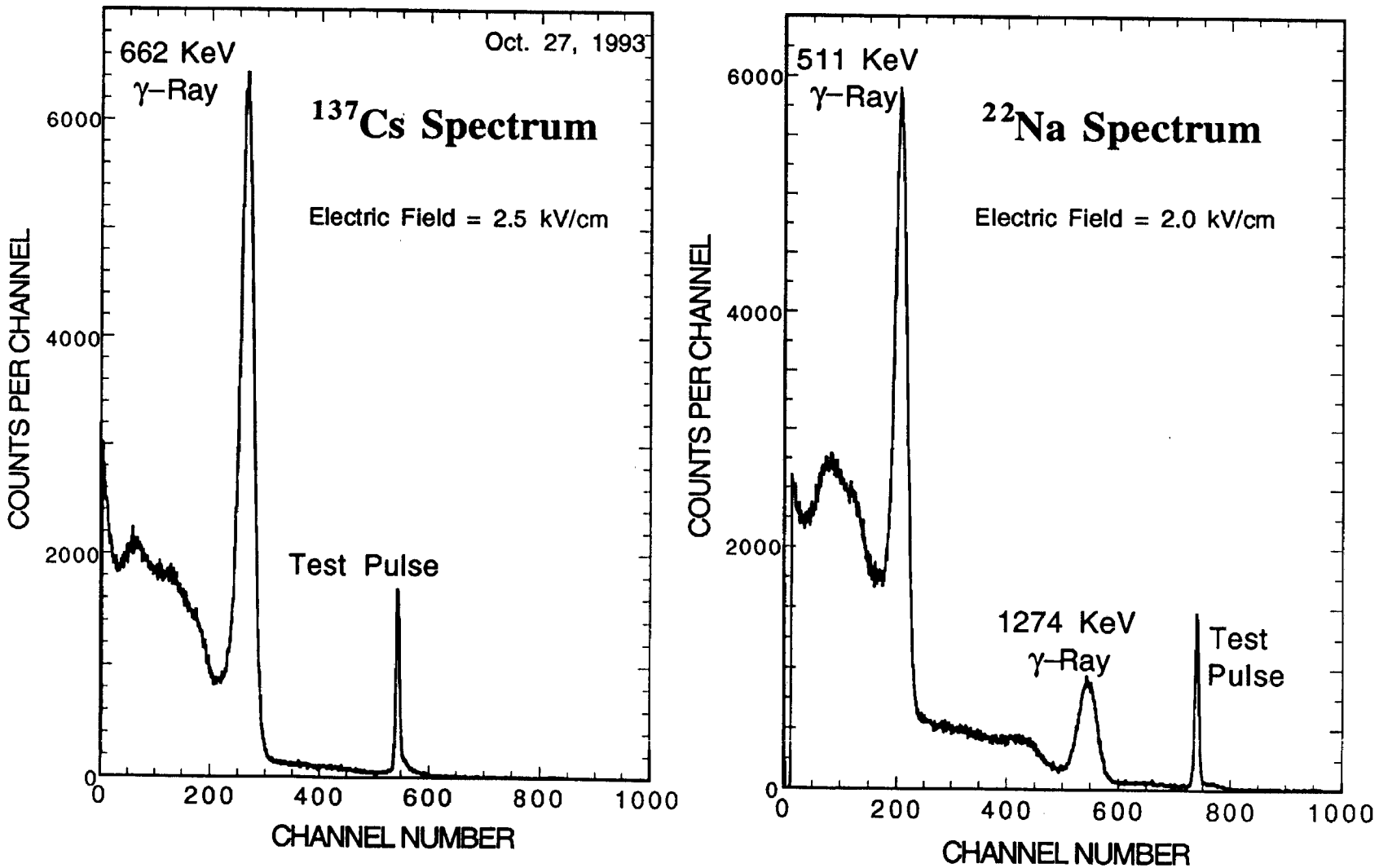

Fig. 10

γ-ray Imaging

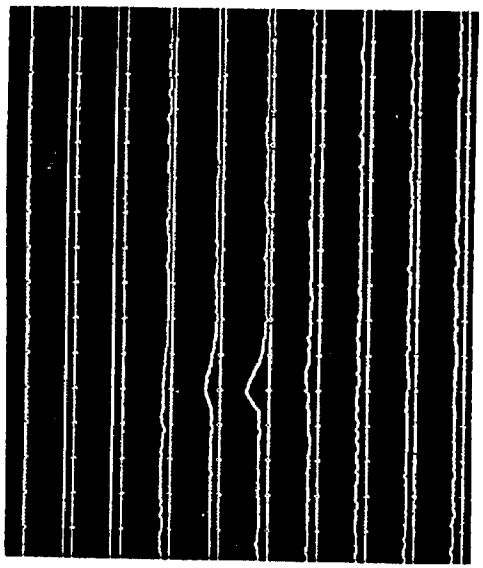

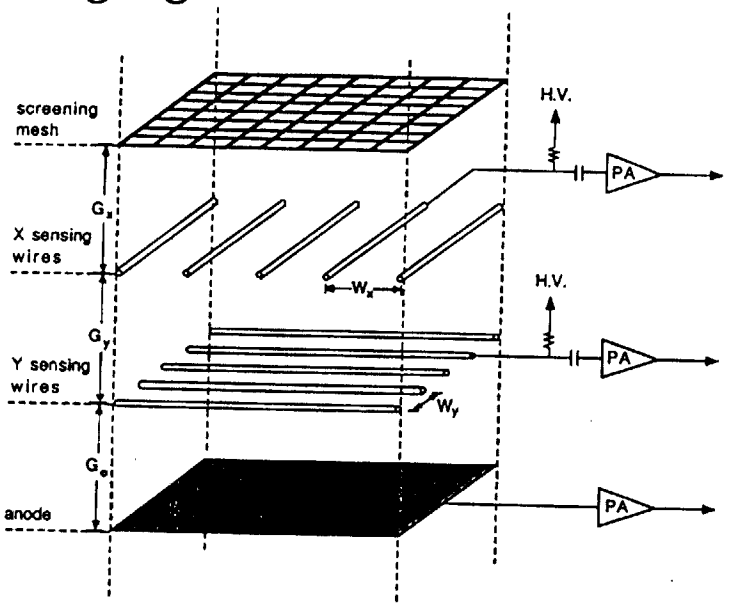

X-Y Spatial Information

Calorimetry

Fig. 11a

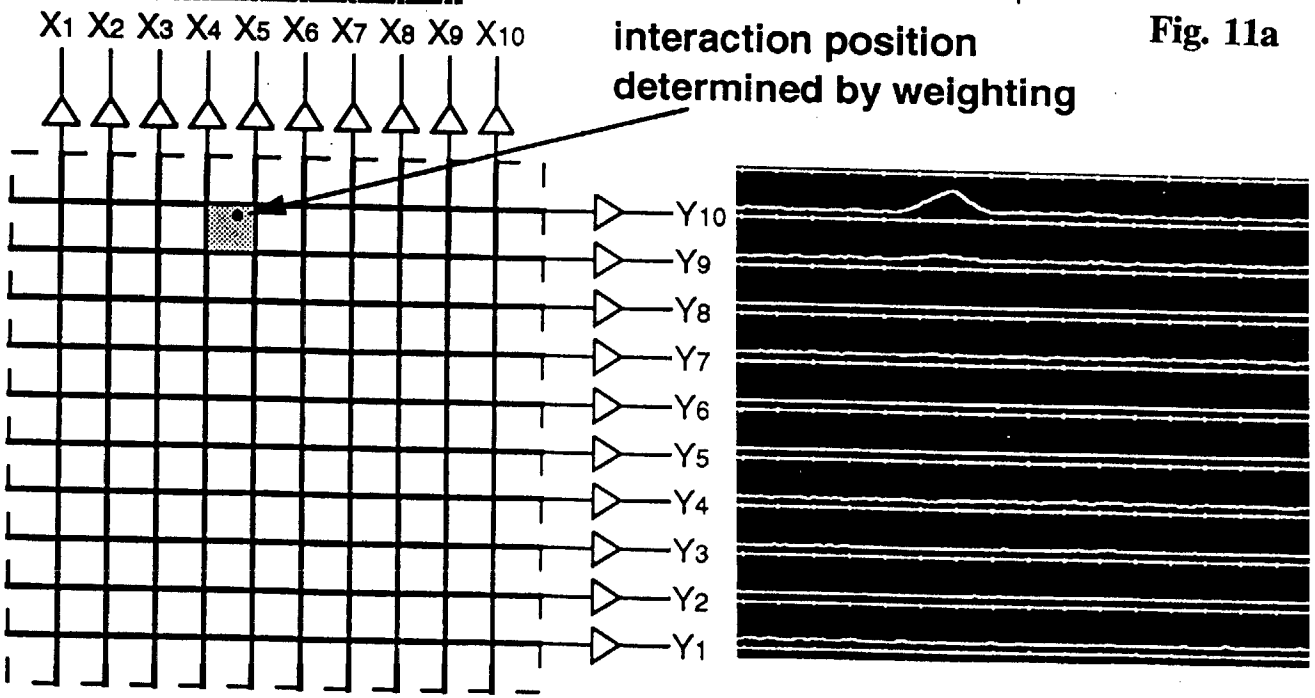

Fig. 11b

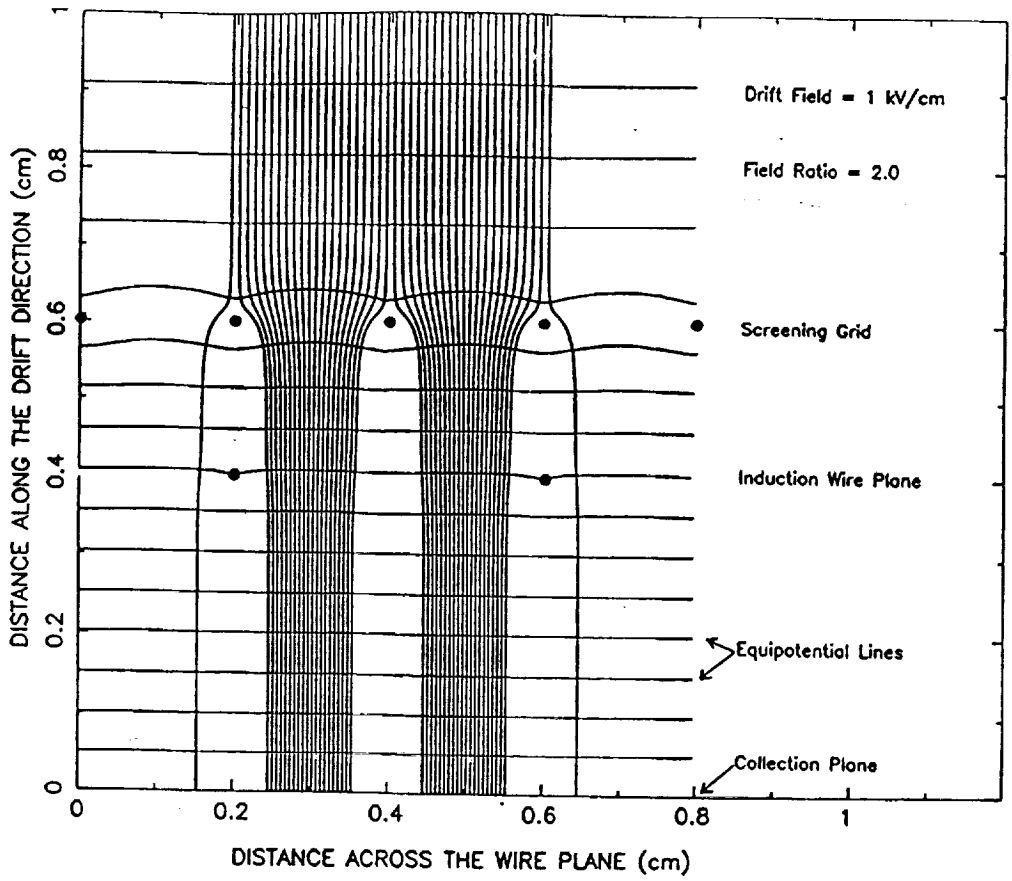
Drift Field = 1 kV/cm
Field Ratio = 2.0
Screening Grid
Induction Wire Plane
Equipotential Lines
Collection Plane
DISTANCE ALONG THE DRIFT DIRECTION (cm)
DISTANCE ACROSS THE WIRE PLANE (cm)
0
0.2
0.4
0.6
0.8
1

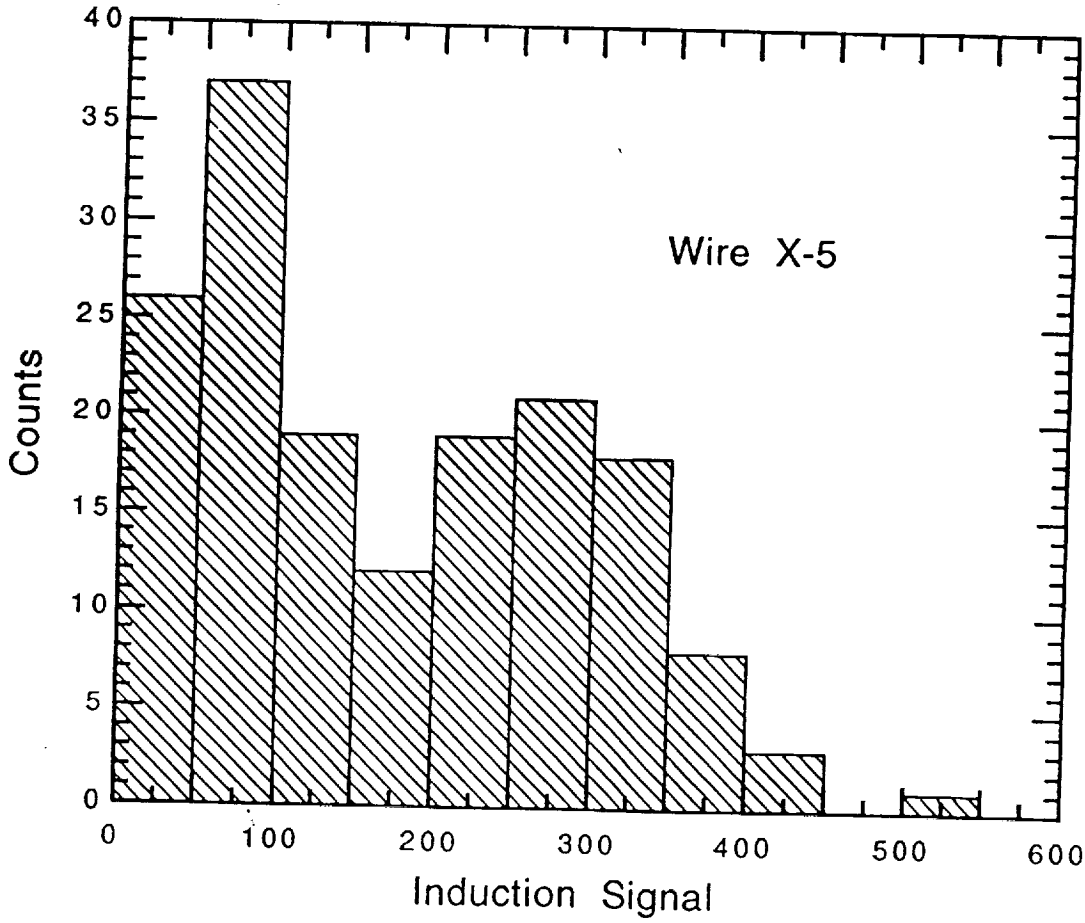
Wire X-5
Counts
Induction Signal
0
5
10
15
20
25
30
35
40
100
200
300
400
500
600

Fig. 12

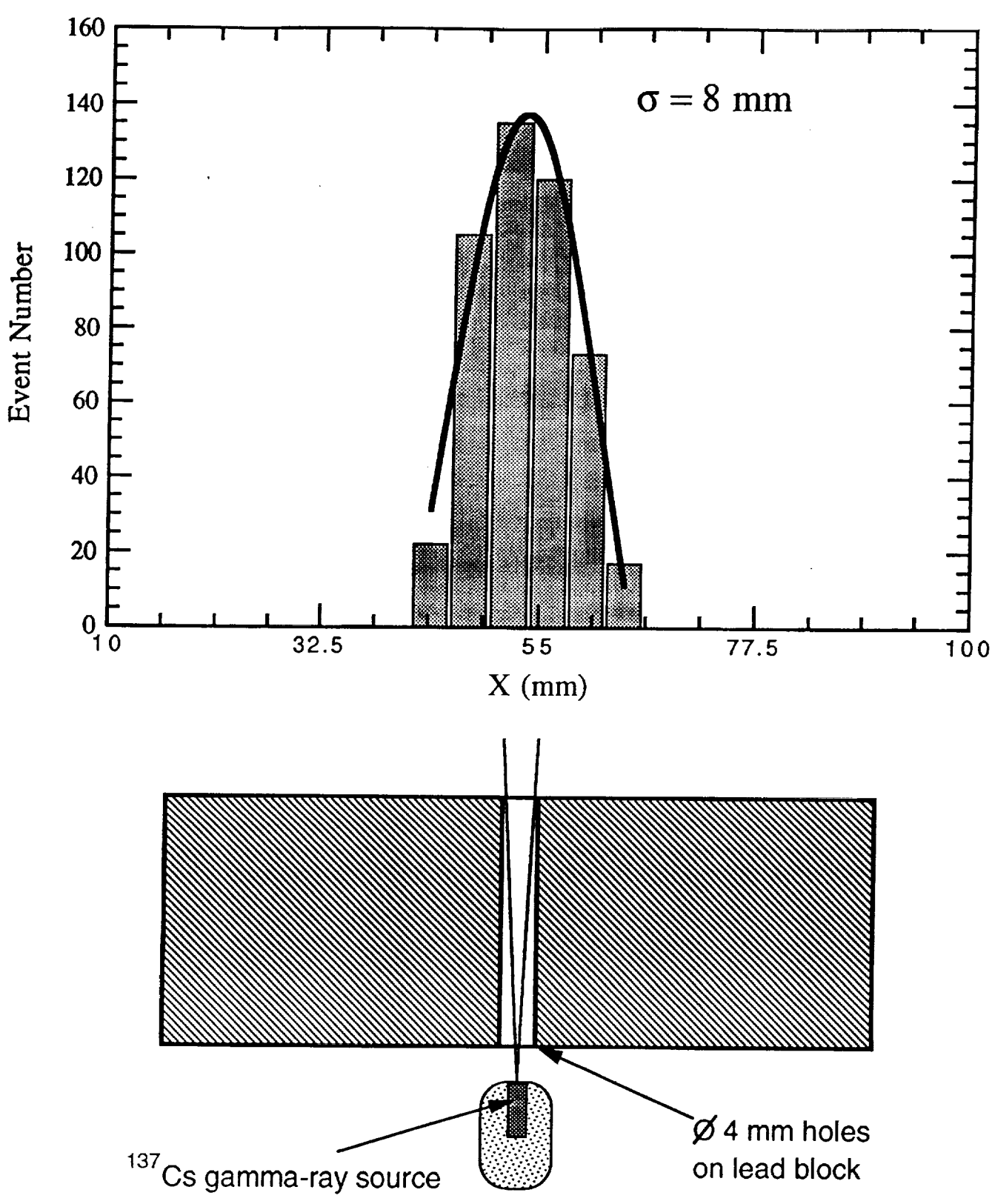
1-D Image of Collimated Gamma-ray Beam
σ = 8 mm
Event Number
X (mm)
160
140
120
100
80
60
40
20
0
10
32.5
55
77.5
100
137Cs gamma-ray source
Ø 4 mm holes
on lead block

Fig. 13

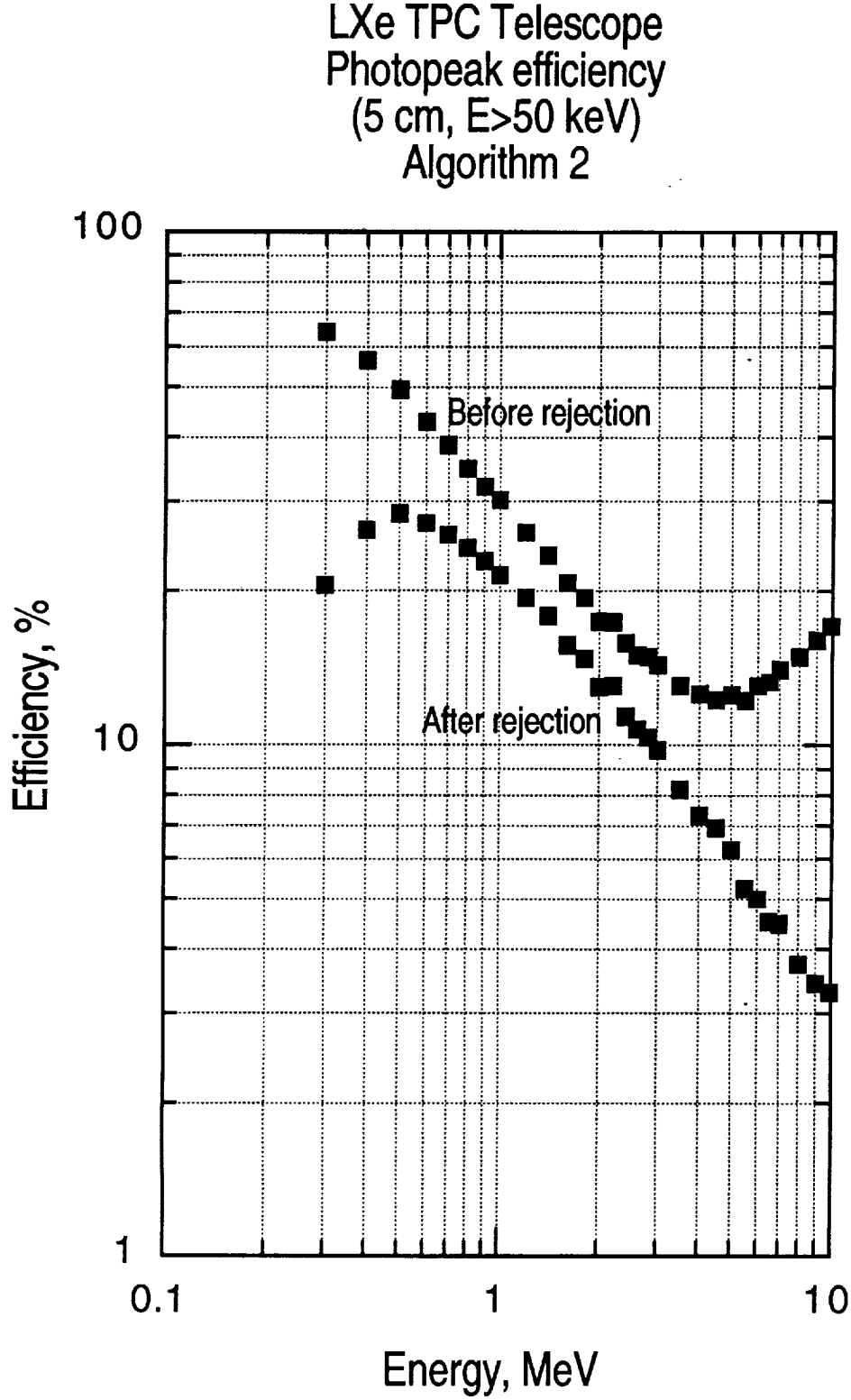
LXe TPC Telescope
Photopeak efficiency
(5 cm, E>50 keV)
Algorithm 2
100
10
1
Efficiency, %
Before rejection
After rejection
0.1
1
10
Energy, MeV

Fig. 14

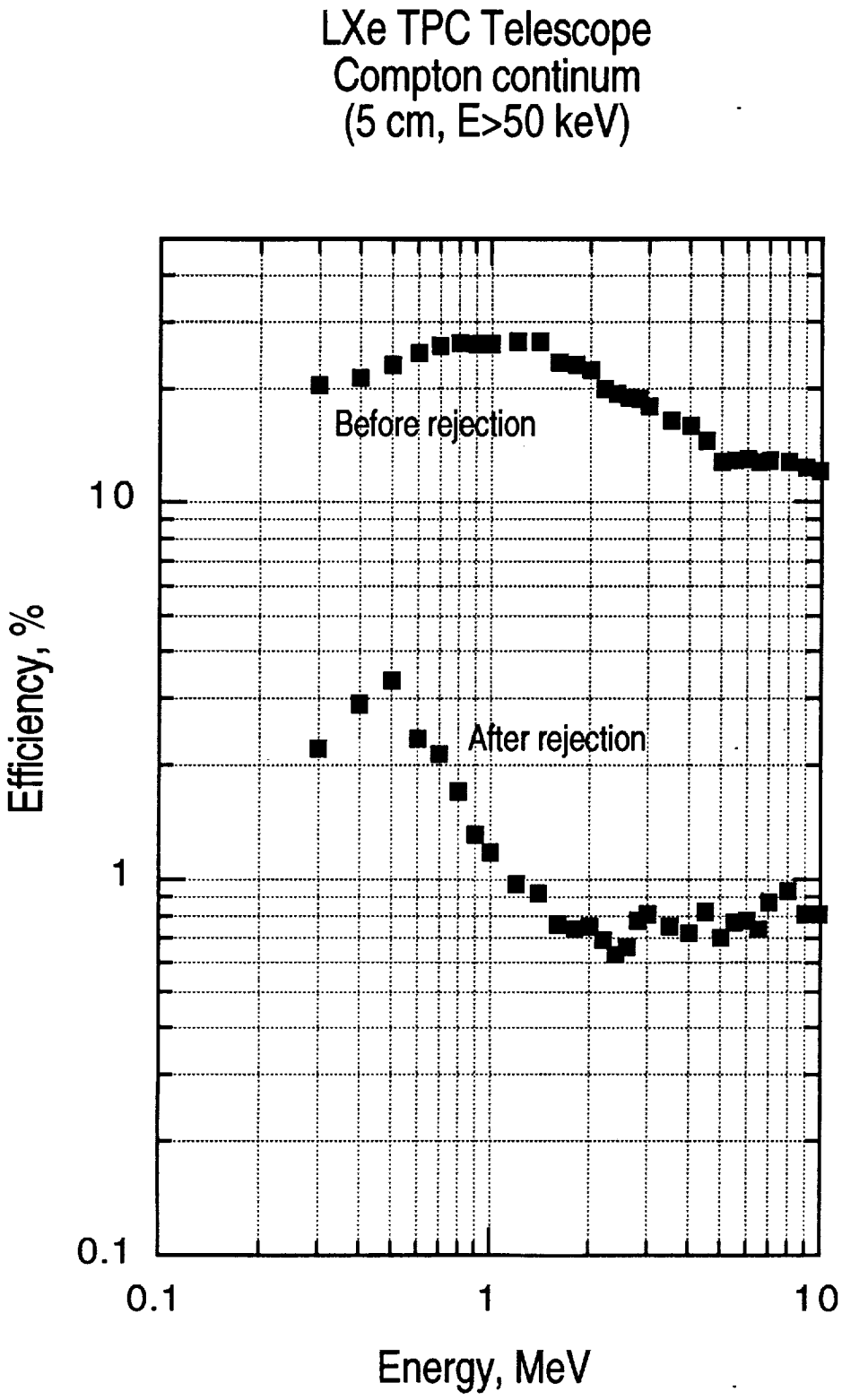
LXe TPC Telescope
Compton continum
(5 cm, E>50 keV)
Before rejection
After rejection
Efficiency, %
10
1
0.1
0.1
1
10
Energy, MeV

Fig. 15

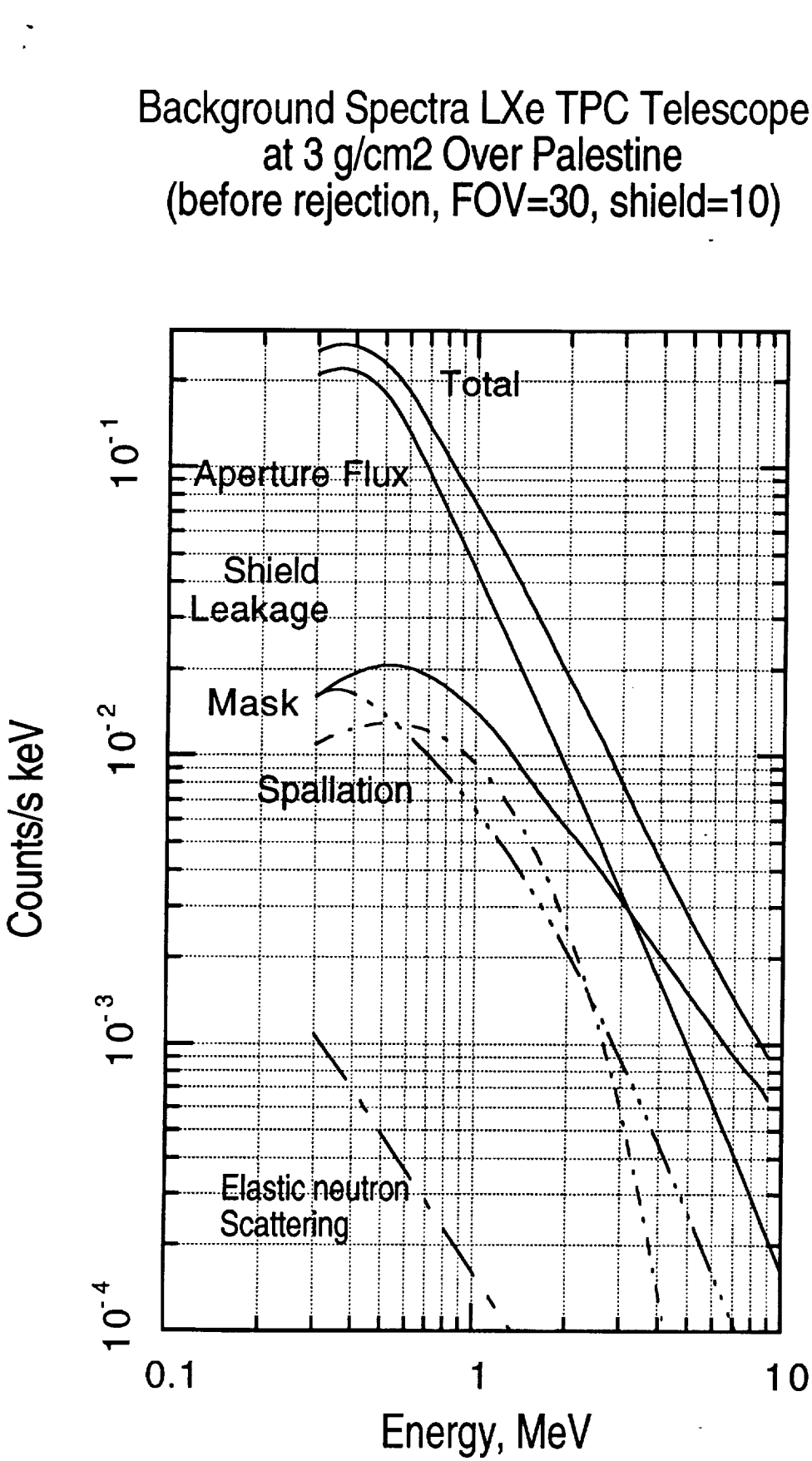
Background Spectra LXe TPC Telescope
at 3 g/cm2 Over Palestine
(before rejection, FOV=30, shield=10)
Total
Aperture Flux
Shield
Leakage
Mask
Spallation
Elastic neutron
Scattering
Counts/s keV
10^-1
10^-2
10^-3
10^-4
0.1
1
10
Energy, MeV

Fig. 16

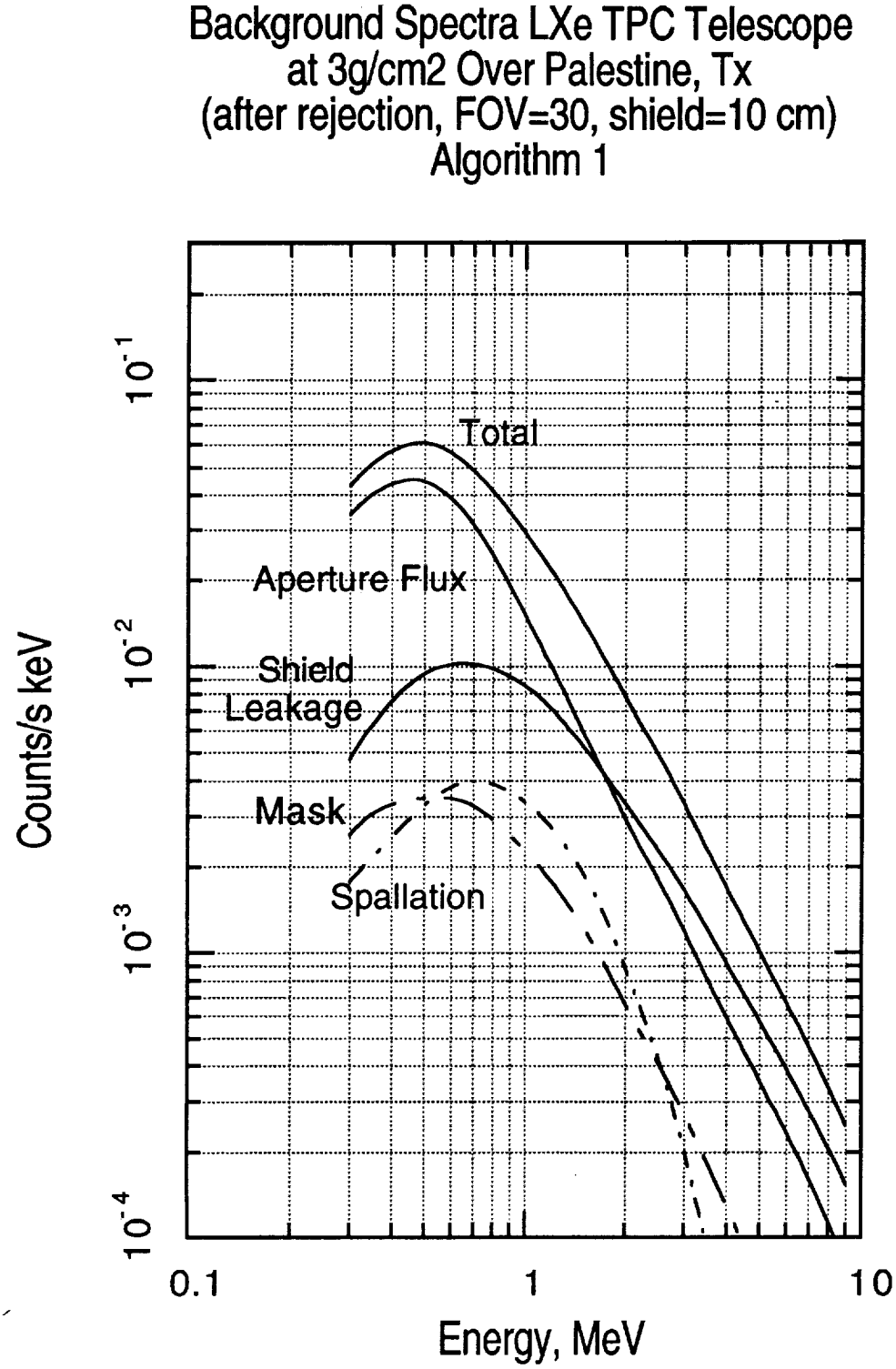
Background Spectra LXe TPC Telescope
at 3g/cm2 Over Palestine, Tx
(after rejection, FOV=30, shield=10 cm)
Algorithm 1
Total
Aperture Flux
Shield
Leakage
Mask
Spallation
Counts/s keV
10^-1
10^-2
10^-3
10^-4
0.1
1
10
Energy, MeV

Fig. 17

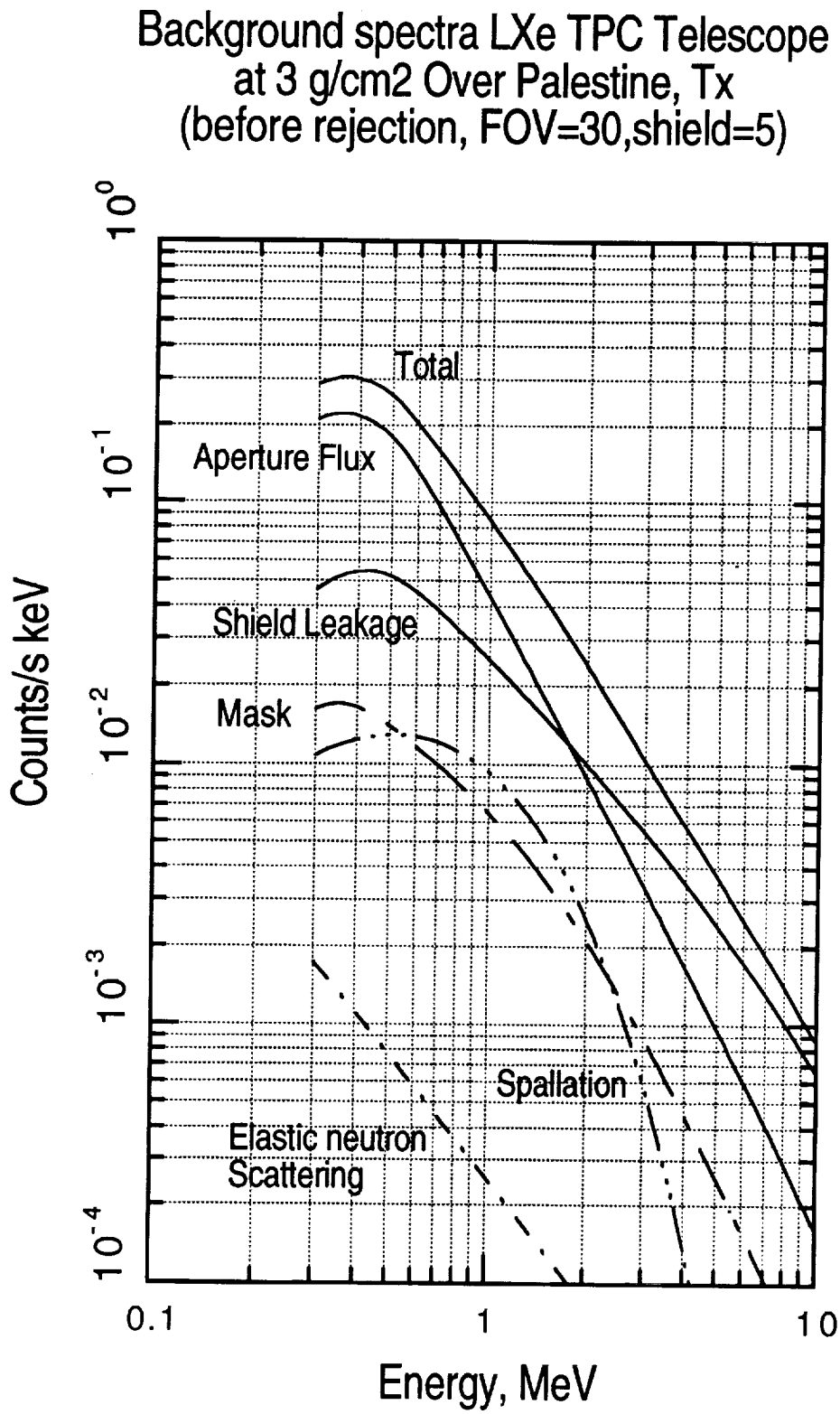
Background spectra LXe TPC Telescope
at 3 g/cm2 Over Palestine, Tx
(before rejection, FOV=30,shield=5)
Counts/s keV
Energy, MeV
Total
Aperture Flux
Shield Leakage
Mask
Spallation
Elastic neutron
Scattering
10^0
10^-1
10^-2
10^-3
10^-4
0.1
1
10

Fig. 18

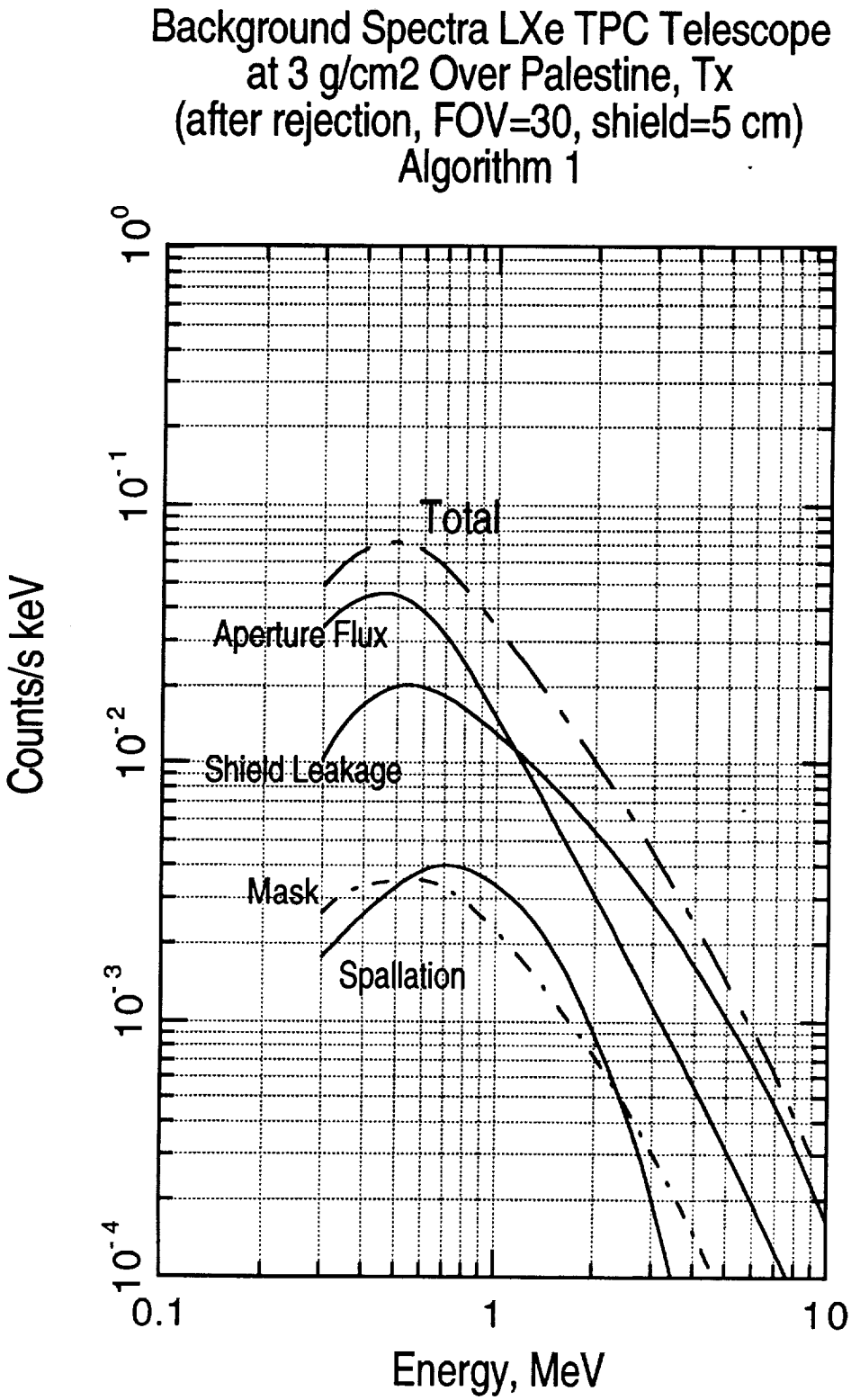
Background Spectra LXe TPC Telescope
at 3 g/cm2 Over Palestine, Tx
(after rejection, FOV=30, shield=5 cm)
Algorithm 1
Counts/s keV
Energy, MeV
Total
Aperture Flux
Shield Leakage
Mask
Spallation
10^0
10^-1
10^-2
10^-3
10^-4
0.1
1
10

Fig. 19

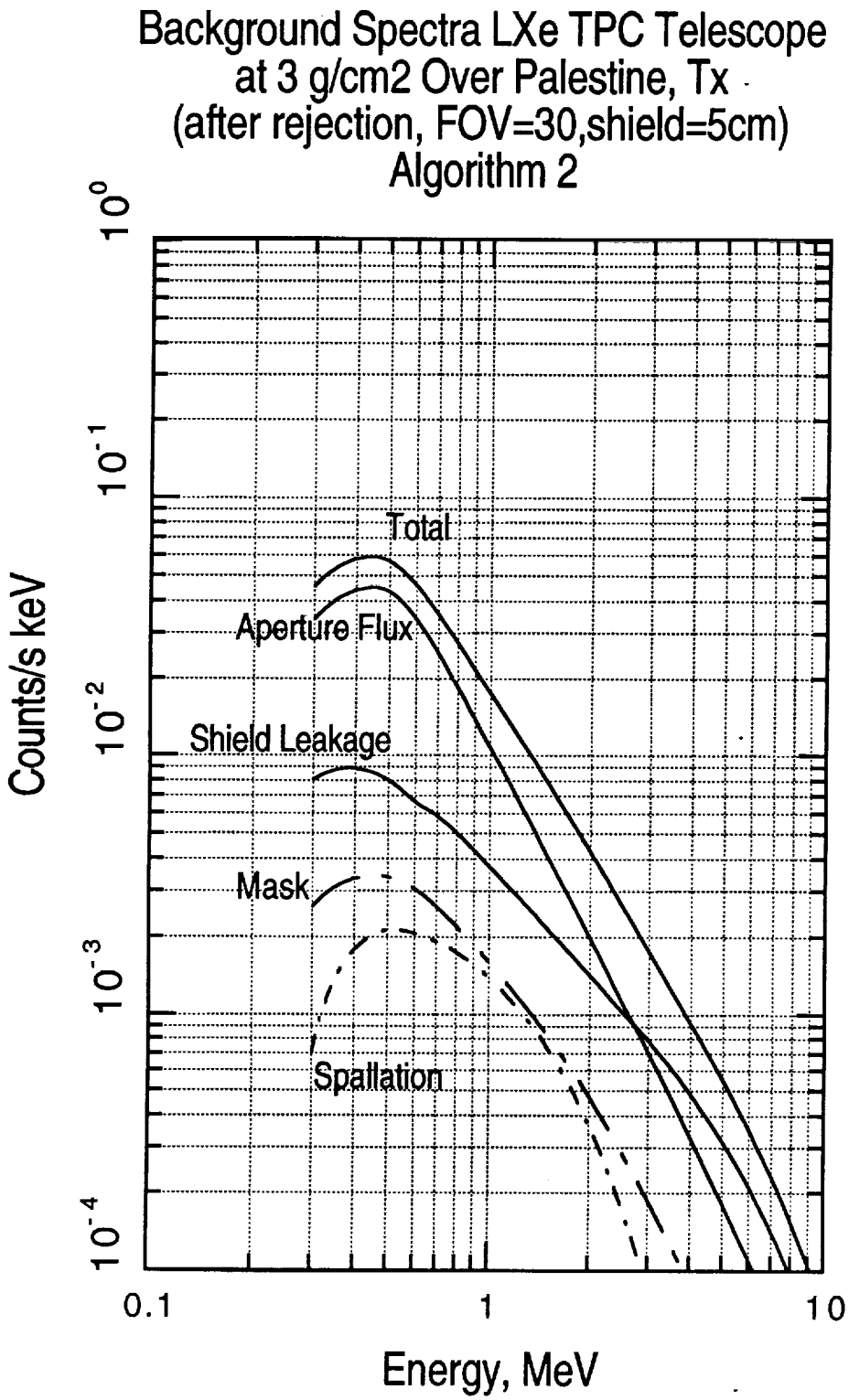
Background Spectra LXe TPC Telescope
at 3 g/cm2 Over Palestine, Tx
(after rejection, FOV=30,shield=5cm)
Algorithm 2
Counts/s keV
Energy, MeV
Total
Aperture Flux
Shield Leakage
Mask
Spallation
10^{0}
10^{-1}
10^{-2}
10^{-3}
10^{-4}
0.1
1
10

Fig. 20

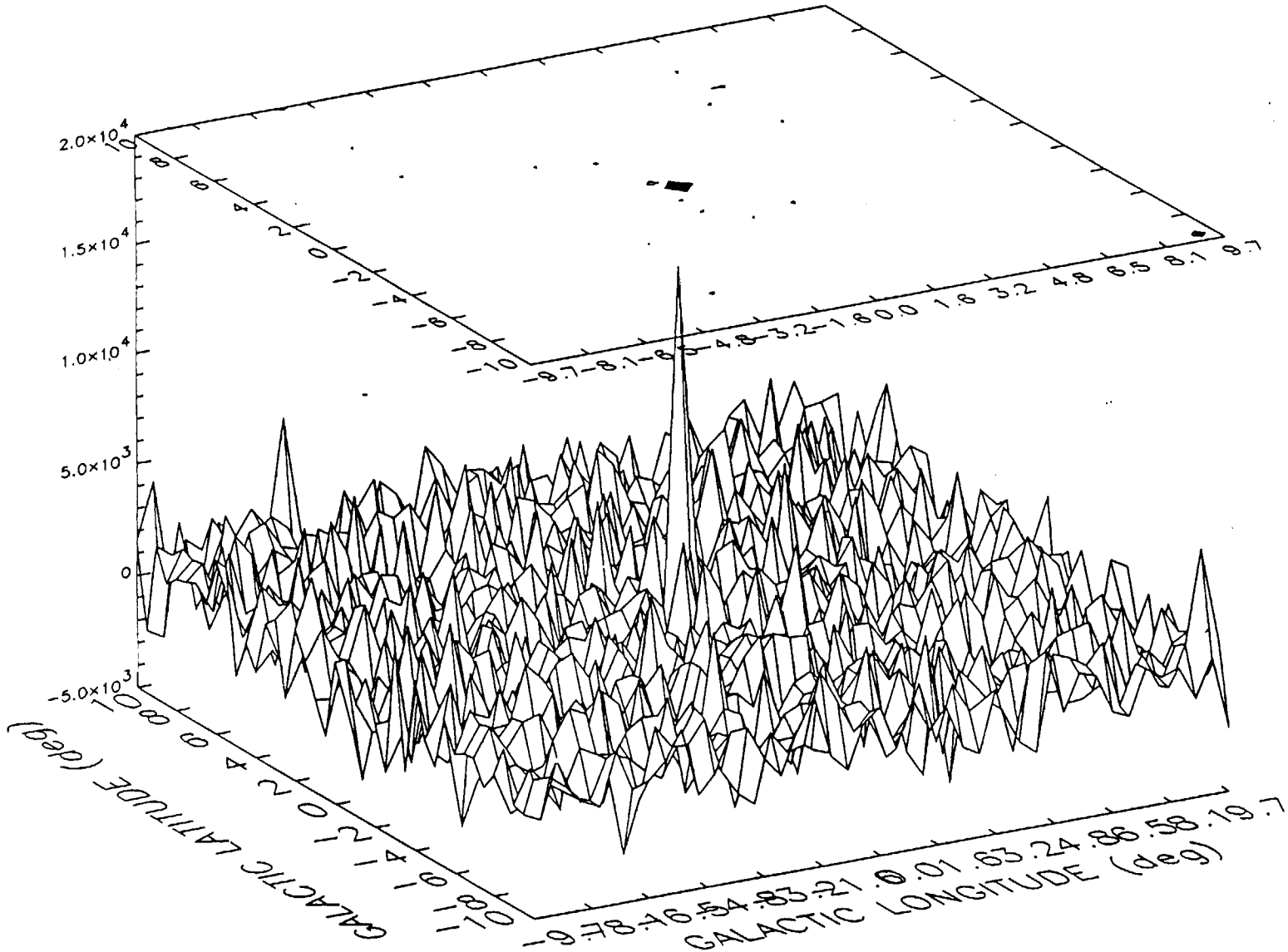
2.0×10^4
1.5×10^4
1.0×10^4
5.0×10^3
0
-5.0×10^3
GALACTIC LATITUDE (deg)
GALACTIC LONGITUDE (deg)

Fig. 21

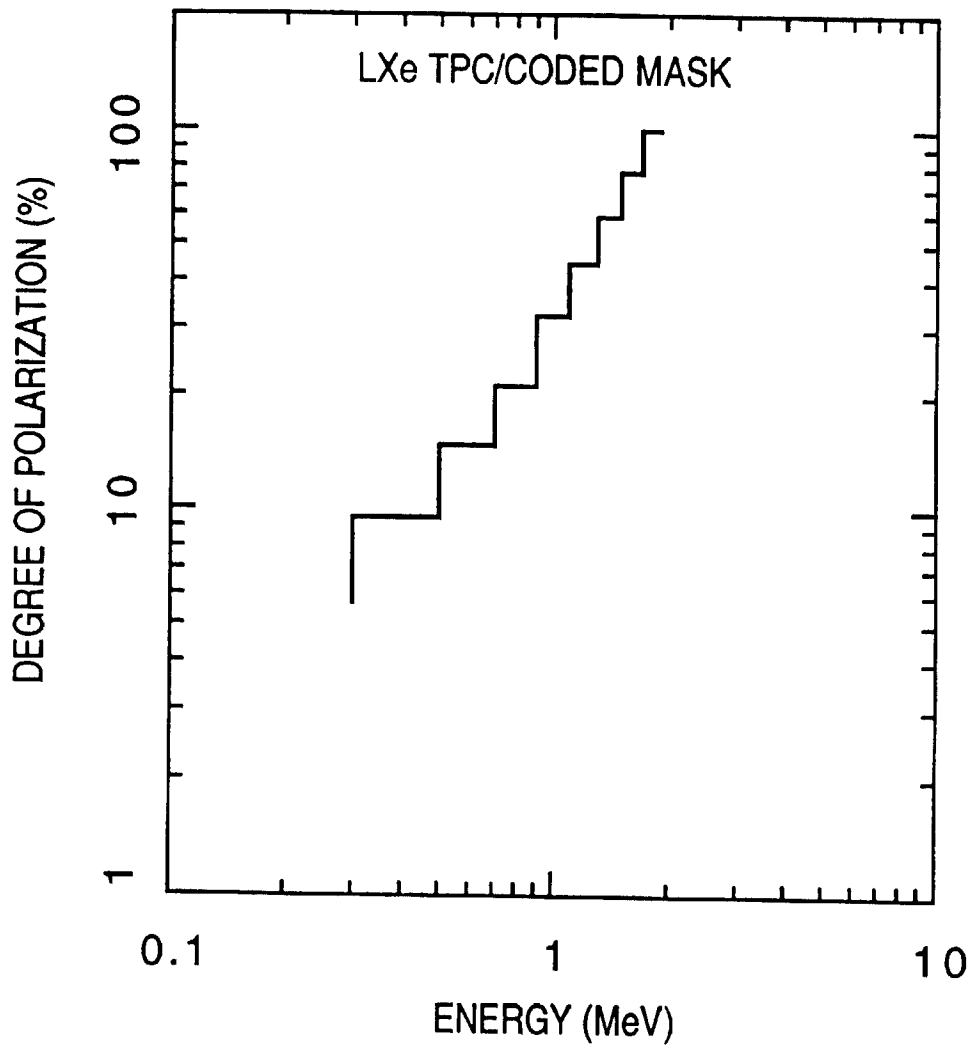
LXe TPC/CODED MASK
DEGREE OF POLARIZATION (%)
100
10
1
0.1
1
10
ENERGY (MeV)

Fig. 22

10Liter LXe-TPC

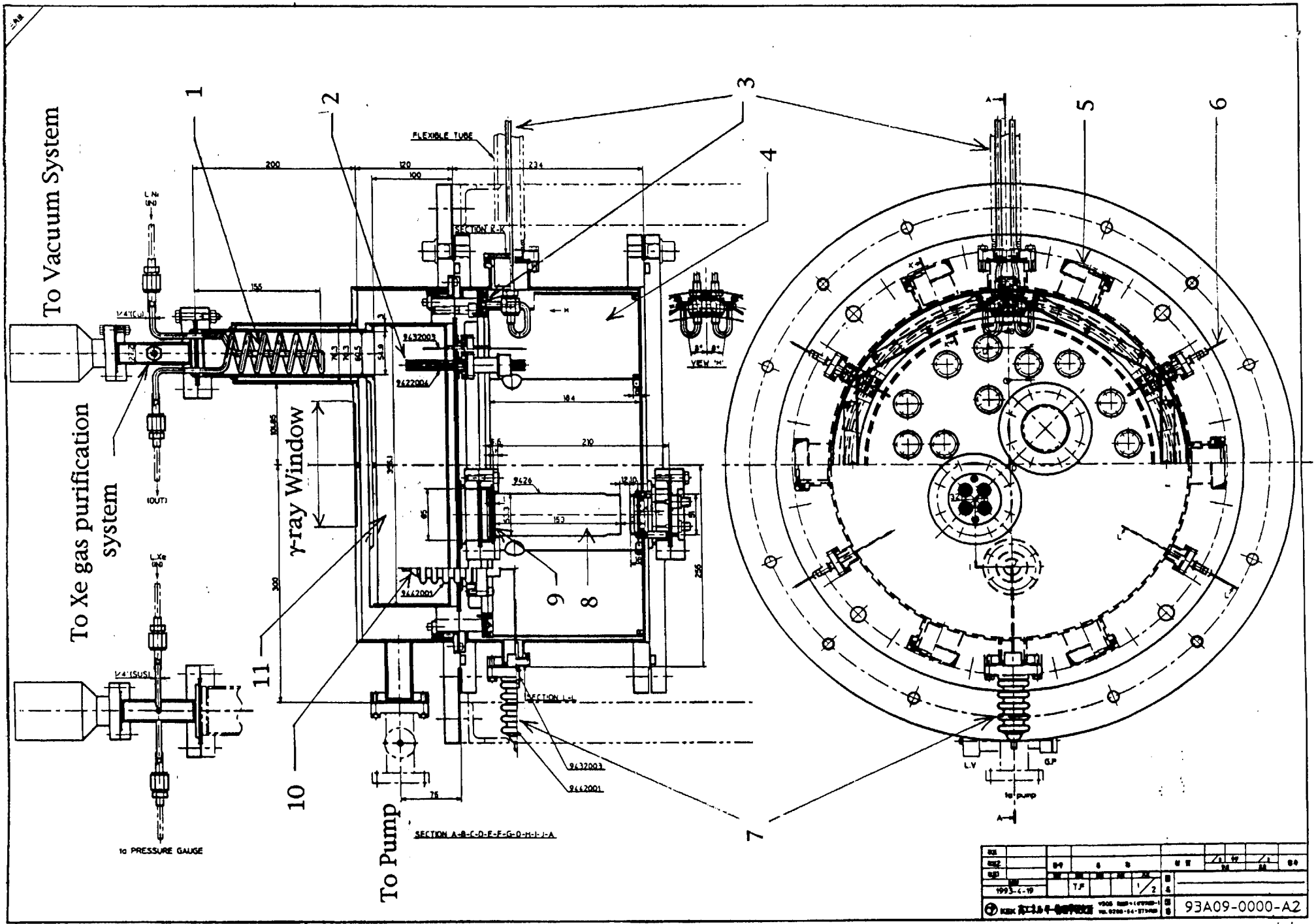

Fig. 23

Legend for Figure 23

1. LN_2 Heat Exchanger (for condensation of Xe-gas)
2. Signal/high voltage feedthroughs
3. Liquid N_2 (for cooling preamplifers)
4. Cryostat (vacuum+Mylar, preamplifiers and PMTs)
5. Burndy connector for signal outputs
6. High voltage feedthrough
7. High voltage feedthrough
8. UV-sensitive photomultiplier
9. Quartz UV window
10. High voltage feedthrough
11. Liquid Xe chamber vessel

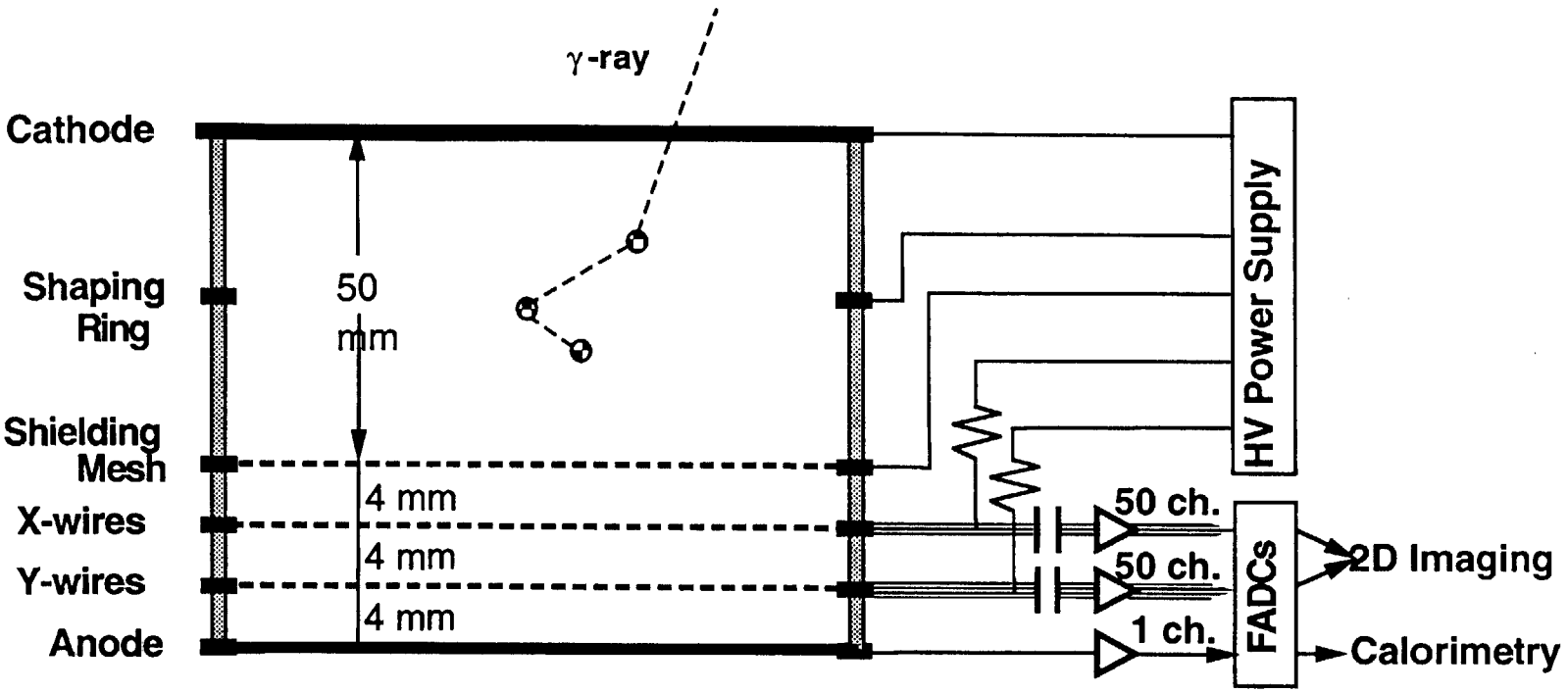

Schematic of the 10L LXe-TPC Electrode Structure

Fig. 24

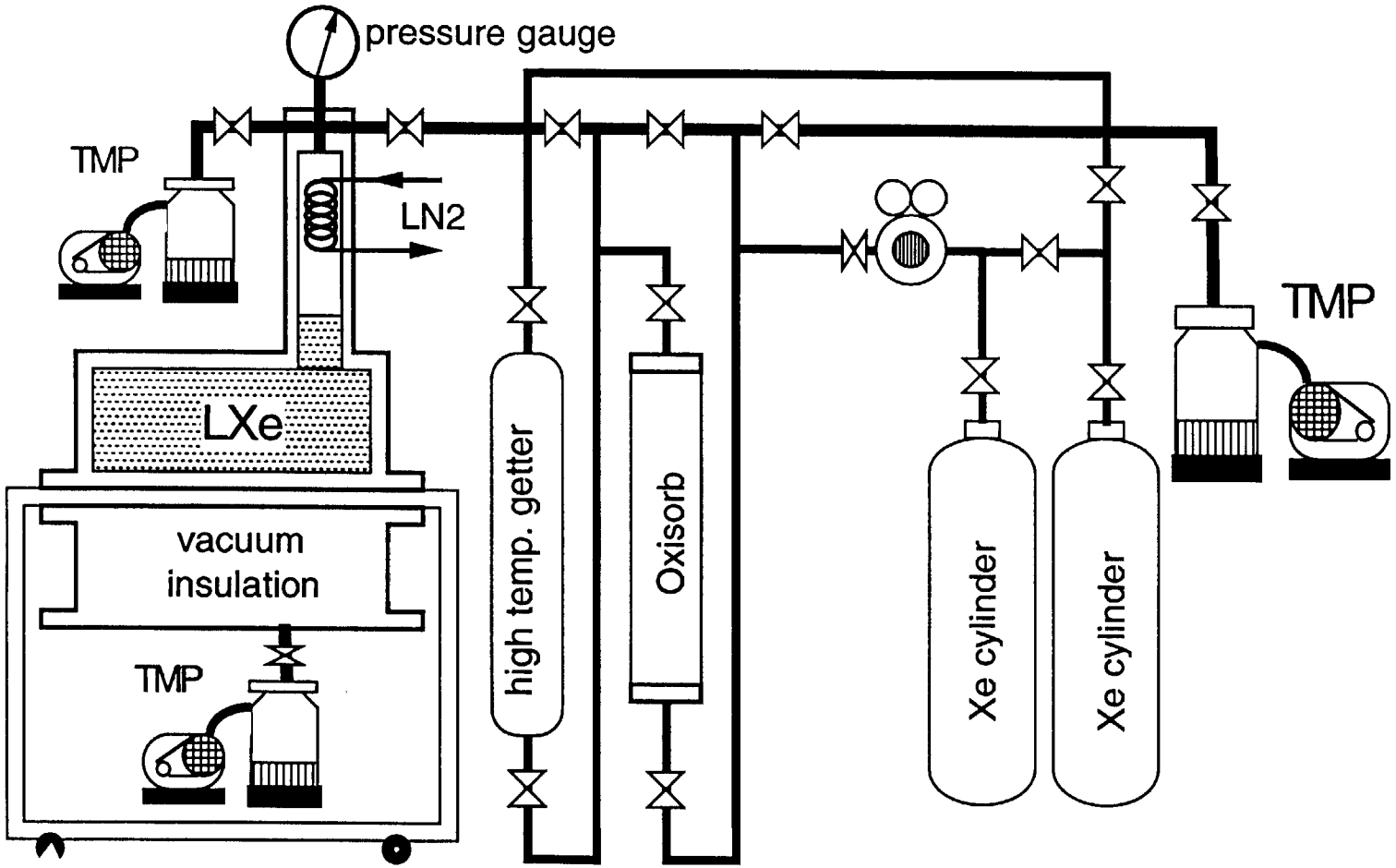

Schematic of the Xe gas purification system

Fig. 25

Data Acquisition Electronics for 10 Liter LXe-TPC

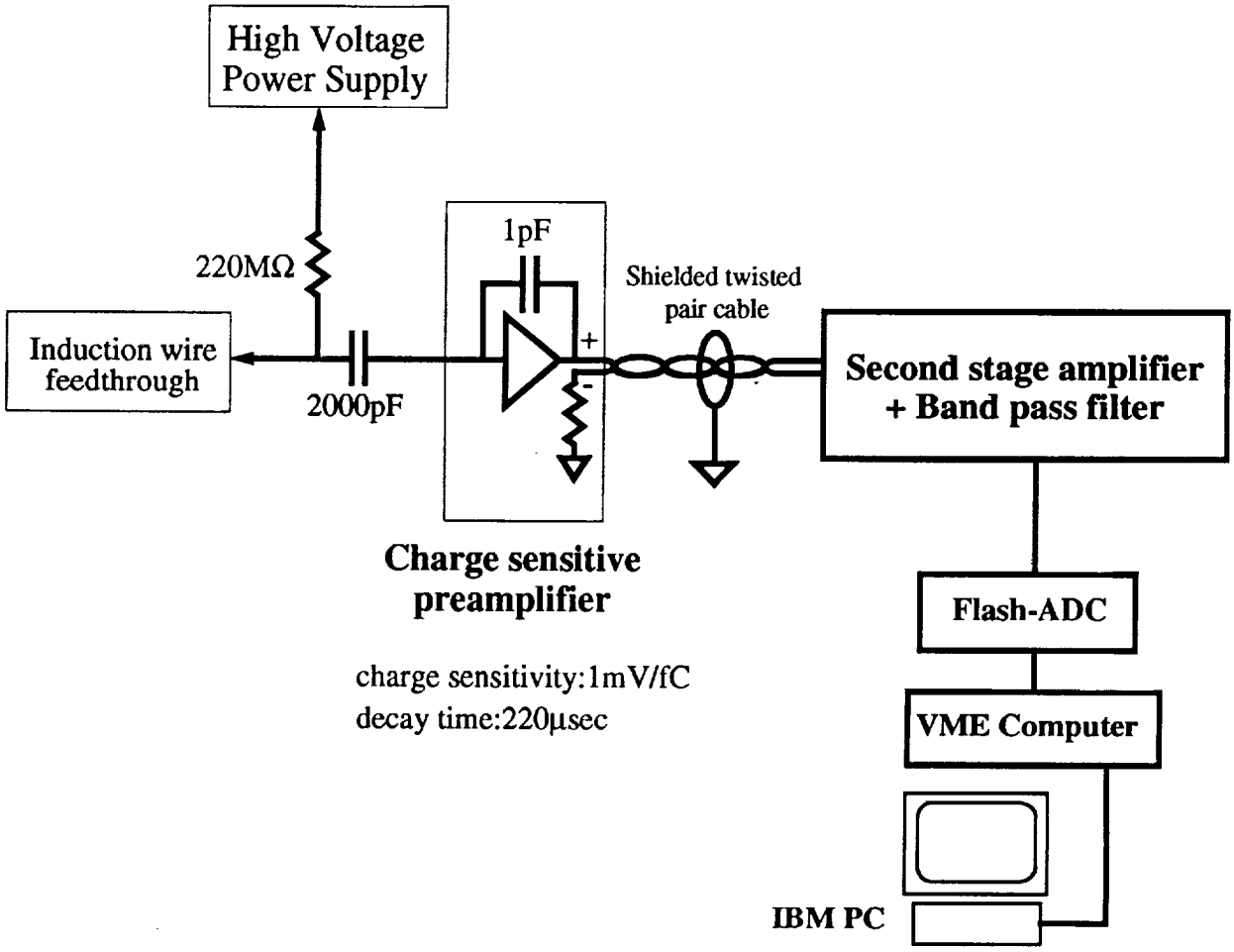

Fig. 26

NORTH-HOLLAND
PHYSICS
PUBLISHING

APPENDIX 1

A Monte Carlo analysis of the liquid xenon TPC as gamma-ray telescope

E. Aprile, A. Bolotnikov, D. Chen and R. Mukherjee

Physics Department and Columbia Astrophysics Laboratory, Columbia University, New York, NY 10027, USA

Extensive Monte Carlo modeling of a coded aperture γ-ray telescope based on a high resolution liquid xenon TPC has been performed. Results on efficiency, background reduction capability and source flux sensitivity are presented. We discuss in particular the development of a reconstruction algorithm for events with multiple interaction points. From the energy and spatial information, the kinematics of Compton scattering is used to identify and reduce background events, as well as to improve the detector response in the few MeV region. Assuming a spatial resolution of 1 mm RMS and an energy resolution of 4.5% FWHM at 1 MeV, the algorithm is capable of reducing the background rate expected at balloon altitude by an order of magnitude, thus significantly improving the telescope sensitivity.

Reprinted from NUCLEAR INSTRUMENTS AND METHODS
IN PHYSICS RESEARCH A

Nuclear Instruments and Methods in Physics Research A327 (1993) 216–221
North-Holland

NUCLEAR
INSTRUMENTS
& METHODS
IN PHYSICS
RESEARCH
Section A

A Monte Carlo analysis of the liquid xenon TPC as gamma-ray telescope

E. Aprile, A. Bolotnikov, D. Chen and R. Mukherjee
Physics Department and Columbia Astrophysics Laboratory, Columbia University, New York, NY 10027, USA

Extensive Monte Carlo modeling of a coded aperture γ-ray telescope based on a high resolution liquid xenon TPC has been performed. Results on efficiency, background reduction capability and source flux sensitivity are presented. We discuss in particular the development of a reconstruction algorithm for events with multiple interaction points. From the energy and spatial information, the kinematics of Compton scattering is used to identify and reduce background events, as well as to improve the detector response in the few MeV region. Assuming a spatial resolution of 1 mm RMS and an energy resolution of 4.5% FWHM at 1 MeV, the algorithm is capable of reducing the background rate expected at balloon altitude by an order of magnitude, thus significantly improving the telescope sensitivity.

1. Introduction

Significant progress in experimental γ-ray astrophysics can only be achieved with the development of instruments with improved imaging capability. Efforts to improve the sensitivity of a γ-ray telescope without a corresponding improvement in angular resolution will result in source confusion in the field-of-view (FOV) and will limit the mapping of extended source distributions. Two important scientific objectives which typify the need for detectors with improved imaging capability, along with good sensitivity and energy resolution, are the 1.8 MeV line emission from radioactive ^{26}Al and the 0.511 MeV positron–electron annihilation emission. For both cases a precise study of the spatial distribution of the emission will uniquely identify the source of radiation. Among the proposed novel techniques for imaging astrophysical γ-ray sources in the low to medium energy region, the liquid xenon time projection chamber (LXe-TPC) is recognized as very promising and worth a strong R&D effort. Like an electronic bubble chamber, a TPC is capable of visualizing the complex histories of γ-ray events with multiple interactions, initiated by either Compton scattering or pair production. As a result of this imaging, efficient background rejection is also achieved, reducing the requirement for a massive anticoincidence shield of the type that is required for germanium and sodium iodide detectors. From the energy and spatial information available for each point of interaction, Compton kinematics enables the reconstruction of the direction of the incoming γ-ray. The direction is not unique unless the Compton scattered electron is also imaged. Given the short range of low energy electrons in liquid xenon, this is not possible for a practical spatial resolution of the order of millimeters. In the LXe-TPC Compton telescope, as proposed by us in ref. [1], the angular resolution for the MeV region is limited by the small separation between two successive γ-ray interactions.

To overcome this limitation and release the strong requirement on the TPC spatial resolution, we propose to combine the imaging capability of the LXe-TPC with that of the coded aperture technique, for studying astrophysical sources in the few MeV region with arc min accuracy. In a coded aperture telescope, a mask consisting of a two-dimensional array of opaque and transparent elements is placed between the source and a position sensitive γ-ray detector. Every source within the FOV casts a shadow of part of the mask onto the detector. By properly decoding the pattern obtained at the detector plane, an image of the source is inferred. The successful application of coded aperture imaging in the low energy γ-ray region has been demonstrated by two balloon borne telescopes: the New Hampshire Directional Gamma-Ray Telescope, DGT [2], the Caltech Gamma-Ray Imaging Payload, GRIP [3], and more recently the SIGMA telescope aboard the GRANAT satellite [4]. All these telescopes use scintillators as position sensitive γ-ray detectors. The advantage of the LXe-TPC/coded telescope is its unique capability to suppress background over a wide energy range, thus improving the sensitivity to weak sources, while maintaining an excellent detection efficiency, energy and angular resolution.

In this paper the technical aspects of the LXe-TPC development are not considered. For this we refer to a previous publication by Aprile et al. [5]. We present here initial results from a Monte Carlo analysis of the expected performance of the LXe-TPC coupled to a coded aperture as γ-ray telescope for 0.3–10 MeV.

2. Monte Carlo analysis and results

2.1. Telescope model

The mode of the γ-ray telescope used in the Monte Carlo simulation is schematically shown in fig. 1. It consists of a coded aperture mask, located 1 m above the LXe-TPC γ-ray detector. An active CsI shield has been included. In practice, the background rejection capability of the TPC reduces the need for massive anticoincidence shield. The sensitive area of the TPC is 39×28 cm^2. The total depth of liquid xenon is 10 cm. The detector's dimensions and mask–detector separation have been determined on the basis of the existing gondola for the DGT telescope which we plan to use for the first balloon flight of the telescope [6]. The TPC is operated in the ionization mode. Both the energy and the spatial distribution of each ionizing event within its sensitive volume is measured. The coordinates in the X–Y plane are inferred from the signals induced on two orthogonal wire planes, while the coordinate along the Z-direction is inferred from the drift time measured with respect to a zero time provided by the fast scintillation signal. As indicated by our first experimental results on the induction signals in a 3.5 l LXe-TPC, to be published elsewhere, the spatial resolution in the plane is better than $S/\sqrt{12}$, where S is the spacing between the induction wires. For the spatial resolution on the coordinate along the drift axis we have previously measured $\sigma_z = 0.18$ mm [5]. For the Monte Carlo calculations, a resolution of $\sigma_x = \sigma_y = 1$ mm and $\sigma_z = 0.2$ mm has been assumed, along with the experimental energy resolution of 4.5% FWHM at 1 MeV, extrapolated according to a $E^{-1/2}$ law [7].

The mask is a 2×2 mosaic of a basic uniformly redundant array (URA) [8]. It consists of a 43×41 element pattern of 0.91 cm $\times$ 0.68 cm $\times$ 1.2 cm thick tungsten blocks. With the assumed separation of 1 m between mask and the detector, an angular pixel size of $0.65° \times 0.49°$ and a FOV of $28° \times 20°$ is defined. Much finer angular resolution is obtained by increasing the mask–detector separation. The precision in point source localization depends, however, also on the detector's spatial resolution and the statistical significance of the source data. We have estimated that a precision at the arcminute level is possible with a practical spatial resolution of 1 or 2 mm.

2.2. Reconstruction algorithm based on Compton kinematics

The interaction of γ-rays in liquid xenon is dominated by Compton scattering and pair production, for energies larger than few hundred keV. The typical event registered by the TPC is therefore characterized by multiple interaction points before the original γ-ray

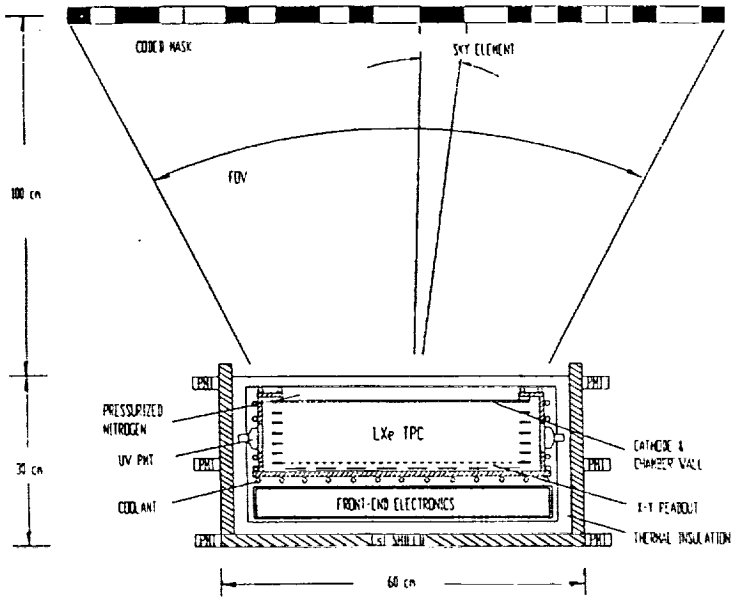

Fig. 1. Schematic of the LXe-TPC/coded mask γ-ray telescope.

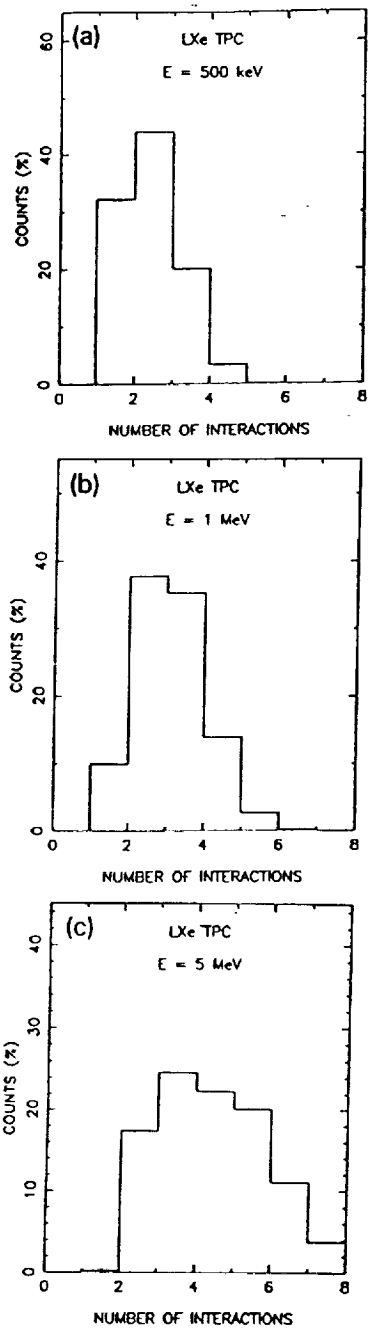

Fig. 2. Distribution of interaction points for γ-ray energies of (a) 500 keV, (b) 1 MeV and (c) 5 MeV.

energy is fully deposited in the liquid. This is illustrated in fig. 2 where the distribution of the number of interaction points for three different γ-ray energies is plotted. The probability that the first interaction point is a Compton scattering is 90% at 1 MeV, decreasing to about 25% at 10 MeV. To improve the signal/noise level in the few MeV region where multiple Compton events dominate, an algorithm based on the kinematics of the Compton process was developed and tested. The algorithm uses the capability of the LXe-TPC to visualize each incoming γ-ray event and to reconstruct the initial direction from the energy deposited in each interaction point and the coordinates of the points. Consider an event in which a γ-ray produces N energy deposition points. Let W_0 be the energy of the incoming photon, W_i the energy of the scattered photon, E_i the energy of the scattered electron and $\cos\theta_i$ the cosine of the scattering angle. If the coordinates and the energy depositions for each interaction point as well as the right order of the successive interactions are known, then from energy and momentum conservation we can write for each interaction point:

$$1-\cos\theta_i = 1/W_i - 1/W_{i-1}, \tag{1}$$

where $W_i = W_{i\pm1} + E_{i+1}$, for $i = 1, N-1$. For any given distribution of interaction points generated inside the sensitive volume, we now assume that the last interaction point is a photo-absorption and that the initial direction of the incoming γ-ray is known. Calling

$$\frac{E_i}{1-\cos\theta_i} = \alpha_i, \tag{2}$$

eq. (1) becomes

$$W_{i-1}W_i = \alpha_i. \tag{3}$$

Similarly, for the $(i+1)$th point,

$$W_iW_{i+1} = \alpha_{i+1}. \tag{4}$$

From eqs. (3) and (4),

$$W_i = \frac{\alpha_i - \alpha_{i+1}}{E_i + E_{i+1}}. \tag{5}$$

Also, if the total energy is contained, W_0 is

$$W_0 = \frac{\alpha_1}{E_2 + E_3 + \cdots E_N}. \tag{6}$$

Alternatively, from energy conservation alone we have an independent estimate of the energy of the scattering photon at each point. We express this as W_i'.

$$W_i' = E_{i+1} + \cdots E_N \tag{7}$$

for $i = 0, N-1$. To test the validity of the assumption that the total energy is contained, as well as if the assumed initial direction of the γ-ray is kinematically possible, the function

$$f = \sum_{i=0}^{N-1} (W_i - W_i')^2 \tag{8}$$

is minimized for all possible combination of points. The calculation takes into account the errors on the energy and spatial coordinates.

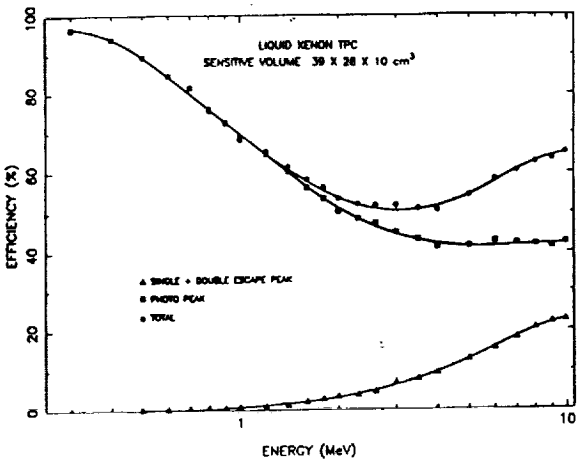

Fig. 3. Efficiency of the LXe-TPC for normally incident photons.

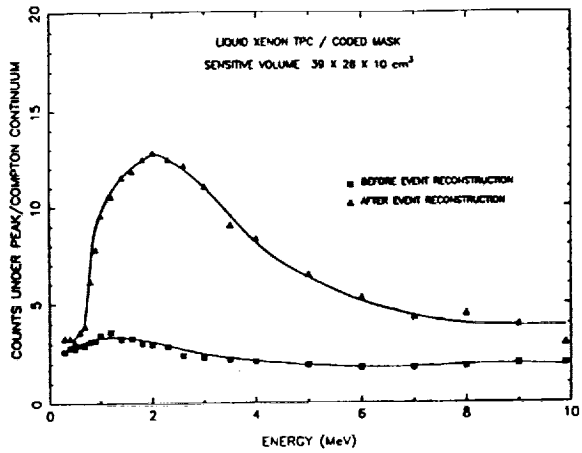

Fig. 5. Ratio of events under the peak to that under the Compton continuum for the LXe-TPC/coded mask before and after event reconstruction.

2.3. Detection efficiency

The Monte Carlo calculations were based on the EGS4 computer code [9]. The excellent γ-ray detection efficiency of liquid xenon over a wide energy range is shown in fig. 3. The full energy peak efficiency was calculated for γ-rays in the range 0.3–10 MeV, normally incident on the forward face of a 10 cm deep liquid xenon detector. The energy of the events in the sample was required to be totally contained. The use of a coded mask reduces the detection efficiency by a factor of two, assuming 100% opacity of the closed mask elements. This is shown in the upper curve of fig. 4. The effect of the 3 mm stainless steel detector wall was also accounted for. The effect of the Compton reconstruction algorithm, described in section 2.2, on the telescope efficiency is also shown in fig. 4 as a □.

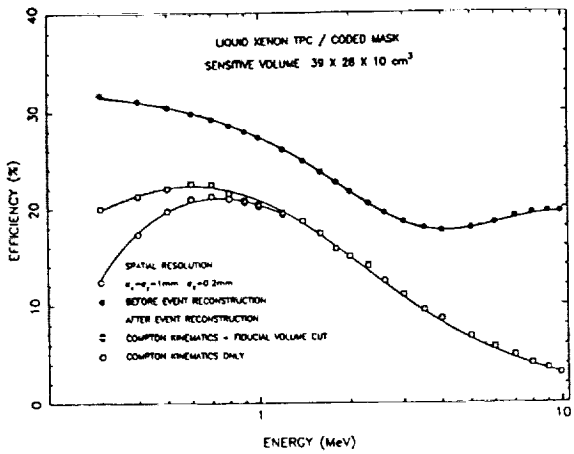

Fig. 4. Efficiency of the LXe-TPC/coded mask, before and after event reconstruction.

Because the algorithm is tailored for events which start with a Compton scattering, all events with a single photo-absorption or starting with a pair production are rejected. To recover the detection efficiency at low and high energy, different reconstruction techniques can be applied. For example, the majority of low energy photons coming from the source will interact in the top region of the LXe-TPC. Fiducial volume cuts for single site events can therefore drastically improve the signal/noise ratio. This is shown in fig. 4 as a •. All single-site events reconstructed outside the first 1 cm layer of liquid xenon from the top were rejected. For high energy events which start with a pair production, tracking of the electron/positron can be used on an event-by-event basis, to estimate the γ-ray direction from the opening angle of the pair. Such an algorithm has however not been applied as one can see from the drastic drop in efficiency at energies above ~2 MeV.

The capability of the reconstruction algorithm to reject events under the Compton continuum is shown in fig. 5, which shows the ratio of the total counts under the peak to that under the Compton continuum. A large improvement in this ratio is achieved for the MeV region. The excellent capability of the same algorithm to recognize γ-ray events entering the TPC normally from the bottom was also tested. Results are shown in fig. 6. For this calculation total energy containment was not required.

2.4. Background reduction and flux sensitivity

The ultimate flux sensitivity is perhaps the most relevant "figure-of-merit" of a γ-ray telescope. Among the factors which determine the sensitivity are: i) the energy of the γ-rays and ii) the detector's effective

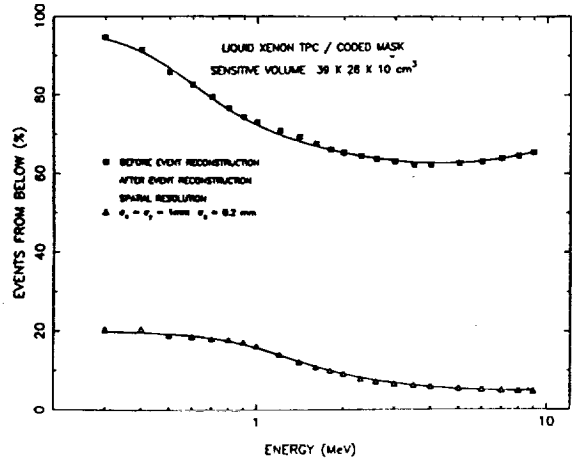

Fig. 6. Percentage of events entering the LXe-TPC from the bottom before and after event reconstruction.

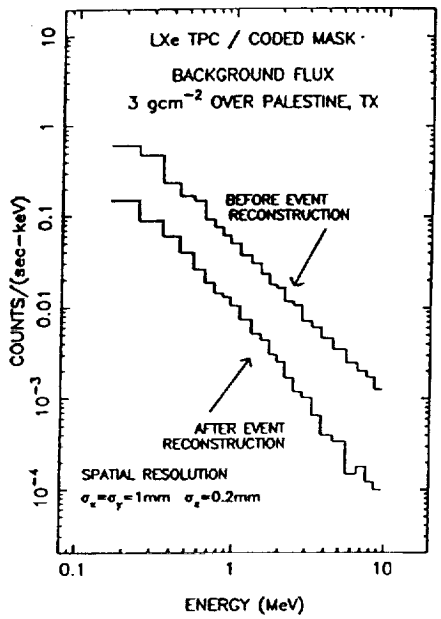

Fig. 7. Calculated background count rate before and after event reconstruction.

area, energy and spatial resolution, the exposure time and the total background rate. To calculate the background expected in the LXe-TPC/coded mask telescope at balloon altitudes, we have taken into account the dominant atmospheric and cosmic diffuse components entering the forward aperture of the telescope or leaking through a thick (5 cm) CsI active shield. The flux and angular distribution of the atmospheric γ-rays used in the calculation were taken from the parameterized forms given by Costa et al. [10] and the cosmic diffuse spectrum used was that given in ref. [11]. The internal backgrounds from natural radioactivity, cosmic ray induced radioactivity and activation of instrument materials have been neglected, as we expect to reject the majority of these single site events. Pulse shape discrimination of the scintillation light pulses offers additional background rejection capability, as it is strongly dependent on the ionization density of the event. For example, neutron induced events can easily be discriminated against, based on the light signature. Fig. 7 shows the calculated background flux, before

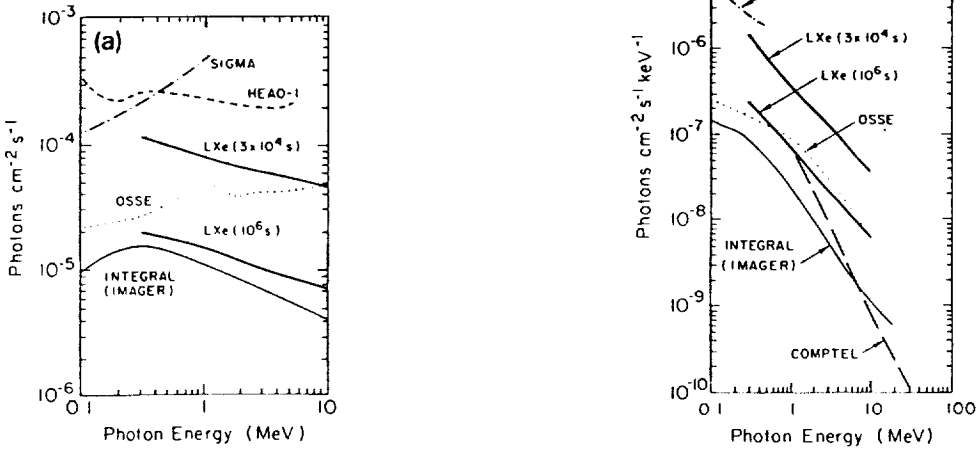

Fig. 8. The 3σ minimum (a) line and (b) continuum flux sensitivity of the LXe-TPC/coded mask γ-ray telescope.

and after applying the Compton event reconstruction of section 2.2. and the fiducial volume cut. We assumed a float altitude of 3 g/cm^2 over Palestine, Texas. The integrated flux over the 0.1–10 MeV region gives about 340 counts/s, consistent with typical background rates measured at these altitudes. A background reduction of almost a factor of 10 is obtained by identifying γ-rays which kinematically could not have come through the FOV of the telescope. It is clear that even better background suppression can be achieved, on an event-by-event basis, using different algorithms for different γ-ray energies, as previously discussed.

From the calculated efficiency and background rate we have estimated the 3σ minimum flux sensitivity of the proposed telescope. The results are shown in figs. 8a and 8b. For a typical exposure of 3×10^4 s, we find a value of 9×10^{-5} photons/cm^{2}s for 511 keV and of 6×10^{-5} photons/cm^{2}s for 1.8 MeV. A continuum sensitivity of 3×10^{-7} photons/cm^{2}s is obtained at 1 MeV. The sensitivity curves of the other instruments, shown for comparison, have been taken from Winkler [12]. When combined with the arcminute source localization accuracy, the high sensitivity of the LXe-TPC telescope makes it competitive with many satellite instruments, even with the much shorter observation time available in a balloon flight.

4. Conclusion

Monte Carlo modeling of a realistic LXe-TPC/coded mask telescope has demonstrated the unique capability of this instrument to suppress background events as a direct consequence of the imaging properties of the LXe-TPC. By using a reconstruction algorithm for multiple site events, based on the kinematics of Compton scattering, we find that the expected background flux at balloon altitude is reduced by nearly an order of magnitude, resulting in superior line flux sensitivity in the MeV region, compared to that of existing scintillator-coded mask or proposed segmented germanium/coded mask γ-ray telescopes. It is clear that this is only a first step towards the application of the liquid xenon technique for precise imaging of cosmic γ-ray sources. The full potential will be realized when a detector with large effective area, improved energy resolution and sub-millimeter spatial resolution becomes practically operational as a Compton/pair production γ-ray telescope.

Acknowledgement

This work was supported by NASA grant NAGW-2013.

References

[1] E. Aprile, R. Mukherjee and M. Suzuki, in: EUV, X-Ray and Gamma-Ray Instrumentation for Astronomy and Atomic Physics, ed. C.J. Hailey and O.H.W. Siegmund, SPIE Conf. Proc. 1159 (1989) p. 295.
[2] P.P. Dunphy et al., Nucl. Instr. and Meth. A274 (1989) 362.
[3] W.E. Althouse et al., Proc. 20th Int. Cosmic Ray Conf. 1 (1987) 84.
[4] J. Paul et al., Cospar Proc. on Recent Result and Perspective Instrumental Developments in X- and Gamma-ray Astronomy, Adv. Space Res. 11 (1991) 289.
[5] E. Aprile et al., Nucl. Instr. and Meth. A316 (1992) 29.
[6] Prof. E. Chupp, Univ. of New Hamsphire, private communications (1992).
[7] E. Aprile, R. Mukherjee and M. Suzuki, Nucl. Instr. and Meth. A302 (1991) 177.
[8] E.E. Fenimore and T.M. Cannon, Appl. Opt. 17, (1978) 337.
[9] R.L. Ford and W.R. Nelson, SLAC-210 (1978).
[10] E. Costa et al., Astrophys. and Space Sci. 100 (1984) 165.
[11] V. Schönfelder, V. Graser and J. Daugherty, Astrophys. J. 217 (1977) 306.
[12] C. Winkler, AIP Conf. Proc. 232 (1991) 483.

APPENDIX 2

The Polarization Sensitivity of the Liquid Xenon Imaging Telescope

E. Aprile, A. Bolotnikov, D. Chen and R. Mukherjee

Physics Department and Columbia Astrophysics Laboratory
Columbia University, New York, NY 10027

Submitted to: *The Astrophysical Journal* supplement series
as part of the proceedings of the
INTEGRAL Workshop, Les Diableret, Switzerland, 2 – 5 February 1993

COLUMBIA UNIVERSITY

DEPARTMENTS OF

PHYSICS and ASTRONOMY

NEW YORK, NEW YORK 10027

Columbia Astrophysics Laboratory Contribution Number 517

The Polarization Sensitivity of the Liquid Xenon Imaging Telescope

E. Aprile, A. Bolotnikov, D. Chen, R. Mukherjee, and F. Xu

Physics Department and

Columbia Astrophysics Laboratory

Columbia University, New York, NY 10027

Abstract

The properties and the expected performance of a liquid xenon (LXe) γ-ray imaging telescope, optimized for the MeV energy region are presented. The unique potential of this telescope as a Compton polarimeter is particularly emphasized. Based on Monte Carlo simulations we show that the modulation factor is as high as 40% at 1 MeV with a detection efficiency close to 20%. These figures of merit combined with the excellent background suppression capability of the three-dimensional position sensitive LXe detector, yield sensitivity at the three sigma level to polarization fractions as small as a few percent for strong sources, even in a balloon flight.

Subject headings: γ-rays; instruments; polarization

1. Introduction

Future missions in low and medium energy γ-ray astronomy will rely on new telescopes with superior imaging capability, high energy resolution, wide sky coverage and high sensitivity. Of the new detector technologies that have been proposed to meet with these requirements, a Liquid Xenon Time Projection Chamber (LXe-TPC) (Aprile, Mukherjee & Suzuki 1989) is among the most promising. The properties of liquid xenon make it an excellent radiation detector medium, particularly for γ-rays. When used in an ionization

chamber, operated in the time projection mode, LXe offers an ideal combination of high detection efficiency, 3-D event imaging with submillimeter spatial resolution and very good energy resolution response. Like an electronic bubble chamber, a LXe-TPC is able to visualize any ionizing event occurring within its sensitive volume. γ-ray events with multiple Compton interactions are recognized as such, thus substantially increasing the detection efficiency in the difficult Compton region. The interaction of γ-rays in most materials is dominated by Compton scattering for energies larger than few hundred keV. As shown in Figure 1, the probability that a γ-ray interacts first via Compton scattering in a 10 cm deep LXe detector varies between 50% at 1 MeV and 10% at 10 MeV. Also shown is the fraction of events with two or more consecutive Compton interactions. In the few MeV region this fraction is not small. These multiple Compton events which have a high probability to be rejected in a conventional double scatter Compton telescope, carry as much information as single Compton events, if all interaction points and the deposited energy in each point are measured. The imaging capability can be used not only to analyze the topology of the events under investigation, but also to reject background. Since the Compton scattering cross-section depends on the polarization of the incident γ-ray, a direct consequence of the LXe-TPC intrinsic imaging capability is its sensitivity as a Compton polarimeter. To estimate this polarization sensitivity a Monte Carlo program that explicitly considers the polarization of Compton scattered γ-rays was written. Results on modulation factor, detection efficiency and background rate in the 0.3–10 MeV energy range are combined to obtain the polarization sensitivity curve for a 100% polarized source with the spectrum of the Crab.

2. Telescope description and properties

Figure 2 shows the schematic of the LXe-TPC γ-ray imaging telescope which we have proposed for the observation of a variety of discrete and diffuse γ-ray sources in the MeV region (Aprile *et al.* 1992a; Aprile *et al.* 1993a). It consists of a 3-D position sensitive

LXe γ-ray detector, an active veto shield, and a coded aperture mask. The coded mask consists of a 2×2 mosaic of a basic Uniformly Redundant Array (URA), with a 85×83 element pattern of $0.91 \times 0.58 \times 1.2$ cm^3 thick blocks of tungsten alloy. With 1 meter distance between the mask and the detector plane, the FWHM angular resolution is $\sim 30'$ and the nominal fully coded FOV is $28° \times 20°$ FWHM. For a 10σ source strength, the point source localization accuracy is estimated to be ~ 1 arcminute, based on the LXe detector spatial resolution of 1 mm RMS. The LXe detector has an active area of 39×28 cm^2, and a thickness of 30 g cm^{-2} which gives good sensitivity up to 10 MeV. The lowest energy threshold will be determined mostly by the S/N ratio achievable in a practical detector operated in the ionization mode. The LXe-TPC works on the principle that the free ionization electrons liberated in the liquid by a charged particle can drift, under a uniform electric field, towards a signal readout structure. The ionization signals induced on the sensing elements provide both the spatial and total energy information for each event. In our design the information in the XY plane is obtained from the signals induced on two orthogonal wire planes while the Z information, along the direction of drift, is inferred from the drift time, measured with respect to a zero time provided by the fast signal from the primary scintillation in LXe. The technical feasibility of such a detector has been studied at Columbia for the past few years (Aprile *et al.* 1992a, 1992b; Aprile, Mukherjee & Suzuki 1991a, 1991b, 1990). We have finished the construction and are currently testing with laboratory γ-ray sources a 10 liters detector, with approximately half the sensitive area and half the drift space as the one proposed for the first balloon flight.

3. Detector Performance: Monte Carlo Results

The Compton scattering process is an unique tool for determining the polarization of the incident γ-ray because there is a large difference in the scattering cross-section for the orthogonal states of polarization. The relation between the energy of the incident γ-ray,

E_0, and that of the scattered γ-ray, E, is given by:

$$E = E_0\left[1 + E_0\left(1 - \cos\theta\right)\right]^{-1} \tag{1}$$

where E and E_0 are expressed in units of m_0c^2, and θ is the scattering angle. If the incident γ-ray is completely polarized, then the differential cross section for being Compton scattered is:

$$d\sigma_\phi = \frac{1}{2}r_0^2\left(\frac{E}{E_0}\right)^2\left[\frac{E}{E_0} + \frac{E_0}{E} - 2\sin^2\theta\cos^2\phi\right]d\Omega \tag{2}$$

where r_0 is the classical radius of the electron, ϕ is the azimuthal angle, and $d\Omega$ is the element of solid angle into which the γ-ray is scattered. The polarization sensitive part of the cross section is contained in the $\cos^2\phi$ term. A measure of the response of the Compton scattering process to polarized radiation is obtained from the "asymmetry ratio", R, defined as

$$R = d\sigma_{90}/d\sigma_0 \tag{3}$$

where $d\sigma_0$ and $d\sigma_{90}$ are the differential scattering cross sections for $\phi = 0°$ and $\phi = 90°$. Figure 3 shows the asymmetry ratio as a function of θ for different incident γ-ray energies. At low energies, for values of θ close to 90°, the Compton scattering process provides ideal response to radiation polarized in the reaction plane. As the energy of the incident γ-ray increases, the angle θ at which R is maximum, $\theta_{\max}$, decreases.

The modulation factor of a Compton polarimeter is defined as:

$$Q(\theta) = \frac{N_\perp(\theta) - N_\parallel(\theta)}{N_\perp(\theta) + N_\parallel(\theta)} \tag{4}$$

where $N_\perp(\theta)$ is the detected count rate of the scattered γ-ray in a direction perpendicular to the γ-ray's electric vector (that is, for $\phi = 90°$) and $N_\parallel(\theta)$ is the detected count rate in the direction parallel to the electric vector (that is, for $\phi = 0°$). Q is a measure of the suitability of the detector as a Compton polarimeter. The advantage of the LXe-TPC over more conventional double scatter polarimeters is that the scatterer and absorber are the same detector, which largely increases the detection efficiency, with 4π acceptance.

To evaluate the performance of the LXe telescope as a Compton polarimeter we have written a Monte Carlo program based on EGS4, which explicitly treats the polarization dependence of the Compton process. For the simulations we assumed a LXe active volume of $39 \times 28 \times 10$ cm^3 and a spatial and energy resolution of: $\sigma_x = \sigma_y = 1$ mm, $\sigma_z = 0.2$ mm, $\Delta E/E = 4.5\%$ FWHM at 1 MeV with a $E^{-0.5}$ dependence. A flux of 100% polarized γ-rays incident normally on the detector plane was generated. As previously mentioned, a large fraction of these events are characterized by multiple Compton scatterings. For each event the detector measures the coordinates and the energy deposited in each interaction point. From the locations of the first two successive interaction points the scattering angle θ and the azimuthal angle ϕ of the scattered γ-ray is inferred, provided that the correct order of interaction points is known. If the energy is totally contained, the original γ-ray energy is also inferred. To find the correct order of the interactions, a reconstruction algorithm based on Compton kinematics was developed (Aprile *et al.* 1993b). The efficiency of the LXe polarimeter lies in its capability to include multiple Compton events which in a conventional double scatter polarimeter are rejected.

As shown in Fig. 2, the detector is most sensitive as a polarimeter for a particular scattering angle, $\theta_{\max}$, when the asymmetry ratio is a maximum. To increase the detector count rate, all events were accepted for which the scattered γ-ray was within some angle bin about $\theta_{\max}$. Figure 4 shows the distribution of the scattered γ-rays in the range $\phi = 0°$ to $\phi = 90°$, for different $\Delta\theta$ bins, where $\Delta\theta = |(\theta - \theta_{\max})|$. The simulations were performed for 100% polarized γ-rays of energy 500 keV, incident normally on the detector surface. The results for the modulation factor, Q, versus incident γ-ray energy are shown in Fig. 5,for $\Delta\theta = 5°$. At 1 MeV Q is as high as 40%. For comparison, the modulation factors for the Ge(Li) polarimeter (Taras 1968), the Si(Li)-Ge polarimeter (Ohya *et al.* 1989), and the CsI(Tl) polarimeter (1 cm^2 cross-sectional area) of the Imager on INTEGRAL (Swinyard *et al.* 1991) are also shown.

The polarization sensitivity of a polarimeter, or the minimum detectable degree of

polarization, for a given source flux and observation time, is determined by the modulation factor, as well as by the detection efficiency and the background rate. The polarization sensitivity, $P_{\rm min}$ of the LXe-TPC polarimeter was calculated at the 3 σ level for a 100% polarized source with the spectrum of the Crab, by using the relation:

$$P_{\rm min}^{3\sigma} = \frac{3}{\epsilon Q I_{\rm source}} \sqrt{\frac{\epsilon I_{\rm source} + B}{\Delta E A t}} \tag{5}$$

where ϵ is the detector efficiency, Q is the modulation factor, $I_{\rm source}$ is the source flux, B is the background rate, t is the observation time, A is the sensitive area of the detector, and ΔE is the energy bin.

The Crab spectrum for the MeV region was taken from the DGT experimental results as $5.1 \times 10^{-3} E^{-1.88}$ cm^{-2}s^{-1}MeV^{-1} (Dunphy *et al.* 1989). The efficiency, and background rate at balloon altitude, were estimated using Monte Carlo simulation (Aprile *et al.* 1993b) and are shown in Fig. 6 and Fig. 7. We note that although the use of the coded mask reduces the detection efficiency by a factor two, a 20% efficiency is still achieved at 1 MeV. For the background estimation, we considered only the dominant atmospheric and cosmic diffuse components and assumed an active 5 cm thick CsI anti-coincidence shield. As shown in Fig. 7, a background reduction of almost a factor of ten is achieved by correctly identifying γ-rays which kinematically could not have come through the telescope's FOV. The background rate, after event reconstruction, as used in the polarization sensitivity calculation, was approximated by a power law as $10 \times E^{-2}$s^{-1}MeV^{-1}. The energy bin ΔE was set equal to 200 keV and the observation time was taken as 10 h, for a typical balloon flight. The results of the calculation are shown in Fig. 8. The histogram stops at 2 MeV since, at higher energies the polarization of the Crab source cannot be measured at the 3 σ level, even if we assume a 100% polarized flux.

4. Conclusions

Based on Monte Carlo simulations we conclude that the LXe-TPC imaging telescope will work as a sensitive Compton polarimeter for cosmic γ-ray sources in the MeV region, even as a balloon payload. A modulation factor of 40% was calculated at 1 MeV. This combined with a detection efficiency close to 20% and the low background rate which can be achieved with an intrinsically imaging γ-ray detector, will permit sensitivity to polarization fractions as small as few percent for strong sources.

This work was supported by NASA grant NAGW-2013.

References

Aprile, E., Bolotnikov, A., Chen, D., & Mukherjee, R. 1992a, "Gamma-Ray Detectors", *SPIE Conference Proceedings*, **1734**, 98.

Aprile, E., Chen, D., Moulson, M., Mukherjee, R., & Suzuki, M. 1992b, Nuclear Instruments and Methods in Physics Research A, 316, 29.

Aprile, E., Bolotnikov, A., Chend, D., & Mukherjee, R. 1993a, Nuclear Physics B (Proc. Suppl.), 32 (1993), 279.

Aprile, E., Bolotnikov, A., Chen, D., & Mukherjee, R. 1993b, Nuclear Instruments and Methods in Physics Research A, 327, 216.

Aprile, E., Mukherjee, R. & Suzuki, M. 1991a, Nuclear Instruments and Methods in Physics Research A, 302, 177.

Aprile, E., Mukherjee, R. & Suzuki, M. 1991b, Nuclear Instruments and Methods in Physics Research A, 300, 343.

Aprile, E., Mukherjee, R. & Suzuki, M. 1990, IEEE Trans. Nucl. Sci., NS-37, 553.

Aprile, E., Mukherjee, R. & Suzuki, M. 1989, "EUV, X-Ray and Gamma-Ray Instrumentation for Astronomy and Atomic Physics," *SPIE Conference Proceedings*, 1159, 295.

Dunphy, P. et al. 1989, Nuclear Instruments in Physics Research A274, 362.

Ohya, S., Miura, H., Nishimura, K., Mutsuro, N., & Aoki, T. 1989, Nuclear Instruments and Methods in Physics Research A, 276, 223.

Swinyard, B.M., Malaguti, G., Caroli, E., Dean, A.J., & Di Cocco, G. 1991, "Production and Analysis of Polarized X-Rays," *SPIE Conference Proceedings*, 1548, 94.

Taras, P. 1968, Nuclear Instruments and Methods in Physics Research A, 61, 321.

Figure Captions

Fig. 1. Expected number of γ-ray events with a single Compton scattering and with two or more consecutive Compton scatterings, vs. incident γ-ray energy.

Fig. 2. Schematic of the LXe-TPC/coded mask imaging γ-ray telescope.

Fig. 3. Asymmetry ratio, R, as a function of the scattering angle θ.

Fig. 4. Distribution of the scattered γ-rays for $\phi = 0° - 90°$, simulated for 100% polarized incident γ-rays of energy 500 keV.

Fig. 5. Modulation factor, Q, vs. incident γ-ray energy for the LXe-TPC. For comparison, results on Q for other polarimeters are also shown.

Fig. 6. Detection efficiency vs. incident γ-ray energy, before and after event reconstruction.

Fig. 7. Background rate (atmospheric and cosmic diffuse components only) before and after event reconstruction.

Fig. 8. The minimum detectable degree of polarization vs. incident photon energy for a 3 σ detection of a 100% polarized γ-ray source with the spectrum of the Crab for an observation time of 10 hours.

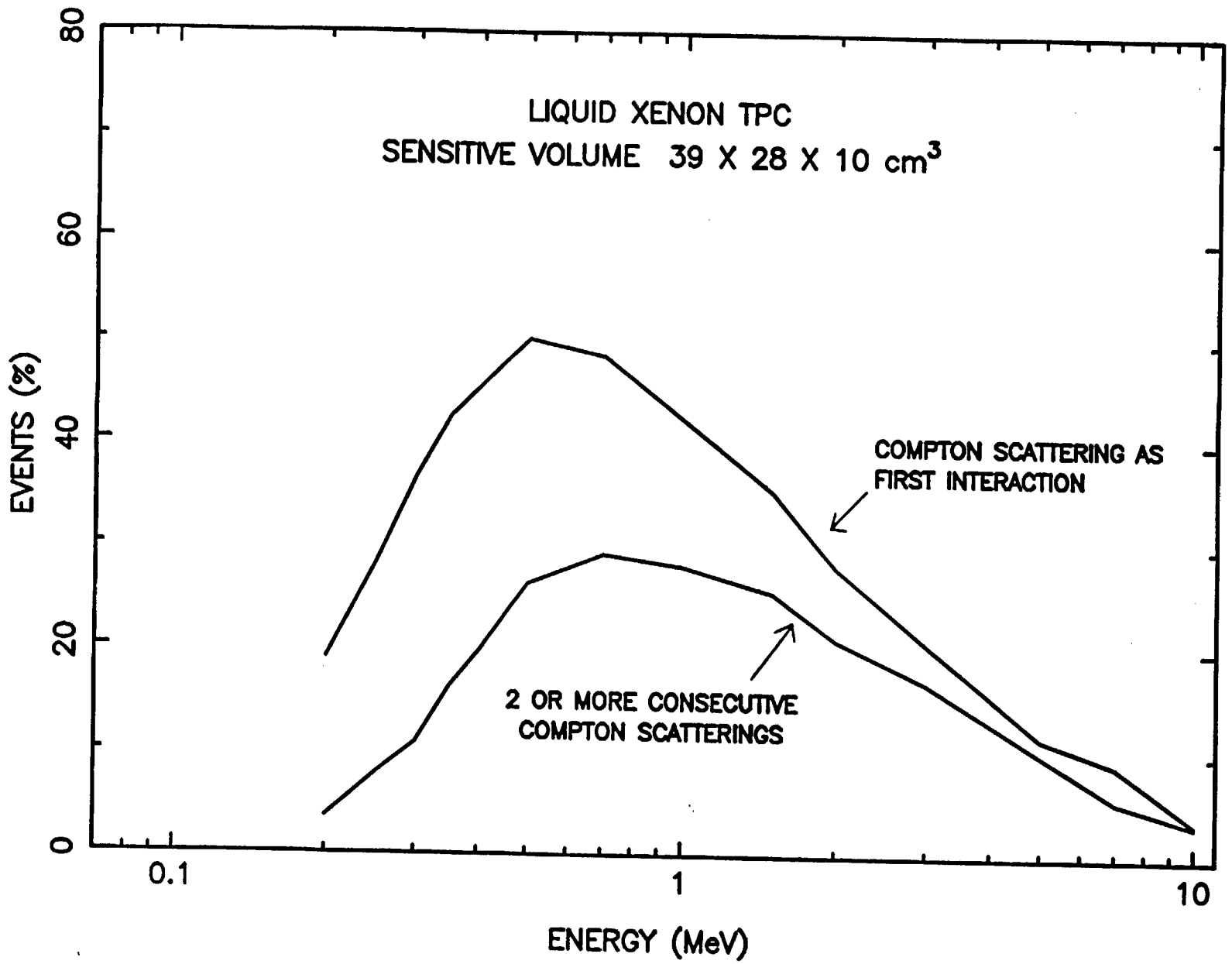
LIQUID XENON TPC
SENSITIVE VOLUME 39 X 28 X 10 cm3
EVENTS (%)
0
20
40
60
80
0.1
1
10
ENERGY (MeV)
COMPTON SCATTERING AS FIRST INTERACTION
2 OR MORE CONSECUTIVE COMPTON SCATTERINGS

FIG. 1

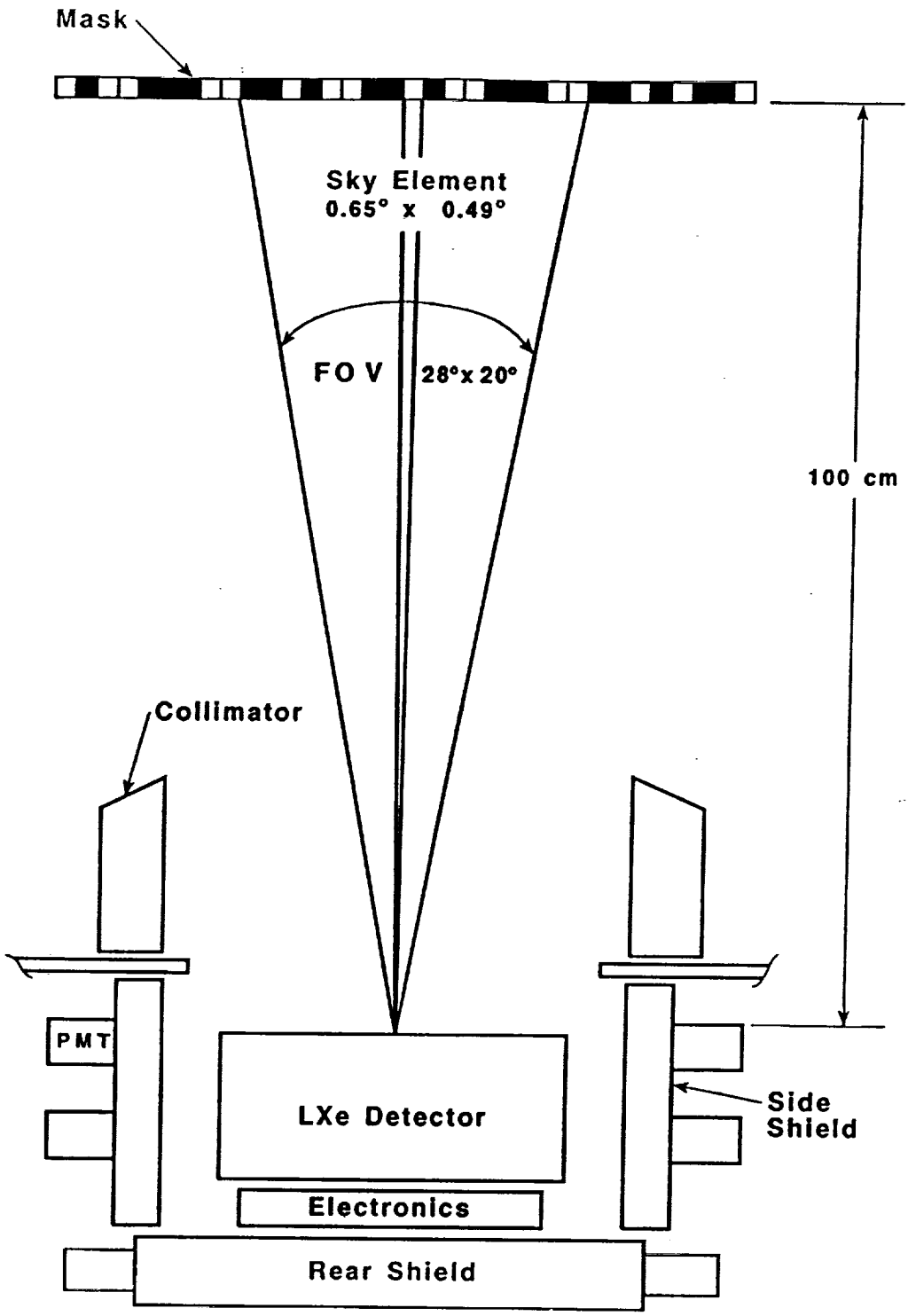
Mask
Sky Element
0.65° x 0.49°
FOV
28°x 20°
100 cm
Collimator
PMT
LXe Detector
Side
Shield
Electronics
Rear Shield

FIG.2

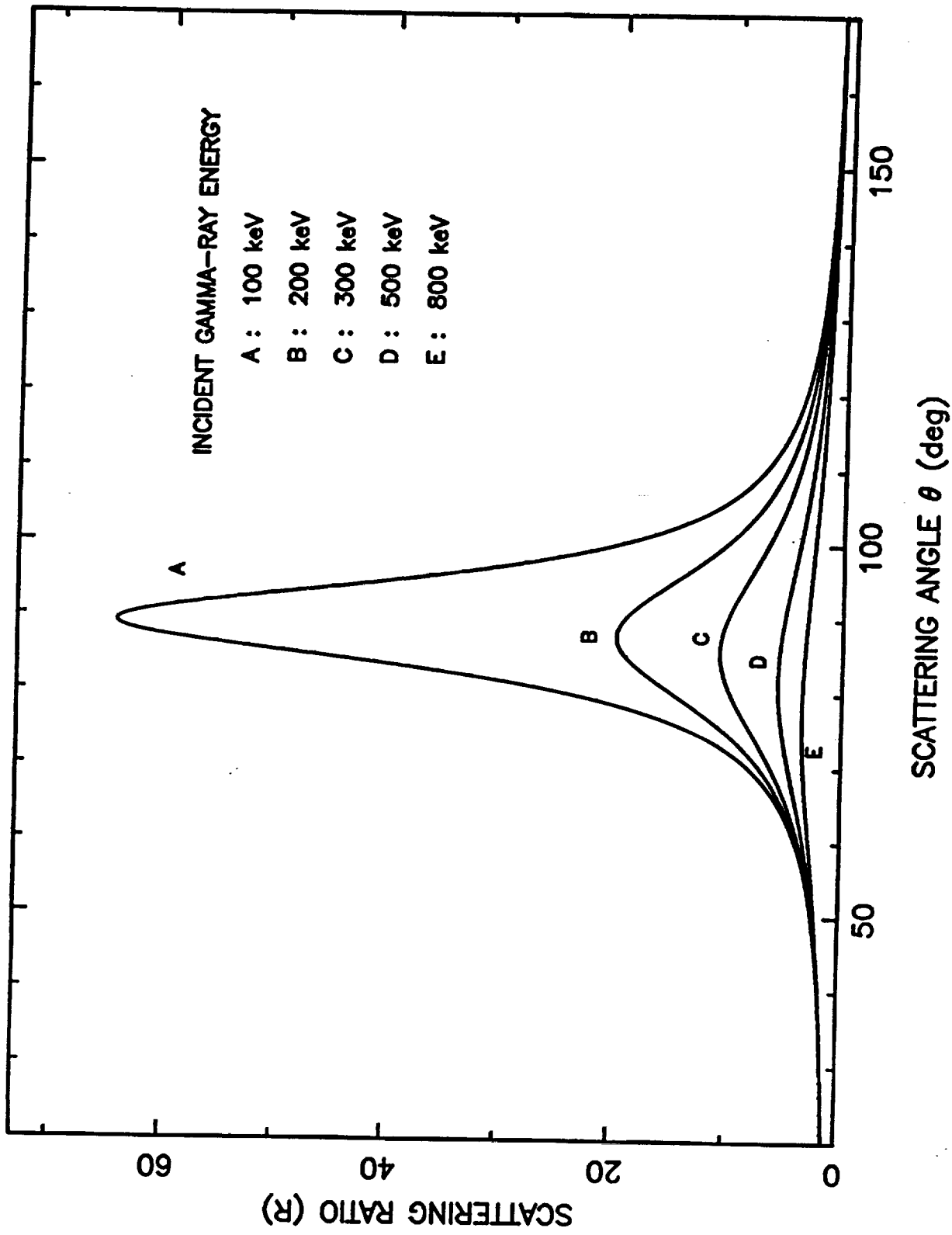
INCIDENT GAMMA-RAY ENERGY
A : 100 keV
B : 200 keV
C : 300 keV
D : 500 keV
E : 800 keV
A
B
C
D
E
SCATTERING RATIO (R)
0
20
40
60
50
100
150
SCATTERING ANGLE θ (deg)

FIG.3

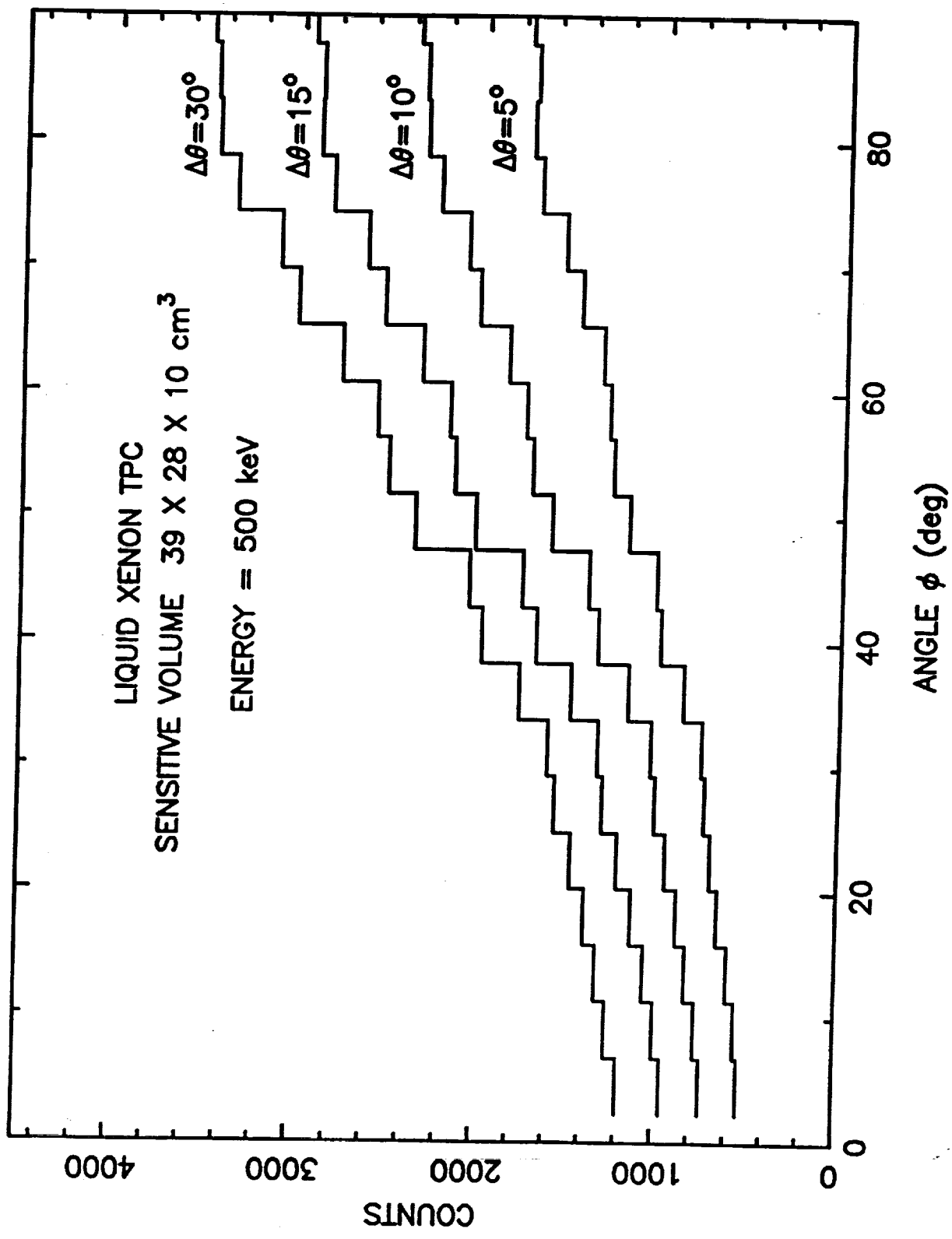
LIQUID XENON TPC
SENSITIVE VOLUME 39 X 28 X 10 cm3
ENERGY = 500 keV
Δθ=30°
Δθ=15°
Δθ=10°
Δθ=5°
COUNTS
0
1000
2000
3000
4000
ANGLE φ (deg)
0
20
40
60
80

FIG. 4

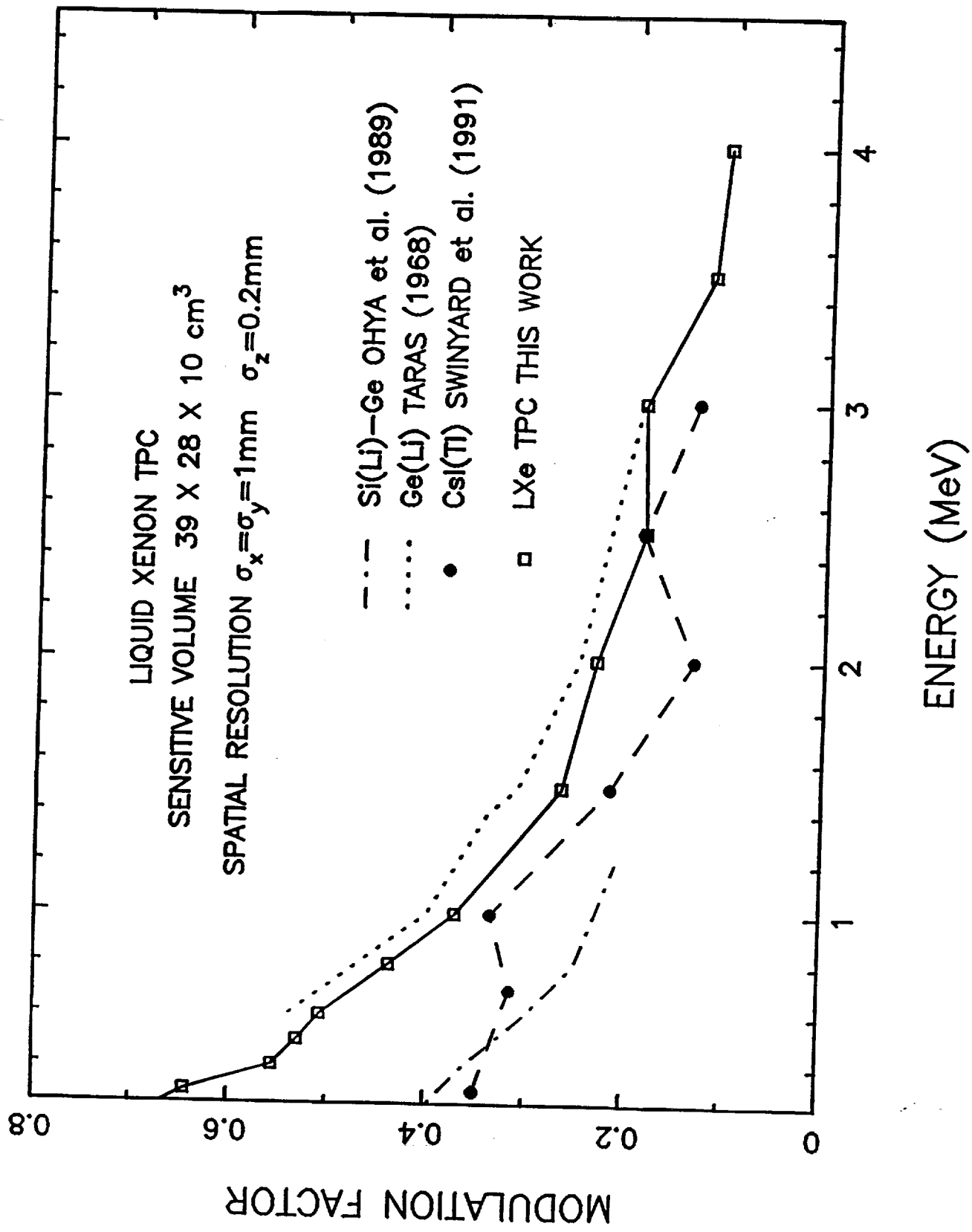
LIQUID XENON TPC
SENSITIVE VOLUME 39 X 28 X 10 cm3
SPATIAL RESOLUTION σx=σy=1mm σz=0.2mm
Si(Li)–Ge OHYA et al. (1989)
Ge(Li) TARAS (1968)
CsI(Tl) SWINYARD et al. (1991)
LXe TPC THIS WORK
MODULATION FACTOR
ENERGY (MeV)
0
0.2
0.4
0.6
0.8
1
2
3
4

FIG. 5

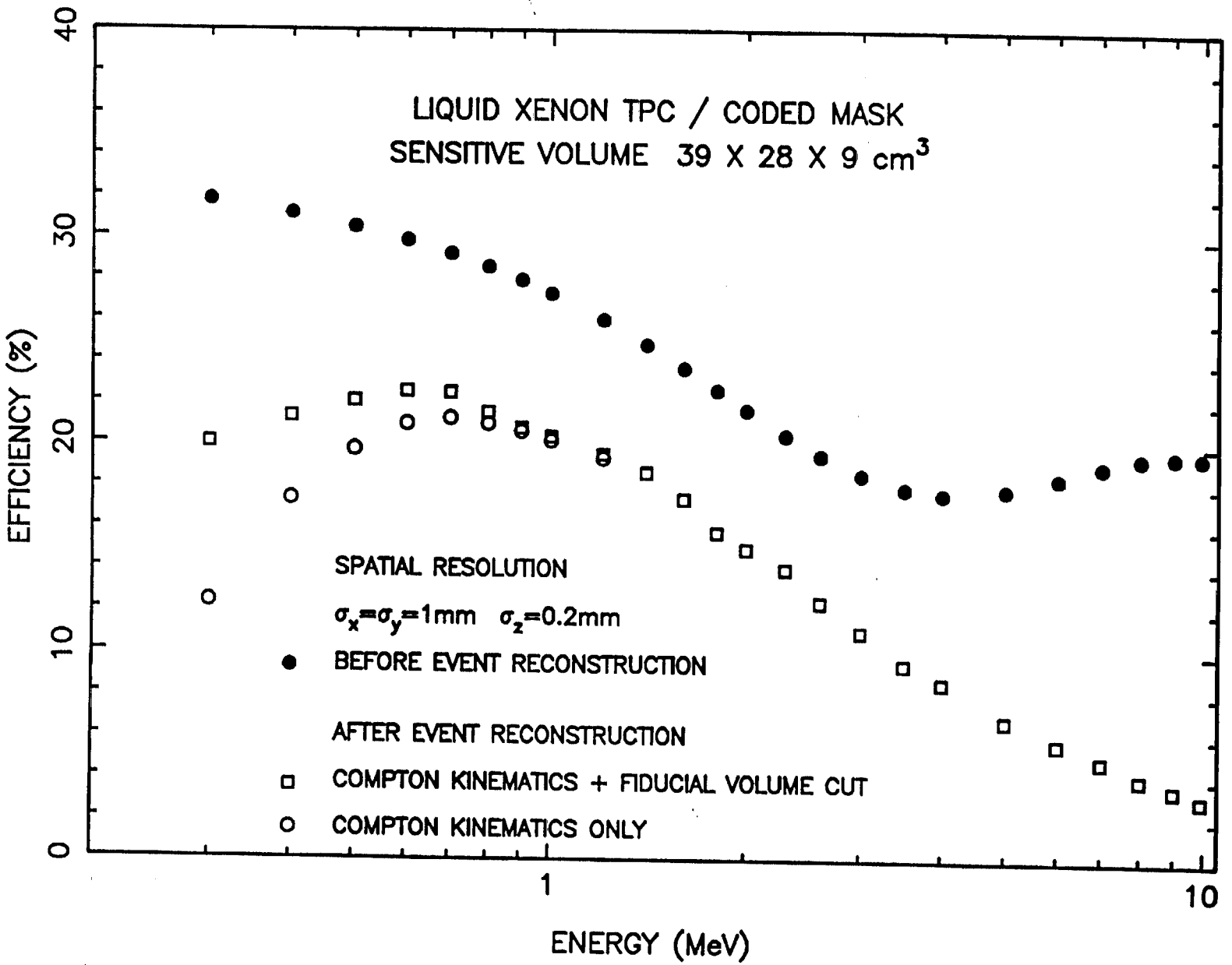
LIQUID XENON TPC / CODED MASK
SENSITIVE VOLUME 39 X 28 X 9 cm3
EFFICIENCY (%)
ENERGY (MeV)
0
10
20
30
40
1
10
SPATIAL RESOLUTION
σx=σy=1mm σz=0.2mm
BEFORE EVENT RECONSTRUCTION
AFTER EVENT RECONSTRUCTION
COMPTON KINEMATICS + FIDUCIAL VOLUME CUT
COMPTON KINEMATICS ONLY

FIG. 4

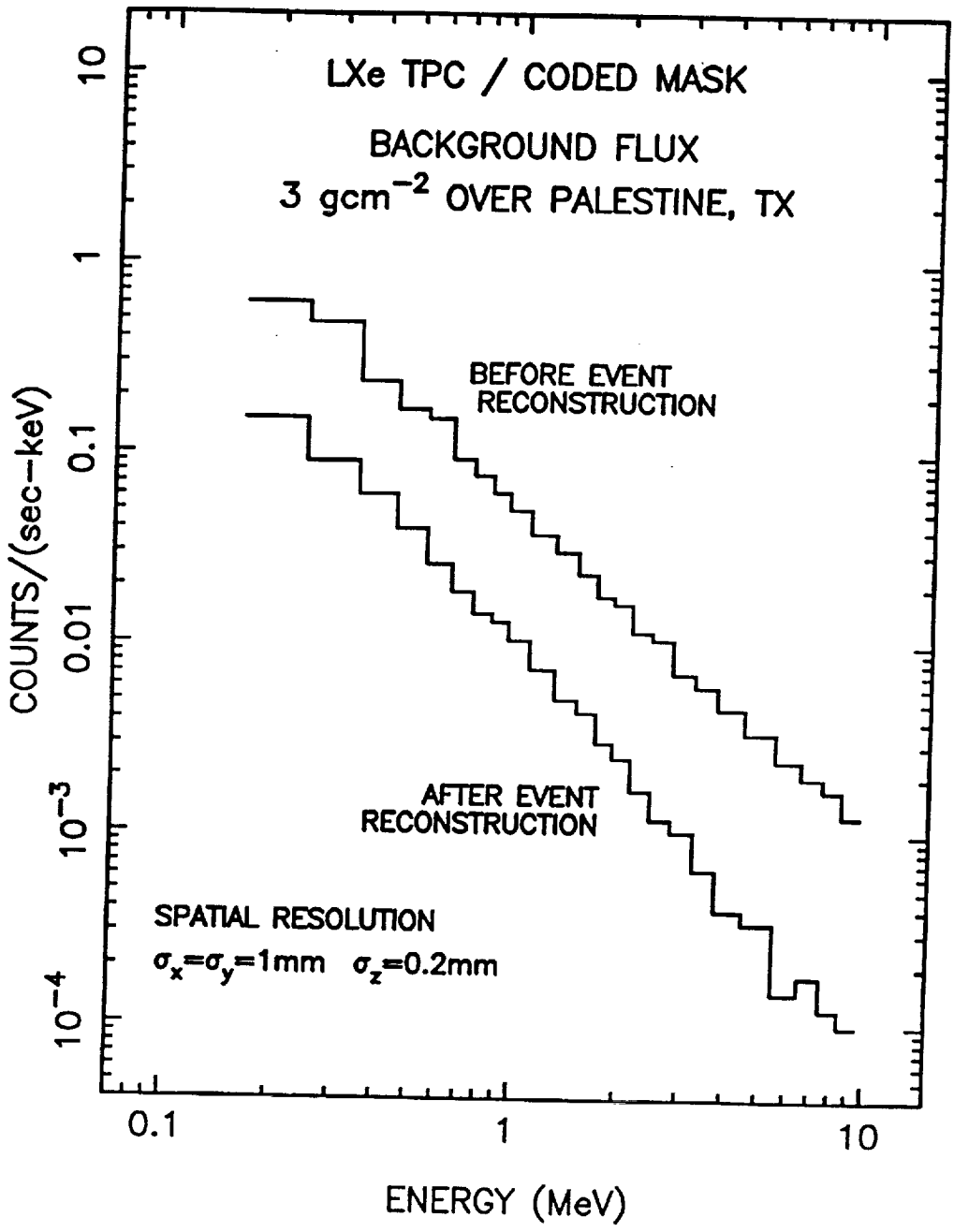
LXe TPC / CODED MASK
BACKGROUND FLUX
3 gcm^{-2} OVER PALESTINE, TX
BEFORE EVENT RECONSTRUCTION
AFTER EVENT RECONSTRUCTION
SPATIAL RESOLUTION
$\sigma_x=\sigma_y=1$mm $\sigma_z=0.2$mm
COUNTS/(sec-keV)
10
1
0.1
0.01
10^{-3}
10^{-4}
0.1
1
10
ENERGY (MeV)

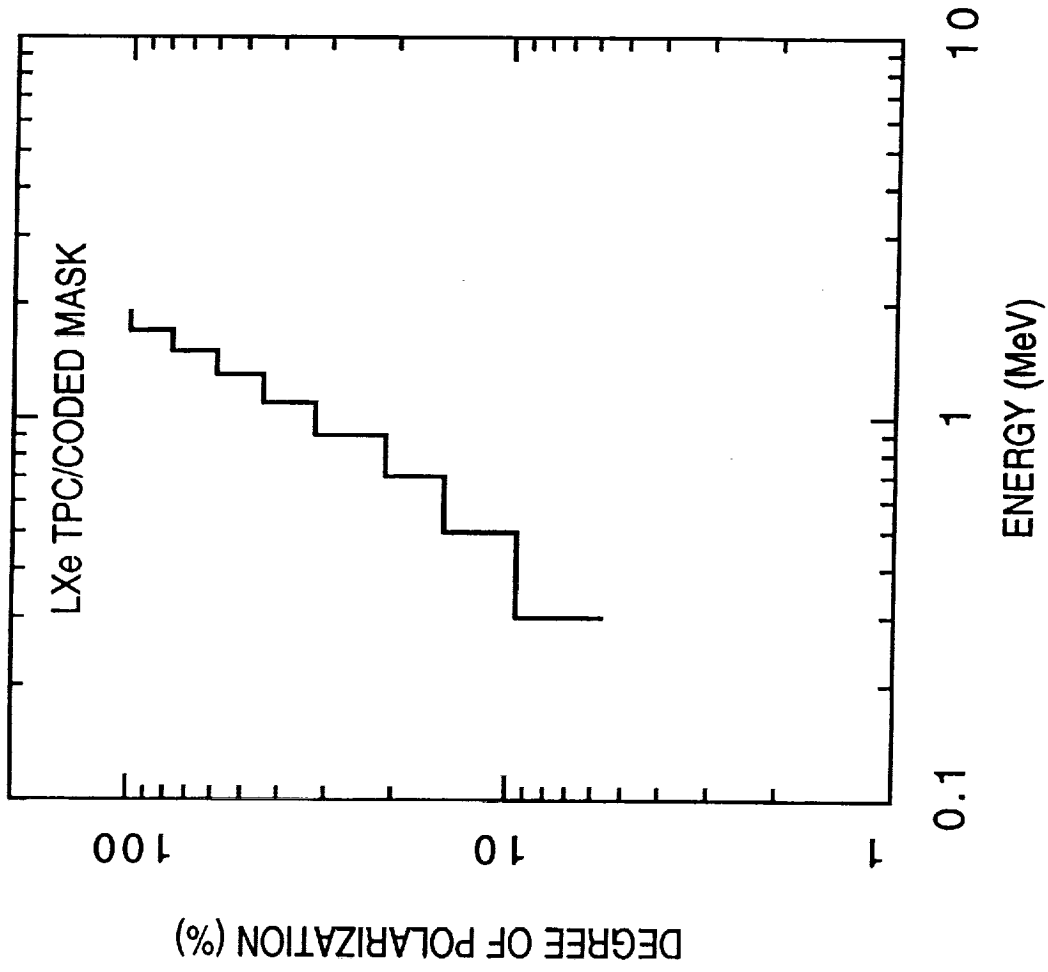
LXe TPC/CODED MASK
100
10
1
0.1
1
10
ENERGY (MeV)
DEGREE OF POLARIZATION (%)

Fig. 8

REPRINTED FROM:

APPENDIX 3

NUCLEAR PHYSICS

Volume 32, Nos. 1–3, 1993

A Liquid Xenon Imaging Telescope for Gamma-Ray Astrophysics: Design and Expected Performance

E. Aprile, A. Bolotnikov, D. Chen and R. Mukherjee

Physics Department and Columbia Astrophysics Laboratory
Columbia University, New York, NY 10027

pp. 279–286

NORTH HOLLAND
AMSTERDAM

Nuclear Physics B (Proc. Suppl.) 32 (1993) 279–286
North-Holland

NUCLEAR PHYSICS B
PROCEEDINGS
SUPPLEMENTS

A Liquid Xenon Imaging Telescope for Gamma-Ray Astrophysics: Design and Expected Performance

E. Aprile, A. Bolotnikov, D. Chen and R. Mukherjee

Physics Department and Columbia Astrophysics Laboratory
Columbia University, New York, NY 10027

A high resolution telescope for imaging cosmic γ-ray sources in the MeV region, with an angular resolution better than 0.5° is being developed as balloon-borne payload. The instrument consists of a 3-D liquid xenon TPC as γ-ray detector, coupled with a coded aperture at a distance of 1 meter. A study of the actual source distribution of the 1.809 MeV line from the decay of ^{26}Al and the 511 keV positron-electron annihiliation line is among the scientific objectives, along with a search for new γ-ray sources. The telescope design parameters and expected minimum flux sensitivity to line and continuum radiation are presented. The unique capability of the LXe-TPC as a Compton Polarimeter is also discussed.

1. INTRODUCTION

Gamma-ray telescopes with true imaging capability and high flux sensitivity are essential for studying the highest-energy phenomena in the universe. Fine imaging provides accurate positioning of the sources detected within the FOV and good angular resolution to map regions of diffuse emission and separate point source contributions. The importance of true source imaging is particularly evident in the study of two of the most pressing problems in low energy γ-ray astronomy: the 1.089 MeV line emission from the decay of ^{26}Al and the 511 keV positron-electron annihilation line emission from the Galactic Center.

In 1977, Ramaty and Lingenfelter [1] suggested that galactic nucleo-synthetic production of ^{26}Al in supernova events over the past few million years could give rise to a detectable γ-ray line at 1.809 MeV. This line arises from the electron capture (18%) or positron decay (82%) of the million-year mean life ^{26}Al and was first detected in 1984 [2] at a flux level of $4.3\pm0.8 \times 10^{-4}$ photons cm^{-2} s^{-1} rad^{-1} at the Galactic Center. Several subsequent confirmations of the line energy and flux level have been made. Some potential sources of ^{26}Al, which have been proposed, are supernovae, novae, red giants in the Asymptotic Giant Branch (AGB), Wolf-Rayet stars or nearby OB stars (see e.g., [3] for a recent review). Since these objects have more or less known or inferred galactic distributions, it is believed that a measurement of the spatial distribution of the ^{26}Al 1.809 MeV line intensity will identify the ^{26}Al source. The only instrument which could measure this radiation with imaging capability, is the Compton telescope, the most advanced version of which is COMPTEL on the *COMPTON* Observatory. COMPTEL however cannot directly measure the 1.809 MeV spatial distribution. The only definite statement that can be made about the ^{26}Al spatial distribution from the latest COMPTEL results, at the present time, is that a point source near the Galactic Center can be excluded [4]. Clearly, there is a requirement to measure directly the spatial distribution of the 1.809 MeV line with a true imaging telescope.

As for the 511 keV line, the debate between point like and diffuse nature of the emission continues to date and can only be fully resolved with a high level imaging map of the Galactic Center region at γ-ray energies.

At the present time the OSSE instrument on the *COMPTON* Observatory is mapping the distribution of the annihilation line [5]. Since the OSSE measurements give the lowest galactic center flux measurements so far Skibo, Ramaty and Leventhal [6] have used these results

and other off-center measurements to test different models for the origin of the diffuse or steady galactic plane 511 keV component. On the other hand, the origin of the variable narrow line galactic 511 keV radiation may be associated with the bright hard X-ray source 1E1740.7-2942 which was studied by the imaging telescope SIGMA on the *GRANAT* satellite during the spring-fall of 1990 and in early 1991. Sunyaev *et al.* [7] have identified three spectral states for this source which range from a "low state," a normal (Cygnus X-1 like) state to a hard state in which a bump appears in the spectrum between (300–600) keV. The broad feature of the spectrum has been interpreted as annihilation of positrons in a hot medium ($\sim$ 40 keV). This is consistent with the temperature of the accretion disk derived from the X-ray continuum spectrum.

Subsequently it was proposed [8,9] that in addition this high energy source injects positrons into a molecular cloud where they slow down and annihilate to produce the narrow component of the 511 keV line emission.

Future studies of the 511 keV emission require the most advanced imaging telescope with good to excellent energy resolution.

Of the techniques proposed for γ-ray imaging and spectroscopy of astrophysical sources, the Liquid Xenon Time Projection Chamber (LXe-TPC) is among the most promising. The properties of liquid xenon make it very efficient for γ-ray detection. When used in an ionization chamber, operated in the time projection mode, this medium offers a combination of high detection efficiency, excellent spatial resolution and very good energy resolution. Like an electronic bubble chamber, a LXe-TPC with three-dimensional position sensitivity is capable of visualizing the complex histories of γ-ray events initiated by either Compton scattering or pair-production. As a result, efficient background rejection is also achieved, reducing the requirement for massive anticoincidence shielding of the type that is required for germanium or sodium iodide γ-ray detectors. The angular resolution of the LXe-TPC as a Compton telescope is however limited, in the few MeV region, by the small separation between two successive γ-ray interactions [13]. To achieve imaging with good angular resolution at low energies, the combination of the imaging LXe-TPC with a coded aperture is proposed.

A unique consequence of the LXe-TPC imaging capability is its sensitivity as a Compton polarimeter. Besides the precise determination of the energy and incident direction of a photon, determination of its polarization state can give further information on the source of γ rays. The main production mechanisms which can give polarized γ rays are: bremsstrahlung from electron beams, electron synchrotron radiation, electron curvature radiation, and γ rays from de-excitation of nuclei excited by directed ion beams. In the case of the Crab Nebula it has been determined that the nebular X-ray emission is polarized [10]. Existence of UHE ($> 10^{14}$) electrons in this source could yield polarized nebular γ-rays of a few MeV. If curvature radiation from electrons is the source of MeV γ rays in pulsars, such as the Crab and Vela, then polarization might also be expected.

In general it has been recognized in the study of X-ray sources, that measurement of the direction and magnitude of the photon polarization could significantly contribute to a better understanding of the physical processes in compact objects, such as pulsars, Black Holes and AGN.

2. TELESCOPE DESIGN

2.1. Introduction

The telescope is schematically shown in Fig. 1. It consists of a coded aperture mask, located 1 meter above a LXe-TPC. The sensitive area of the TPC is 39 x 28 cm^2. The active depth of liquid xenon is 10 cm. Fig. 2 shows the LXe-TPC in more detail. The event trigger to the readout electronics is provided by the fast primary scintillation light detected by two UV sensitive PMTs. The intrinsic instrumental angular resolution in the coded mask configuration is determined by the size of the mask unit cell, the mask-detector separation, and by the accuracy to which the photon interaction points in the detection plane can be determined. The coded mask that we have assumed in our design and Monte Carlo simulations consists of a 85 x 83 element pattern of

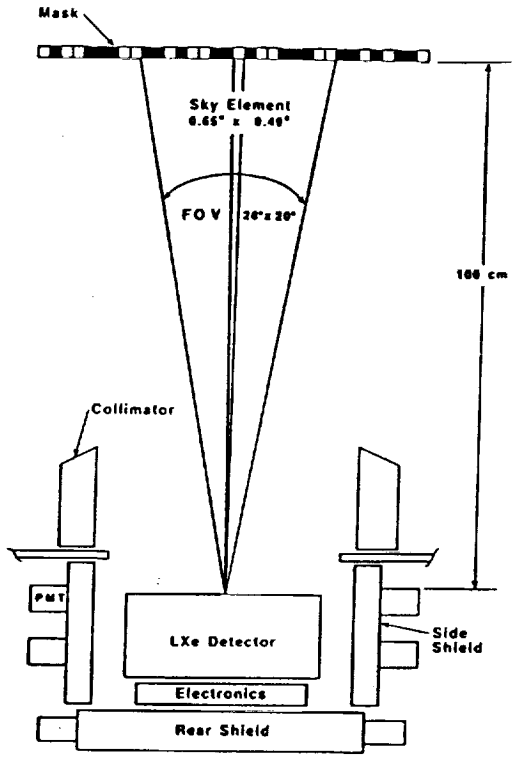

Energy Range	0.3-10 MeV
Energy Resolution	4.5% FWHM at 1 MeV
Spatial resolution	1 mm
Geometrical area	1200 cm^2
FOV (Fully Coded)	28° x 20° FWHM
Angular resolution	30′
Point source location accuracy	1′ (10σ source)
Min Flux (Line) 3σ at 1 MeV	8×10^{-5} ph $cm^{-2}s^{-1}$ (3×10^4s)
Min Flux (Continuum) 3σ at 1 MeV	3×10^{-7} ph $cm^{-2}s^{-1}keV^{-1}$ (3×10^4s)

Fig. 1. Schematic of the LXe-TPC/coded mask imaging γ-ray telescope.

$0.91 \times 0.58 \times 1.2$ cm^3 thick blocks of tungsten alloy. The 1 meter separation between the mask and the LXe detector plane is determined by the University of New Hampshire gondola [11] which we plan to use for the first balloon flight. This defines a pixel element of angular dimension 0.65° × 0.49°. The nominal FOV is 28° × 20°

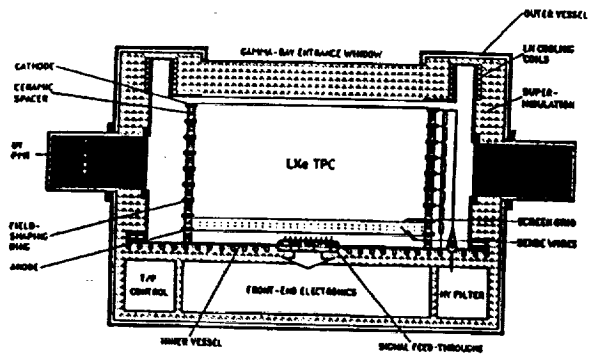

Fig. 2. Schematic of the LXe-TPC detector.

and the source localization accuracy is estimated to be ~ 1 arcminute, for a 10σ source strength. For background suppression at balloon altitude an active shield has been assumed around the detector. The type and amount of shield needed will ultimately be determined by the type of event triggering and selection on board, by dead time consideration, telemetry rate as well as cost and weight consideration.

2.2. The LXe-TPC: Status of Development

A LXe-TPC works on the principle that free ionization electrons liberated by a charged particle in the liquid can drift, under a uniform electric field, from their point of creation towards a signal read-out region. Here the charge signals induced or collected on sensing electrodes are detected to yield both the spatial distribution of the ionizing event and its energy.

For γ-rays it is the electrons or positrons created by photoabsorption, Compton scattering or pair production, which will ionize as well as excite the xenon atoms creating a large number of electron-ion pairs and scintillation photons. For 3-D imaging of γ-ray events in LXe we plan to use a sensing electrodes geometry based on the original design by Gatti *et al.* [12]. Two orthogonal induction wire planes separated from the drift region by a screening grid, give the X-Y event information. The measured drift time, referred to the scintillation trigger, and the known drift velocity provides the Z-information. The total event energy is measured from the total charge collected on an anode plate, placed below the induction

wires.

In order to verify the feasibility of such a detector, the Columbia group started in 1989 an intensive R&D program on LXe. The attenuation length of electrons and UV photons in purified liquid xenon, the ionization and scintillations yields of electrons and alpha particles, the energy and spatial resolution have been studied.

The experimental results obtained on these aspects relevant for the development of a liquid ionization TPC, are documented in several references [13-18]. Especially relevant are the latest experimental results obtained with a 3.5 liter 2D-TPC prototype [19] equipped with a multi-wire structure to detect the induction signals in liquid xenon. The results demonstrate both the capability of a large volume LXe detector to provide similar or better energy resolution than the previously reported value of 4.5% FWHM for 1 MeV radiation, as well as the imaging capability.

Figure 3 shows an example of collection and induction signals produced by a γ-ray event in the LXe-TPC prototype. The induction signal, which has the expected triangular shape, has a large S/N ratio of 12:1, even for a typical point-like charge deposition produced by a γ-ray interaction. The dependence of the induced signal on the lateral position of the drifting electron cloud

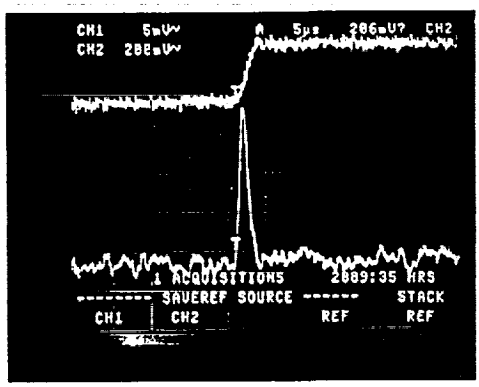

Fig. 3. Collection signal (upper trace Gain=1) and induction signal (lower trace Gain=400) produced by a γ-ray event in the 3.5 liter LXe-TPC prototype.

with respect to the wire cell [19], offers the possibility to derive the spatial coordinate of each event by weighting the signal amplitude on neighbouring wires. Thus the spatial resolution in the X-Y plane, can be better than $s/\sqrt{12}$, where s is the wire spacing.

Experimental work on the operation and performance of the LXe TPC prototype implemented for full 3-D imaging and triggered by the scintillation light is in progress.

3. TELESCOPE PERFORMANCE: MONTE CARLO RESULTS

3.1. Background Rate and Minimum Flux Sensitivity.

To calculate the background expected in the LXe-TPC/coded mask telescope at balloon altitudes, we have taken into account the dominant atmospheric and cosmic diffuse components, entering the forward aperture of the telescope or leaking through the active shield (5 cm thick CsI). The flux and angular distribution of the atmospheric γ-rays used in the calculation were taken from the parameterized forms given by Costa *et al.* [20] and the cosmic diffuse spectrum used was that given by Shoiifelder, Graser and Daugherty [21]. The internal backgrounds from natural radioactivity, cosmic ray induced radioactivity and activation of instrument materials have been neglected, as the majority of these single site events can be rejected by simple fiducial volume cuts.

The results of the calculation are shown in Fig. 4. The integrated flux over the 0.1–10 MeV region gives about 340 counts/sec, consistent with typical background rates measured at the assumed altitude. An event reconstruction algorithm based on the kinematics of Compton scattering was developed and used for identification and rejection of background events [22]. As shown in Fig. 4, a background reduction of approximately a factor of 10 is obtained by identifying γ-rays which kinematically couldn't have come through the FOV of the telescope, and by applying a fiducial volume cut to remove low energy events.

Based on the calculated γ-ray detection efficiency [22] and the calculated background rate,

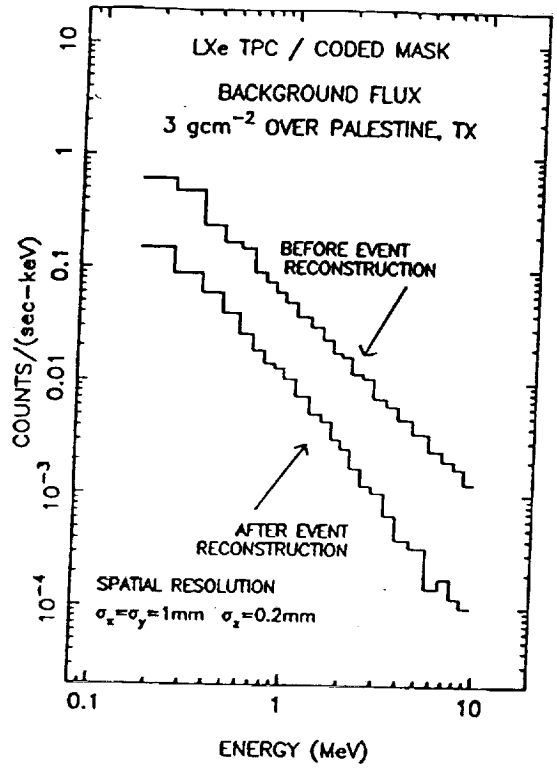

Fig. 4. Monte Carlo calculation of the background flux at balloon altitude.

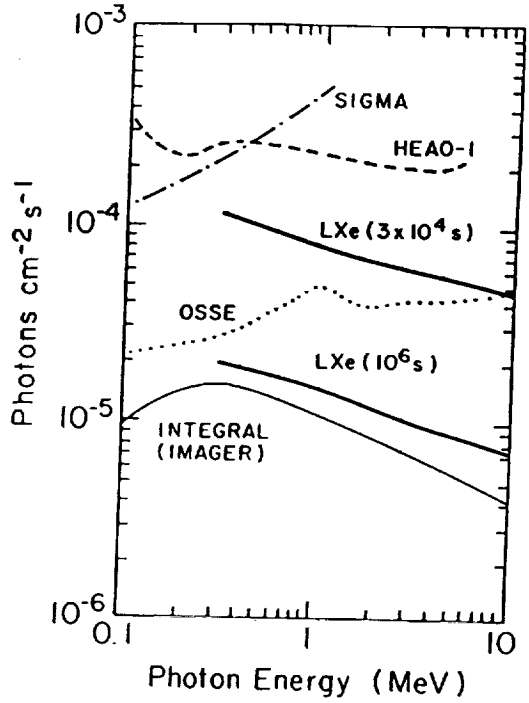

Fig. 5. 3σ minimum line flux sensitivity of the LXe-TPC/coded mask γ-ray telescope.

we have obtained the 3σ minimum flux sensitivity shown in Fig. 5. With a typical balloon flight exposure of 3×10^4s, the 3σ line sensitivity is 6×10^{-5} photons cm^{-2} s^{-1} (1.8 MeV line) and 9×10^{-5} photons cm^{-2} s^{-1} (511 keV line). The continuum sensitivity is 3×10^{-7} photons cm^{-2} s^{-1} keV^{-1} at 1 MeV. The sensitivity curves of the instruments, shown for comparison, have been taken from Winkler [23]. When combined with the excellent source localization accuracy, the high sensitivity of the LXe-TPC telescope makes it competitive with many satellite instruments, even with the much shorter observation time available in a balloon flight.

3.2. Simulated Observations of the Crab and 511 keV Line

The Crab Nebula/Pulsar will be the primary target for the first verification balloon flight of the LXe-TPC coded mask γ-ray telescope. This source is one of the most intense in our energy range and is stable, both in intensity and spectrum. Monte Carlo simulations of the expected Crab signal were performed using the complete telescope system shown in Fig. 1.

The Crab Nebula was assumed to be a point source in the sky with a spectrum equal to 5.5×10^{-4} (E/100 keV)$^{-2.2}$ photons cm^{-2} s^{-1} keV^{-1} at 10 MeV [24]. The source was aligned with the telescope axis and the observing time was 10^4 s. The estimated background of Fig. 4, after event reconstruction, was uniformly distributed in the detector's plane and added to the shadowgram of the source. Figure 6 shows the resulting deconvolved image of the Crab, for the energy interval 0.3 – 0.5 MeV. The Crab signal dominates over the background up to several MeV with a S/N of about 20σ.

Simulated observations have also been performed for the low and high state of the 511 keV Galactic Center annihilation line. A 10^4 s exposure time was assumed. The source was placed in the center of the FOV, and superimposed on

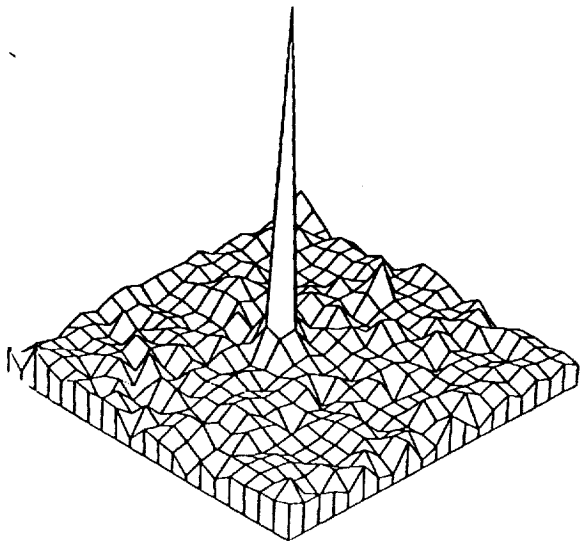

Fig. 6. Monte Carlo simulation of the Crab as a point γ-ray source in the energy range (0.3–0.5 MeV).

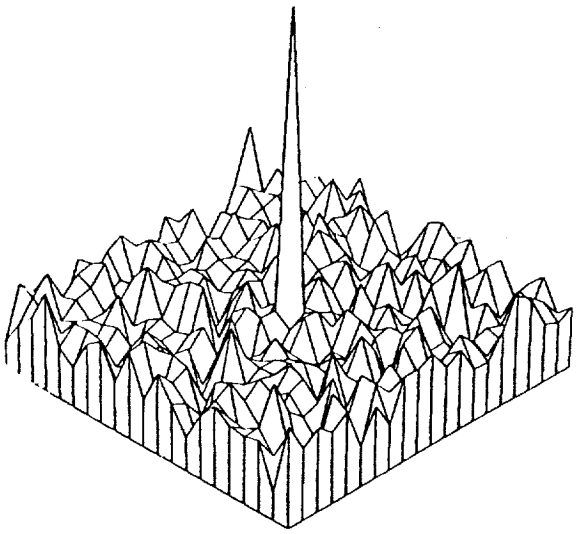

Fig. 7. Monte Carlo simulation of the 511 keV Galactic Center point source observed for High State.

a uniformly distributed background of 4×10^{-2} counts s^{-1} keV^{-1}, as from our estimate. The intensity of the 511 keV line source was chosen to be 2×10^{-4} photons cm^{-2} s^{-1} for the "low state" and 1×10^{-3} photons cm^{-2} s^{-1} for the "high state". Figure 7 shows the result of the 511 keV image for the "high state". Even in the "low state", the 511 keV flux can be detected by our instrument at a satisfactory significance level of $\sim 4\sigma$.

3.3. Polarization Sensitivity

The LXe-TPC imaging capability is also ideal to measure the linear polarization of the incident γ-ray undergoing Compton scattering. The linear polarization of γ-rays can be measured based on the principle that the Compton scattering process is sensitive to the polarization of the incident γ-ray, the cross-section for Compton scattering being the largest for the case when the direction of the scattered γ-ray is normal to the polarization vector of the incident γ-ray. The advantage of a LXe-TPC Compton Polarimeter over the conventional NaI(Tl), CsI(Tl) or Ge(Li) double scatter Compton telescopes is the enhanced detection efficiency offered by a single detector working both as scatterer and absorber, as well as its combination of good energy and position sensitivity.

A Monte Carlo program was developed to estimate the polarization sensitivity of the LXe-TPC for a 100% polarized γ-ray beam of energy varying from 300 keV to 4 MeV, incident normally on the detector surface. Figure 8 shows the result. For comparison, the polarization sen-

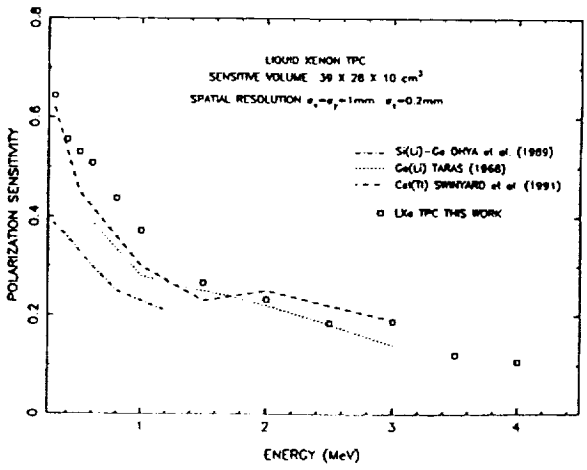

Fig. 8. Monte Carlo calculation of the LXe-TPC polarization sensitivity.

sitivity of the Ge(Li) polarimeter [25], the Si(Li) [26] and the CsI(Tl) polarimeter of the Imager on INTEGRAL [27] are also shown. The unique feature of the LXe-TPC is its capability to infer the scattering angle θ and the azimuthal angle ϕ, with an accuracy of about 0.5° [13], for each scattered γ-ray. We can thus obtain the azimuthal angular distribution of the scattered γ-rays by selecting events from different intervals of scattering angle. By applying the detector's response function, calculated or measured during calibration tests with polarized beams, we can deconvolute the original γ-ray polarization. Figure 9 shows the modulation curve in the range $\phi = 0°$ to $\phi = 90°$, simulated for 100% polarized γ-rays of energy 500 keV.

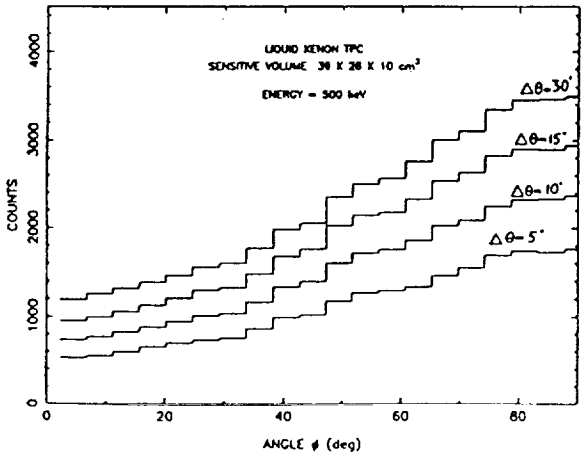

Fig. 9. Modulation curve of the LXe-TPC for 100% polarized γ-rays of energy 500 keV.

4. CONCLUSION

The design and expected performance of a γ-ray imaging telescope tailored to the 0.3–10 MeV energy region have been discussed. The telescope combines the excellent properties of a liquid xenon TPC as 3-D position sensitive γ-ray detector with the well established imaging properties of a coded aperture mask, to achieve high efficiency, good spectroscopy and angular resolution over the entire energy range of interest. The high sensitivity to MeV γ-ray lines and continuum complemented with the good imaging capability will permit the observation of a variety of astrophysical sources. Important contributions to the field of low energy astrophysics as well as new discoveries are expected even in the maiden balloon flight which is planned for the end of 1994.

This work was supported by NASA (Award NAGW 2013).

5. REFERENCES

[1] R. Ramaty, and R.E. Lingenfelter, *Ap.J. (Letters)*, **213**, L5 (1977).
[2] W.A. Mahoney *et al.*, *Ap.J.*, **286**, 578 (1984).
[3] N. Prantzos, *Astron. Astrophys. Suppl.*, in press (1992).
[4] R. Diehl *et al.*, *Astron. Astrophys. Suppl.*, in press (1992).
[5] W.A. Purcell, *et al.* in *The Compton Observatory Science Workshop*, NASA Conf. Publ. 3137, eds. C.R. Shrader, N. Gehrels and B. Dennis, 43 (1992).
[6] J.G. Skibo, R. Ramaty, M. and Leventhal, *Ap.J.*, in press (1992).
[7] R. Sunyaev, *et al.*, *Ap. J. (Letters)*, **383**, L49 (1991).
[8] J. Bally and M. Leventhal, *Nature*, **353**, 234 (1991).
[9] I.F. Mirabel *et al.*, *Nature*, **358**, 215 (1992).
[10] M.C. Weisskopf *et al.*, *Ap.J. (Letters)*, **220**, L117 (1978).
[11] P.P. Dunphy *et al.*, *Nucl. Instr. and Meth.*, **A274**, 362 (1989).
[12] E. Gatti *et al.*, *Trans. Nucl. Sci.*, **NS-26**, 2910 (1970).
[13] E. Aprile, R. Mukherjee, and M. Suzuki, "EUV, X-Ray and Gamma-Ray Instrumentation for Astronomy and Atomic Physics," *SPIE Conference Proceedings*, ed. C.J. Hailey and O.H.W. Siegmund, **1159**, 295 (1989).
[14] E. Aprile, R. Mukherjee, and M. Suzuki, *IEEE Trans. Nucl. Sci.*, **NS-37**, No. 2, 553 (1990).
[15] E. Aprile, R. Mukherjee, R. and M. Suzuki, *Nucl. Instr. and Meth.*, **A302**, 177 (1991).
[16] E. Aprile, R. Mukherjee, and M. Suzuki, *Nucl. Instr. and Meth.*, **A300**, 343 (1991).

[17] E. Aprile, R. Mukherjee, and M. Suzuki, *Nucl. Instr. and Meth.*, **A302**, 177 (1991)
[18] E. Aprile *et al.*, *Nucl. Instr. and Meth.*, **A316**, 29 (1992).
[19] E. Aprile *et al.*, accepted for publication in *SPIE proceedings* (1992).
[20] E. Costa, *et al.*, *Astrophysics and Space Science*, **100**, 165 (1984).
[21] V. Schönfelder, V. Graser, V. and J. Daugherty, *Ap.J.*, **217**, 306 (1977).
[22] E. Aprile *et al.*, accepted for publication in *Nucl. Instr. and Meth.* (1992).
[23] C. Winkler, *Gamma-Ray Line Astrophysics*, *AIP Conf. Proc.*, **232**, p. 483 (1991).
[24] J.C. Ling, and C.D. Dermer, *B.A.A.S.*, **22**, 1271 (1990).
[25] P. Taras, *Nucl. Instr. and Meth.*, **61**, 321 (1968).
[26] S. Ohya *et al.*, *Nucl. Instr. and Meth.*, **A276**, 223 (1989).
[27] B.M. Swinyard *et al.*, *SPIE*, Vol. 1548 *Production and Analysis of Polarized X-rays*, 94 (1992).